MOLECULAR BEAM STUDIES OF STRATOSPHERIC PHOTOCHEMISTRY

Thesis by

Teresa Anne Moore

In Partial Fulfillment of the Requirements

for the Degree of

Doctor of Philosophy

California Institute of Technology

Pasadena, California

1998

(Defended October 6, 1997)

ACKNOWLEDGMENTS

Many people contributed to this work and to my graduate career at Caltech, and I'm sure I have left some of them off of this short list. To those persons and to the people listed below, I extend my thanks for their help, support, and encouragement. Without them, this work would not have been possible.

First I must acknowledge my husband Dustin Laurence, who stood by me during this whole endeavor, especially when I left him for nine months (March - December 1996) to finish the experiment after the beam machine moved to Montana. He gave up the most so that the ClOOCl experiment could be completed.

Also thanks to my advisor Mitchio Okumura, who showed me how to be a scientist, and to my "unofficial" advisor Tim Minton, on whose Crossed Molecular Beams Apparatus all of these experiments were done. They were the major influences on my scientific career.

Thanks to Janet Minton, who welcomed me into their household in Montana for several months until I got a place of my own, as well as on several of the "just one more experiment" trips near the end of the ClOOCl experiment. Thanks to Chrissy Minton, who gave up her bedroom during these later trips, and to Michelle Minton who shared her room with Chrissy so I could have someplace to stay.

Also thanks to James Seale, who came in to take data in the mornings so I could catch a few hour's nap after a long night of data taking; to Donna Garton, who helped set up and take data for the ClOOCl elastic scattering experiments; and to postdoc Thomas Schindler, who came up to Montana for several weeks to help take ClOOCl photolysis and scattering data and to let me visit home for a few weeks. These people were a great help in the last few

months of the ClOOCl experiment, when I was about ready to give up and go home. Alex Ide also helped in the preliminary setup for the ClOOCl experiment in Montana.

The entire Okumura group deserves recognition for their support; Yi-Bin Cao, Jong-Ho Choi, Matt Johnson, and Chrissy Nelson were senior group members who helped me get started, also Keith Kuwata, Jim Spotts, Alex Wong, and Julio Lobo listened to countless practice talks and helped out in many ways. Postdoc Bermi (Bernd-Michael) Haas and undergrad PC (Pratap Chakrabarty) helped in the very early ClOOCl source design phase. Chrissy Nelson was the senior graduate student on the early $ClONO_2$ experiments and helped me learn the CMBA. Undergrad Jessie Haldeman helped make Cl_2O and $ClONO_2$ for the early photolysis experiments at 193 and 248 nm. Our group secretary, Lena Lenore, was also helpful and encouraging.

Other people at Caltech and JPL also played a part: Yuk Yung, who let me use his model to look at the effect of changing the $ClONO_2$ branching ratio; Stan Sander and his postdocs (Troy, Chip Miller, Scott Nickolaisen, possibly others) for helpful advice; Randy Friedl for discussions about Cl_2O and $ClONO_2$ synthesis and ClOOCl cracking patterns, among other things; Greg McDermott at SRI who showed us a much better way to make N_2O_5; and probably many others who I can't think of at the moment.

During my undergraduate years, I was greatly influenced by and owe a lot to several people: Lee Spangler, my undergrad research advisor, who gave me my start in research; and Brad Mundy and Dallas Johnson, who made freshman chemistry lecture and labs sufficiently interesting that I switched my major from chemical engineering to chemistry.

Mr. Frank (math) and Mr. Schladweiler (chemistry and biology) at Roundup High

School were major influences on my decision to go to college and major in a technical field. I also owe a great deal to Mr. Helgeson, my fifth grade teacher, who took me out of the "dumb" group and put me in the "smart" group. Who knows where I would be today without that statement of faith in my ability? And of course, to my parents and grandparents, who always believed in me and supported me in all of my college and career choices.

ABSTRACT

Photochemistry of chlorine oxide containing species plays a major role in stratospheric ozone depletion. This thesis discusses two photodissociation studies of the key molecules $ClONO_2$ and ClOOCl which were previously thought to only produce Cl-atom (ozone depleting) products at wavelengths relevant to the stratosphere. The development of a molecular beam source of ClOOCl and the photodissociation dynamics of the model system Cl_2O are also discussed.

In the first chapter, the photochemistry of $ClONO_2$ is examined at 308 nm using the technique of photofragment translational spectroscopy. Two primary decomposition pathways, leading to $Cl + NO_3$ and $ClO + NO_2$, were observed, with a lower limit of 0.33 for the relative yield of ClO. The angular distributions for both channels were anisotropic, indicating that the dissociation occurs within a rotational period.

Chapter two revisits the photodissociation dynamics of Cl_2O at 248 and 308 nm, on which we had previously reported preliminary findings. At 248 nm, three distinct dissociation pathways leading to Cl + ClO products were resolved. At 308 nm, the angular distribution was slightly more isotropic that previously reported, leaving open the possibility that Cl_2O excited at 308 nm lives longer than a rotational period.

Chapter three describes the development and optimization of a molecular beam source of ClOOCl. We utilized pulsed laser photolysis of Cl_2O to generate ClO radicals, and cooled the cell to promote three body recombination to form ClOOCl. The principal components in the beam were Cl_2, Cl_2O, and ClOOCl.

In the fourth chapter, the photodissociation dynamics of ClOOCl are investigated at

248 and 308 nm. We observed multiple dissociation pathways which produced ClO + ClO and $2Cl + O_2$ products. The relative Cl:ClO product yields are 1.0:0.13 and 1.0:0.20 for ClOOCl photolysis at 248 and 308 nm, respectively. The data at 308 nm was more difficult to interpret because of extensive interference from Cl_2 and Cl_2O byproducts. The upper limit for the relative yield of the ClO + ClO channel was 0.19 at 248 nm and 0.31 at 308 nm. These results substantially confirm the current assumption but decrease somewhat the efficiency of the ClOOCl ozone-depleting catalytic cycle. At 248 nm, ClOOCl photolysis exhibited novel dissociation dynamics which appeared to depend on the symmetry of the excited state.

TABLE OF CONTENTS

Introduction

Significant ozone depletion has been occurring over Antarctica every spring since the late 1970's, as reported by Farman and coworkers in 1985.[1] Since then, considerable progress has been made in trying to understand the mechanisms of this ozone depletion. The current models link ozone depletion to catalytic cycles of active chlorine species.[2] Chlorine enters the stratosphere primarily as a component of chlorofluorocarbons (CFCs), which are stable in the troposphere but photodissociate in UV light once they get above the ozone layer.[3] These reactive chlorine species can catalytically destroy ozone through the mechanism

$$Cl + O_3 \rightarrow ClO + O_2$$

$$ClO + O \rightarrow Cl + O_2.$$

Most of the active chlorine species react to form more stable reservoir species such as hydrogen chloride and chlorine nitrate:[4]

$$Cl + CH_4 \rightarrow HCl + CH_3$$

$$ClO + NO_2 \rightarrow ClONO_2.$$

These reservoir species can photodissociate or undergo other gas phase reactions in the unperturbed stratosphere.

The Antarctic "ozone hole" develops in the perturbed stratosphere in the early polar spring. After the autumnal equinox, the polar regions fall into darkness and the solar UV heating ceases. Thermal radiation quickly cools the polar stratosphere to temperatures much lower than those of the mid latitudes. This cooling causes a pressure gradient which creates a polar vortex, effectively isolating the air over the pole from the rest of the stratosphere.[5] Temperatures fall low enough to form polar stratospheric clouds (PSCs) of nitric acid

hydrates, possibly nitric acid trihydrate,[6] and liquid aerosols consisting of ternary solutions of sulfuric acid, nitric acid, and water. The formation of these clouds dehumidifies and denitrifies the stratosphere, trapping most of the NO_x as nitric acid. Chlorine nitrate can react with water or adsorbed species such as HCl on the surface of the PSCs:[7]

$$ClONO2\ (g) + HCl\ (s) \rightarrow Cl_2\ (g) + HNO_3\ (s)$$

$$ClONO_2\ (g) + H_2O\ (s) \rightarrow HOCl\ (g) + HNO_3\ (s).$$

In this reaction scheme, the reservoir chlorine species are converted to active forms of chlorine which escape back into the stratosphere while the NO_x products are trapped in the PSCs as nitric acid. Therefore, the reactive chlorine species can not react with NO_x to re-form the reservoir species chlorine nitrate, and the chlorine is essentially all converted from inactive to active forms. The low temperature and high ClO concentrations during the polar night allow for three body recombination to form the dimer, ClOOCl.

When the polar night is over, photochemistry begins to occur and the active chlorine species can engage in photochemical catalytic ozone depleting cycles. In particular, ClOOCl photolysis is a key step in the catalytic ozone-depleting cycle[8]

$$ClO + ClO + M \rightarrow ClOOCl + M$$

$$ClOOCl + h\nu \rightarrow ClOO + Cl$$

$$ClOO + M \rightarrow Cl + O_2 + M$$

$$2[\ Cl + O_3 \rightarrow ClO + O_2\ ]$$

$$\text{net:}\quad 2O_3 \rightarrow 3O_2$$

which is thought to be responsible for a majority of Antarctic springtime ozone depletion. Current models assume that only Cl-atom products are formed from ClOOCl photolysis.

Photodissociation of ClOOCl to form ClO products would result in a null cycle, which would not deplete ozone. The branching ratio of ClOOCl photolysis into Cl and ClO products is critical in determining the effectiveness of this mechanism for destroying ozone.

ClOOCl has several possible photolysis channels:[9]

$$\begin{aligned} ClOOCl + h\nu &\rightarrow ClO + ClO \quad \Delta H_0^\circ = 17.1 \text{ kcal/mol} \\ &\rightarrow ClOO + Cl \qquad = 21.2 \text{ kcal/mol} \\ &\rightarrow 2Cl + O_2(^3\Sigma^-_g) \qquad = 25.9 \text{ kcal/mol} \\ &\rightarrow 2Cl + O_2(^1\Delta_g) \qquad = 48.4 \text{ kcal/mol} \\ &\rightarrow Cl + O + ClO \qquad = 80.5 \text{ kcal/mol} \\ &\rightarrow Cl_2 + O_2 \qquad = -31.2 \text{ kcal/mol.} \end{aligned}$$

Dissociation to produce solely Cl atom products requires that the stronger Cl–O bond break preferentially over the peroxy bond. The bond-selective nature of this dissociation has been rationalized by the argument that an $n \rightarrow \sigma^*$ transition localized on the ClO chromophore is excited.[8] Ab initio calculations[10] have confirmed the conjecture that the excitation involves the promotion of an electron to a ClO antibonding sigma orbital. However, a localized transition does not necessarily imply that preferential Cl–O bond fission should occur.

Two experiments have found that the quantum yield for Cl atom production from ClOOCl photolysis is unity or greater, but large uncertainties remain in both measurements. Cox and Hayman[11] examined steady-state photolysis of Cl_2O at 254 nm and modeled the disappearance of Cl_2O and the appearance of ClOOCl in a static photolysis cell held at 203-233K. They reported a yield of 3.8 ± 1.6, which is unphysically high. In a more direct study, Molina *et al.*[12] reported a Cl atom quantum yield of 1.03 ± 0.12 from ClOOCl photolysis at

308 nm in a flow cell. They used resonance fluorescence to detect Cl atoms and calibrated the Cl signals relative to Cl_2 photolysis. No ClO was inferred from titration with NO. Their value for the quantum yield depends on the ratio of the ClOOCl absorption cross section at 245 and 308 nm, for which they used a value of 22, which is larger than more recent literature values. If the cross section ratio of 13 from the 1997 JPL evaluation of photochemical data[13] were used, the corresponding Cl atom yield would be reduced to 0.6. The absorption spectrum has also been recently measured by Huder and DeMore,[14] who observed a smaller cross section in the long-wavelength tail. Using their 245/308 nm ratio of 18.7, Molina's quantum yield for Cl would become 0.88.

The mechanism in which the stronger bond is preferentially broken has been rationalized by the argument that the excitation of the $n \rightarrow \sigma^*$ transition localized on the ClO bond in $ClONO_2$ leads only to Cl + NO_3 products. Early gas cell experiments of the photodissociation of $ClONO_2$ only detected products from the Cl + NO_3 dissociation channel, despite the fact that the ClO + NO_2 channel lies 14 kcals/mol lower in energy.[15,16,17,18,19]

We examined $ClONO_2$ photolysis at 193, 248, and 308 nm in a molecular beam study, with direct detection of both Cl and ClO photoproducts, and found a substantial yield of ClO products.[20,21,22] Our results for 308 nm photolysis are detailed in Chapter 1. The observation of ClO products from $ClONO_2$ photolysis has since been corroborated in kinetics experiments by other groups.[23,24,25]

Our $ClONO_2$ results demonstrate how molecular beam techniques can complement the kinetics experiments by allowing direct detection of primary products and by giving

insights into the dissociation dynamics. The photodissociation dynamics of $ClONO_2$ cannot be described by a simple bond-selective ClO picture even when a localized transition is excited, and the photolysis of ClOOCl is therefore likely to be equally complex. Given the uncertainties in the previous ClOOCl photolysis experiments and the importance of the ClOOCl photolysis mechanism for polar stratospheric ozone depletion, we endeavored to design a molecular beam source for ClOOCl (described in Chapter 3). Our ClOOCl source was based on photolysis of Cl_2O to provide ClO, so a significant Cl_2O contamination was also present in the beam, requiring study of the Cl_2O photolysis as well. Also, because Cl_2O photolysis produces Cl + ClO in a 1:1 ratio, the results can be utilized to determine the relative detection efficiencies for Cl and ClO, which was necessary to determine the relative yields for Cl and ClO producing channels from ClOOCl photolysis. Chapter 2 examines the results from the Cl_2O photolysis experiments.

The results of our ClOOCl photolysis experiment are presented in Chapter 4. We did indeed observe both Cl and ClO products from ClOOCl photolysis, although Cl products did dominate. We obtained an upper limit for the relative yield of ClO products of 31% at 308 nm and 19% at 248nm. We also observed slow signal that could correspond to excited ClOOCl* which lives longer than a rotational period, which might be quenched under stratospheric conditions. Because of the extreme importance of the ClOOCl ozone depleting cycle, these new results should be included in models of the stratosphere.

References

1. J. C. Farman, B. G. Gardiner, and J. D. Shanklin, *Nature*, **315**, 207 (1985).

2. J. G. Anderson, D. W. Toohey, W. H. Brune, *Science*, **251**, 39 (1991).

3. M. B. McElroy and R. J. Salawitch, *Science*, **243**, 763 (1989).

4. M. R. Schoeberl and D. L Hartmann, *Science*, **251**, 46 (1991).

5. M. A. Tolbert and A. M. Middlebrook, *J. Geophys. Res.*, **95**, 22423 (1990).

6. M. A. Tolbert, M. J. Rossi, R. Malhotra, and D. M. Golden, *Science*, **238**, 1258 (1987).

7. M. J. Molina, T.-L. Tso, L. T. Molina, and F. C.-Y. Wang, *Science*, **238**, 1253 (1987).

8. L. T. Molina and M. J. Molina, *J. Phys. Chem.* **91**, 433 (1987).

9. Heat of formation for ClOOCl from S. L. Nickolaisen, R. R. Friedl, and S. P. Sander, *J. Phys. Chem.* **98**, 155 (1994).

10. J. F. Stanton and R. J. Bartlett, *J. Chem. Phys.*, **98**, 9335 (1993).

11. R. A. Cox and G. D. Hayman, *Nature* **332**, 796 (1988).

12. M. J. Molina, A. J. Colussi, L. T. Molina, R. N. Schindler, and T.-L. Tso, *Chem. Phys. Lett.* **173**, 310 (1990).

13. W. B. DeMore, S. P. Sander, D. M. Golden, R. F. Hampson, M. J. Kurylo, C. J. Howard, A. R. Ravishankara, C. E. Kolb, and M. J. Molina, *Chemical Kinetics and Photochemical Data for Use in Stratospheric Modeling, Evaluation Number 12*, JPL Publication 97-4, JPL (1997).

14. K. J. Huder and W. B. DeMore, *J. Phys. Chem.* **99**, 3905 (1995).

15. J. S. Chang, J. R. Barker, J. E. Davenport, and D. M. Golden, *Chem. Phys. Lett.*, **60**, 385 (1979).

16. S. M. Adler-Golden and J. R. Wiesenfeld, *Chem. Phys. Lett.*, **82**, 281 (1981).

17. W. J. Marinelli and H. S. Johnston, *Chem. Phys. Lett.*, **93**, 127 (1982).

18. J. J. Margitan, *J. Phys. Chem.*, **87**, 674 (1983).

19. J. P. Burrows, G. S. Tyndall, and G. K. Moortgat, *J. Phys. Chem.*, **92**, 4340 (1988).

20. T. K. Minton, C. M. Nelson, T. A. Moore, and M. Okumura, *Science*, **258**, 1342 (1992).

21. C. M. Nelson, T. A. Moore, M. Okumura, and T. K. Minton, *Chem. Phys.*, **207**, 287 (1996).

22. T. A. Moore, M. Okumura, M. Tagawa, and T. K. Minton, *Faraday Discuss. Chem. Soc.*, **100**, 295 (1995).

23. A. R. Ravishankara, *Faraday Disc. Chem. Soc.*, **100**, 333 (1995); J. B. Burkholder, *Abs. Pap. Chem. Soc.*, **210**, 51 (1995).

24. G. S. Tyndall, C. S. Kegley-Owen, J. J. Orlando, and J. G. Calvert, *J. Chem. Soc., Faraday Trans.* **93**, 2675 (1997).

25. L. Goldfarb, A.-M. Schmoltner, M. K. Gilles, J. B. Burkholder, and A. R. Ravishankara, *J. Phys. Chem. A,* **101**, 6658 (1997); R. J. Yokelson, J. B. Burkholder, R. W. Fox, and A. R. Ravishankara, *J. Phys. Chem. A*, **101**, 6667 (1997).

Chapter 1.*

Dissociation Dynamics of $ClONO_2$ and Relative Cl and ClO Product Yields following Photoexcitation at 308 nm

Chlorine nitrate photolysis at 308 nm was investigated with a molecular beam technique. Two primary decomposition pathways, leading to Cl + NO_3 and ClO + NO_2, were observed. The branching ratio between these two respective channels was determined to be 0.67±0.06:0.33±0.06. This ratio is an upper limit, because some of the ClO photoproducts may have undergone secondary photodissociation. The angular distributions of the photoproducts with respect to the direction of polarization of the exciting light were anisotropic. The anisotropy parameters were $\beta = 0.5 \pm 0.2$ for the Cl + NO_3 channel and $\beta = 1.1 \pm 0.2$ for the ClO + NO_2 channel, indicating that dissociation of $ClONO_2$ by either pathway occurs within a rotational period. Weak signal at mass-to-charge ratios of 35 and 51, arising from products with laboratory velocities close to the beam velocity, was observed. While this signal could result from statistical dissociation channels with a total relative yield of 0.07 or less, it is more likely attributable to products from ClO secondary photodissociation or from dissociation of clusters.

---

* This chapter has been published. The reference is: Teresa A. Moore, Mitchio Okumura, Masahito Tagawa, and Timothy K. Minton, *Faraday Discuss. Chem. Soc.* **100**, 295 (1995).

Introduction

Chlorine nitrate ($ClONO_2$) plays a key role in stratospheric chemistry as a reservoir for reactive chlorine and nitrogen oxides.[1,2] Photolysis is a major decomposition process for $ClONO_2$,[3] and has been the subject of many studies.[4,5,6,7,8,9,10,11,12] At wavelengths less than 250 nm, photodecomposition follows two primary channels:[9]

$$ClONO_2 + h\nu \rightarrow ClO + NO_2 \qquad \Delta H = 26 \text{ kcal/mol} \qquad (1)$$

$$\rightarrow Cl + NO_3 \qquad \Delta H = 40 \text{ kcal/mol} \qquad (2)$$

Channel (2) can lead directly to loss of two ozone molecules via the following reactions:[13]

$$NO_3 + h\nu \rightarrow NO + O_2 \qquad (3a)$$

$$NO + O_3 \rightarrow NO_2 + O_2 \qquad (3b)$$

$$Cl + O_3 \rightarrow ClO + O_2. \qquad (3c)$$

Toumi *et al.* have recently shown in model studies that this catalytic cycle[13] including steps (2) and (3a-c) becomes the dominant ozone loss mechanism in the latter stages of springtime Arctic ozone depletion.[14] In this model, the extent of ozone loss depends upon the quantum yield of channel (2), especially at λ>300 nm. Toumi *et al.* used the value of 0.9 for this quantum yield, which was recommended by the 1992 JPL evaluation of kinetic data.[15] However, results from our laboratory at shorter wavelengths (193 and 248 nm) showed the $Cl + NO_3$ product yield to be significantly lower,[9] a conclusion later corroborated by other groups.[10,11,12] A lower yield at longer wavelengths would diminish the predicted contribution of the $ClONO_2$ catalytic cycle to Arctic ozone depletion and reduce the predicted magnitude and duration of the ozone loss episode.

Sander and co-workers have recently obtained evidence from flow tube studies that

excited $ClONO_2$ formed by wavelengths longer than 300 nm lives long enough to be quenched under stratospheric conditions.[12] Quenching of $ClONO_2$ photolysis would profoundly affect the partitioning of the Cl and NO_x budgets and would largely eliminate the $ClONO_2$ catalytic cycle as a candidate loss mechanism for stratospheric ozone. In their experiment, Sander and co-workers observed products from channels (1) and (2) when $ClONO_2$ was excited by a broadband Xe lamp; however, at wavelengths longer than 300 nm they found that the total quantum yield was significantly quenched at N_2 buffer gas pressures above 50 Torr. Under their conditions (approximately 50 Torr and 200 K), the mean time between gas-kinetic collisions is 3 ns, so an excited molecule must have a lifetime on the order of nanoseconds or longer to be quenched rather than dissociated.

Previous flow tube studies revealed no direct evidence of a relatively long-lived state following UV excitation of $ClONO_2$.[4,8,10,11] However, recent *ab initio* calculations by Graña *et al.* do predict the existence of a metastable state.[16] These authors performed high level configuration interaction (CI) and coupled-cluster calculations to predict the vertical excitation energies and oscillator strengths for transitions to eight singlet and eight triplet states of $ClONO_2$ between 400 nm and 160 nm. They also found a bound, metastable triplet state, with a nonplanar geometry, lying 62 kcal/mol above the ground state equilibrium configuration. If $ClONO_2$ were formed in this state either by direct excitation or by relaxation from an initially prepared state, the excited $ClONO_2$ could conceivably persist for nanoseconds or longer.

The fate of chlorine nitrate excited at wavelengths greater than 300 nm has important implications for stratospheric ozone depletion. To address questions concerning the

dissociation pathways and the possibility of a long-lived excited state, we extended our previous photodissociation studies of $ClONO_2$ to a longer wavelength. With the use of molecular beam methods, we can directly detect photoproducts, measure their relative yields, and determine angular and translational energy distributions in the absence of collisions. Furthermore, we can infer the timescale for dissociation from the anisotropy of the product angular distribution. In our earlier experiments, we observed comparable yields of Cl and ClO products from $ClONO_2$ photolysis at both 193 and 248 nm.[9] We calibrated the relative detector sensitivity for Cl and ClO by performing an experiment on Cl_2O photolysis at 308 nm and found Cl:ClO branching ratios of 0.57:0.43 and 0.67:0.33 for $ClONO_2$ photolysis at 248 and 193 nm, respectively. Furthermore, we observed anisotropic angular distributions for the two channels and inferred that the dissociation is prompt, occurring within a rotational period (τ_{rot} ~ 9 ps at the rotational temperature of the beam). Here we present results from a similar investigation of $ClONO_2$ photolysis at 308 nm.

Experiment

The molecular beams apparatus and methods have been described in detail elsewhere.[9,17] Briefly, a molecular beam was crossed with a laser beam in a low pressure region at the center of rotation of a rotatable mass spectrometer detector[18] (see fig. 1). Collisionless conditions allowed for detection of primary dissociation products recoiling away from the beam direction. Center-of-mass (c.m.) product translational energy and angular distributions were derived from the arrival time distributions of the neutral photoproducts over a calibrated flight length as a function of detector angle away from the beam direction.

Continuous molecular beams were formed by passing H_2 over $ClONO_2$ at −50° C or He over Cl_2O at −74° C and expanding the mixture through a 0.1 mm diameter quartz nozzle maintained at +5° C. $ClONO_2$ was seeded in hydrogen rather than helium in order to obtain a faster beam, which enhanced the signal through kinematic focusing. Stagnation pressures of the gas mixtures were 300 Torr for the $ClONO_2$ experiment and 200 Torr for the Cl_2O experiment. The $ClONO_2$ data was obtained in two sets, with corresponding beam velocities 1350 m/s and 1580 m/s, as determined by beam time-of-flight (TOF) distributions taken with the aid of a chopper wheel. The Cl_2O beam velocity (1480 m/s) was determined by examining the arrival time of the laser-induced depletion of signal at a mass-to-charge ratio (*m/e)* of 37 with the detector directly viewing the molecular beam.[19,20]

Cl_2O was synthesized by oxidation of Cl_2 on HgO and was purified by pumping on the sample at −118° C (ethanol slush bath).[21] $ClONO_2$ was synthesized from the reaction of Cl_2O with N_2O_5 and purified first by cannulation and then by pumping on the sample at −95° C (methanol slush bath).[22] Purity was checked by a survey of beam TOF distributions at all masses where signal was observed. The only impurities in either molecular beam could be attributed to dimers and/or clusters. A small peak in the beam TOF at *m/e* = 143 ($ClONO_2 \cdot NO_2^+$) indicated that clusters were present in the $ClONO_2$ beam; however, the product signals observed were insensitive to the relative magnitudes of the cluster signals.

The molecular beam was crossed in the interaction region with a laser beam at 308 nm from a Lambda Physik EMG103 excimer laser operating at 200 Hz. The laser beam was randomly polarized in a plane perpendicular to the scattering plane and parallel to the molecular beam axis. The laser beam was focused to a spot size of 2.5 mm × 2.5 mm, where

it intersected the molecular beam. The laser pulse energy used for the $ClONO_2$ experiment was 170 mJ. The consequent laser fluence was high enough that secondary photodissociation of the primary ClO products was a concern; however, the low absorption cross section[15] of $ClONO_2$ at 308 nm ($\sigma = 1.6\times10^{-20}$ cm^2) required the use of relatively high laser fluences to make the primary photoproduct signals observable. For the Cl_2O experiment, a pulse energy of 126 mJ was used for data collection at $m/e = 51$, and the laser was attenuated with a stack of quartz plates to 36 mJ/pulse for data collection at $m/e = 35$ in order to minimize secondary photodissociation of the ClO product. TOF distributions were collected at $m/e = 35(Cl^+)$, $51(ClO^+)$, $30(NO^+)$, $46(NO_2^+)$, $16(O^+)$, and $81(ClONO^+)$, and angular distributions of product signals detected at $m/e = 35$, 51, and 46 were measured.

Results and Analysis

Analysis of TOF and angular distributions was carried out by a forward convolution technique.[20,23,24,25] For each channel, trial c.m. translational energy $P(E_T)$ and angular $w(\theta)$ distributions were transformed to the laboratory frame of reference to obtain a predicted number density TOF distribution $N(t)$ that could be compared with the experimental data. The $P(E_T)$ and $w(\theta)$ distributions were then adjusted iteratively until the predicted TOF distributions agreed with the observed distributions at all angles.

The data were similar to our earlier results at 193 and 248 nm.[9] A single peak was prominent at $m/e = 51$ (see figs. 2 and 3), which we assigned to ClO from the $ClO + NO_2$ channel by analogy with our previous results. The $m/e = 35$ TOF distribution contained two main components, the slower of which matched the peak at $m/e = 51$, indicating that it must

arise from fragmentation of ClO to Cl^+ in the ionizer.[26] We assigned the fast component at $m/e = 35$ to Cl from the Cl + NO_3 channel. We used the TOF spectra taken at $m/e = 35$ and 51 to derive the c.m. translational energy distributions for the two dissociation channels (fig. 4).

We verified our assignments of the two dissociation channels by using the $P(E_T)$ and $w(\theta)$ distributions derived from the ClO^+ and Cl^+ data to predict the TOF distributions for the respective counterfragments, NO_2 and NO_3 (fig. 5). No signal was observed at $m/e = 62$, the NO_3 parent mass, but the TOF spectrum collected at $m/e = 46$ (NO_2^+) was fitted well with the distribution predicted for the NO_3 fragment by the $P(E_T)$ and $w(\theta)$ distributions for the Cl + NO_3 channel. Apparently, the NO_2^+ signal comes not from NO_2, but from NO_3 which fragments to NO_2^+ in the ionizer. The bimodal TOF distribution at $m/e = 30$ (NO^+) could not be fit from the $P(E_T)$ and $w(\theta)$ distributions for either the Cl + NO_3 or ClO + NO_2 channels alone, but it could be fit with a sum of contributions from the predicted TOF distributions for both NO_3 and NO_2 fragments. Hence, both NO_3 and NO_2 photofragments lead to NO^+ in the ionizer (similar ionizer fragmentation patterns were observed in our previous study.)[9] The ability to fit both counterfragments of each dissociation channel with the use of the same $P(E_T)$ and $w(\theta)$ distributions thus confirms our original assignments of the two primary photodissociation channels.

Laboratory angular distributions of ClO, Cl, and NO_3 were obtained from the integrated TOF data detected at $m/e = 51$, 35, and 46, respectively. At $m/e = 51$ and 46, where the TOF distributions corresponded only to a single photoproduct, the signal for each detector angle was simply integrated. The Cl angular distribution was extracted from the $m/e = 35$ TOF

distributions by integrating the calculated TOF distributions for the Cl^+ signal arising from the $Cl + NO_3$ channel (obtained from the optimized $P(E_T)$ and $w(\theta)$ distributions).

The c.m. angular distribution must have the form $w(\theta) \propto 1 + \beta P_2(\cos\theta)$, where P_2 denotes the second-order Legendre polynomial and θ the angle between the electric field vector of the excitation photon and the product recoil direction in the c.m. reference frame.[23,27] β is the anisotropy parameter and must lie in the range $-1 \leq \beta \leq 2$. We obtained $\beta = 1.1 \pm 0.2$ for the $ClO + NO_2$ channel from the ClO angular distribution and $\beta = 0.5 \pm 0.2$ for the $Cl + NO_3$ channel from both the Cl and NO_3 angular distributions. The fits used to determine the anisotropy parameters are shown in fig. 6.

The broad, slow signal at *m/e* = 35 may be explained by a number of possible mechanisms: spontaneous secondary dissociation, dissociation of clusters formed in the beam expansion, secondary photodissociation of primary ClO photoproducts, or a third primary channel leading to products with low c.m. translational energies. We can rule out spontaneous secondary dissociation because the $P(E_T)$ distribution (fig. 4B) implies that no ClO photoproducts have enough internal energy to dissociate. Clusters were present in the beam, but we expect the contribution from dissociation of clusters to the *m/e* = 35 TOF to be small because changes in the stagnation pressure did not significantly alter the magnitude of the slow signal relative to the fast peaks. The most likely explanation for the tail at *m/e* = 35 is secondary photodissociation of ClO. The ClO absorption cross section is larger than that of $ClONO_2$ at 308 nm, and at the high laser fluences used, some secondary photodissociation of ClO is expected. However, we could not model the secondary photodissociation, because the signal-to-noise ratio was too low. We therefore could not

eliminate the possibility of a third primary dissociation channel forming products with low translational energies.

Direct dissociation on a triplet surface to ClONO + O(^3P) could conceivably contribute to a slow signal at *m/e* = 51 and 35 through fragmentation to ClO^+ or Cl^+ in the ionizer. ClONO might also fragment to NO_2^+ or NO^+ and give rise to a slow signal at *m/e* = 46 and 30. The energy available for translation after breaking the O-N bond is only about 26 kcal/mol, and the ClONO fragment will recoil slowly from the relatively light O-atom counterfragment. Therefore, the minimum flight time possible at a detector angle of 30° is 133 μs (not including ion flight time), and any signal present should manifest itself as a peak in the slow tail of the product TOF distributions. The only TOF distributions which showed an obvious hint of slow signal were the Cl^+ distributions. If all slow signal at *m/e* = 35 not assigned to the dominant channels did come from ClONO, then the ClONO + O yield would be ~ 0.07. Even this small yield is suspect because 1) no photofragment signal was detected at the ClONO parent mass (*m/e* = 81), 2) no obvious slow signal was seen at other masses, and 3) ClONO can only be formed by a spin-forbidden process at an excitation wavelength of 308 nm.

Statistical dissociation of $ClONO_2$ could also lead to products with low translational energies. The c.m. translational energy distributions for products of a statistical dissociation process have a maximum near zero and decay rapidly with E_T; therefore, the observed signal would have low c.m. velocities. At the smallest detector angle used here, 15°, we can detect Cl products from the Cl + NO_3 channel with total c.m. translational energies $E_T \geq 0.7$ kcal/mol and ClO products from the ClO + NO_2 channel with $E_T \geq 1.4$ kcal/mol. The experiment

should therefore be sensitive to statistical dissociation channels with available energies of a few kcal/mol above threshold.

We can estimate the maximum possible yield from statistical dissociation by fitting the slow component to a statistical model, but the modeling will depend upon the final dissociation channel. Several dissociation channels are energetically available to $ClONO_2$ with 92.8 kcal/mol of internal energy (i.e., the photon energy of 308 nm light). While statistical dissociation of $ClONO_2$ on the ground electronic state potential energy surface will lead predominantly to ClO and NO_2 in their ground electronic states, an excited state of $ClONO_2$ may correlate to a higher energy asymptote and dissociate to form excited state products. The statistical decay rate will be slower and the translational energy release smaller for channels with lower available energy. We therefore considered dissociation via two excited state channels which consume most of the 308 nm photon energy:

$$ClONO_2 \rightarrow Cl\,(^2P) + NO_3(\tilde{A}\,^2E') \qquad \Delta H = 83 \text{ kcal/mol} \qquad (4)$$

$$\rightarrow ClO\,(a\,^4\Sigma^-) + NO_2(X\,^2A_1) \qquad \Delta H \approx 77 \text{ kcal/mol} \qquad (5)$$

We proposed the existence of a bound ClO quartet state in a previous study of photoproducts from Cl_2O dissociation,[17] and this hypothesis was confirmed theoretically by Langhoff, who computed the energy and geometry of this state.[28] In order to estimate the maximum possible yield of these channels, we first performed RRKM calculations to obtain a c.m. translational energy distribution for each channel.[29] We then compared the slow component of the TOF distribution at the relevant *m/e* to the TOF distribution predicted by the RRKM $P(E_T)$ distribution. We obtained upper limits on the yields by assuming that the signal in the slow components arose solely from statistical dissociation (see fig. 2 and 3). We estimated a yield

of 0.05 for dissociation to ground state ClO and NO_2 products, based on the signal at m/e = 51. We then determined the ClO contribution to the slow component at m/e = 35 by using the same ClO ionizer fragmentation pattern observed for the main peaks. We assumed that the remainder of the slow signal at m/e = 35 corresponded to Cl products from statistical decay to ground state Cl and NO_3 products and obtained a maximum yield of 0.02 for this channel. Thus, the maximum total relative yield for statistical dissociation to ground state products via either channel is 0.07. For the excited state products, we found a maximum possible total yield of 0.03 based on the data collected at 15° (fig. 3). However, the RRKM $P(E_T)$ distributions for the excited state product channels predict negligible contributions to the slow signal at larger detector angles, because the $P(E_T)$ distributions fall off quickly with E_T. Our inability to achieve a consistent fit of all the data under the assumption of excited state products makes it highly unlikely that channels (4) or (5) play any role in $ClONO_2$ photodissociation at 308 nm. In any case, these yields are upper limits because it is improbable that all of the slow signal arises from statistical dissociation. Secondary photodissociation, observed unambiguously in our previous experiments at shorter wavelengths, may even account for all of this broad underlying signal at m/e = 35. Regardless of the actual product channel assumed, we conclude that any statistical dissociation process is at most a minor channel.

We performed a photodissociation experiment on Cl_2O at 308 nm in order to calibrate the relative detection efficiency for Cl and ClO and thereby determine the branching ratio between the two channels in the photodissociation of $ClONO_2$. The Cl_2O data (not shown) were analogous to previous observations and were fit with the same $P(E_T)$ and $w(\theta)$

distributions as before.[17] The relative yields for the two photodissociation channels of $ClONO_2$ following excitation at 308 nm were determined to be 0.67±0.06 for the $Cl + NO_3$ channel and 0.33±0.06 for the $ClO + NO_2$ channel. Our results may underestimate the ClO yield because the primary ClO product has a significant probability of undergoing secondary photodissociation during the laser pulse; therefore, the Cl:ClO branching ratio of 0.67:0.33 is an upper limit.

Discussion

Excited-State Lifetime

The anisotropy of the angular distributions allows us to determine whether the main products associated with the dominant peaks were formed by prompt dissociation, i.e., occurring in less than a rotational period, τ_{rot}. If the excited molecule has time to rotate before dissociating, then the molecule will change orientation, causing the angular distribution to become more isotropic. Rotational averaging thus reduces the absolute magnitude of β, though not necessarily exactly to zero. We can estimate upper limits on the minimum values of β for the two channels with the use of expressions that Yang and Bersohn have derived for calculating β when the dissociating molecule is long-lived.[30] We assume 1) the transition dipole moments are parallel to the axes of the respective dissociating bonds, 2) the geometry of $ClONO_2$ does not change on going to the dissociative state, and 3) $ClONO_2$ can be approximated as a symmetric top ($\kappa = -.89$). We find that the upper limits on the anisotropy parameters for a long-lived state of $ClONO_2$ are $\beta = 0.07$ for dissociation to $ClO + NO_2$ and $\beta = 0.13$ for dissociation to $Cl + NO_3$. Effects such as vibrational averaging and breakdown

of the symmetric top assumption will reduce β further. The calculated values lie below the uncertainties in the anisotropy parameters for the two main channels, $\beta = 1.1 \pm 0.2$ for ClO + NO_2 and $\beta = 0.5 \pm 0.2$ for Cl + NO_3. The observed anisotropies thus indicate that dissociation via either channel occurs within τ_{rot}. Assuming a typical rotational temperature of ~50 K in the molecular beam, τ_{rot} would be approximately 9 ps. We conclude that the main products observed in this experiment are formed in less than ~9 ps, which is shorter than the mean collision time (~5 ns) under stratospheric conditions, and thus cannot arise from a long-lived excited state.

We could not rule out assignment of the slow signal at *m/e* = 35 and 51 to a third dissociation channel, such as statistical decomposition, with low c.m. translational energies; however, the contribution from such a process will be small. Dissociation via a statistical process should be dominated by fission of the weakest bond, making ground state ClO and NO_2 the most likely major products if $ClONO_2$ dissociates on its ground electronic state surface. We derived an upper limit of 0.05 for the yield of this channel from the *m/e* = 51 data (figs. 1 and 2). However, the RRKM lifetime for ground state $ClONO_2$ with 92.8 kcal/mol of internal energy will be on the subpicosecond timescale. To account for a nanosecond lifetime, we would have to invoke a rate limiting step, such as internal conversion or intersystem crossing from an initially prepared state. Statistical dissociation of metastable $ClONO_2$ could occur on a nanosecond timescale only if the available energy is small (on the order of 10 kcal/mol or less for $ClONO_2$), e.g. dissociation to a channel near threshold leading to excited state products. Dissociation to channels (4) and (5) may have lifetimes as long as nanoseconds, but we did not have enough information to calculate accurate decay rates for

processes so close to threshold. The bound triplet state predicted by Graña *et al.* is a candidate for this metastable state, but there is no information on its possible decomposition pathways. Although the translational energy release would be even lower than for dissociation to ground state products, our experiment still places an upper limit of 0.03 on the total relative yield for the plausible product channels (4) and (5) near 93 kcal/mol (see fig. 2). Thus, the slow product signal could account for only a small fraction of the total observed products; furthermore, all of these estimates are upper bounds, because secondary photodissociation of ClO will likely contribute substantially to the observed slow signal at *m/e* = 35.

Given our beam velocity, laser spot size, and the solid angle viewed by the detector, we can only detect fragments from excited $ClONO_2$ molecules that dissociate within 2.5 μs. Our sensitivity allows us to detect molecules with dissociation lifetimes $\tau \leq 10$ μs; metastable states which live longer would go unobserved in our experiment. Such lifetimes are significantly longer than typical mean collision times of 1-10 ns in flow tube experiments, where unit quantum yields are observed for $ClONO_2$ photolysis at buffer gas pressures of 5-10 Torr.[7,10,11] If dissociation occurs through a state with a lifetime of 10 μs or longer, then the metastable $ClONO_2$ must undergo $> 10^3$ gas kinetic collisions without being quenched at these pressures. Thus, the molecular beam and flow tube studies are together consistent with a long-lived metastable only if that state has a lifetime $\tau > 10$ μs and is very inefficiently quenched.

Our results would also be consistent with the experiment of Sander and co-workers if a metastable state of $ClONO_2$ is prepared by excitation at wavelengths longer than 308 nm.

Sander and co-workers photolyzed chlorine nitrate with a broad band, filtered Xe lamp whose output extended from *ca.* 300 nm to visible wavelengths.[12] Such long wavelength radiation would be absorbed in the 370-380 nm region, where Molina and Molina[3] observed a weak absorption band that was distinct from absorption bands deeper in the ultraviolet. This band lies close to 362 nm, the wavelength that Graña *et al.* predict for the lowest vertical triplet excitation.[16] This state is predicted to be directly dissociative, but may lead by curve crossing to the bound metastable state. Additional experiments at longer wavelengths are necessary to examine the possibility that this band involves a transition leading to formation of a long-lived state; however, the small absorption cross-section, nine times lower at 362 nm than at 308 nm, will make these measurements difficult.

Product Yields

We found channels (1) and (2) to dominate $ClONO_2$ photochemistry at 308 nm; the total yield of all other possible channels must be ≤ 0.07. The Cl/ClO product branching ratio was determined to be 0.67/0.33. The relative yield of 0.33 for ClO is a lower limit, because some of the ClO products may have undergone secondary photodissociation. This branching ratio does not agree with a number of earlier studies done at $\lambda > 300$ nm by Smith *et al.*,[4] Chang *et al.*,[13] Knauth and Schindler,[6] and Margitan.[7] The last three experiments all found near unit quantum yields of Cl atoms and failed to detect ClO products, even for photolysis at wavelengths less than 300 nm. The JPL evaluation,[15] which recommends quantum yields of 0.9 ± 0.1 for the $Cl + NO_3$ channel and 0.0 for the $ClO + NO_2$ channel, was based primarily on the results of the most direct study, that of Margitan. However, our results are more

consistent with recent unpublished flow tube studies[10,11,12] which detect both channels with similar relative yields.

The decreased yield for dissociation of the weakest bond, ClO–NO_2, in the present study relative to our earlier results suggests that photons at 308 nm excite transitions favoring fission of the Cl–O bond. Graña *et al.* calculate that the lowest singlet state $1^1A''$ possesses ClO $n \rightarrow \sigma^*$ character and has a vertical excitation wavelength of 284 nm with an oscillator strength approximately 1% of the band strength at 190 nm. The next highest state, the $2^1A''$ state, is predicted to be a $\pi \rightarrow \pi^*$ transition localized on the NO_2 group at 252 nm but with zero oscillator strength. While excitation to the $1^1A''$ state could explain the higher Cl yield at 308 nm relative to 248 nm, it is not consistent with the observed angular distributions which are indicative of a parallel transition. To excite a state of A'' symmetry, the transition moment must be out-of-plane and perpendicular to either dissociation coordinate in the ground state geometry. A perpendicular transition would result in a negative value of β unless the dissociating bond rotates significantly out of plane prior to dissociation. There are many states of both symmetries at slightly higher energies, and excitation at 308 nm could instead readily excite the Franck-Condon wing of a dissociative A' state. It is possible that there are simultaneous parallel and perpendicular transitions to multiple excited states or a transition to a mixed state with the dipole transition moment aligned midway between the two bond axes, making the net β small and positive. The complexity of the $ClONO_2$ excited state manifold suggests that photodissociation of $ClONO_2$ cannot be described by a simple bond-selective picture but rather that curve crossings and the dynamics of nuclear motion following excitation may largely determine the final product branching ratio.

The dominance of direct dissociation processes at excitation wavelengths as long as 308 nm implies that it is important to consider a catalytic cycle involving $ClONO_2$ photolysis in models of stratospheric ozone depletion. However, our finding of a significant yield for the $ClO + NO_2$ channel will lead to a decrease in the ozone-depleting efficiency of the $ClONO_2$ cycle from what has been predicted. At mid-latitudes, where this cycle contributes only 3-5% of the ozone loss,[2] the new product yield ratio will not affect the predicted ozone depletion. The impact will be greater on model predictions of ozone loss in the Arctic polar spring as well as in the Antarctic collar region, where Toumi *et al.* have shown that this cycle plays a major role.[14]

Acknowledgments

The experiments were performed at the Jet Propulsion Laboratory, California Institute of Technology, under contract with the National Aeronautics and Space Administration (NASA), and were supported by the NASA Upper Atmosphere Research Program under contract NAGW-3893 and by E. I. duPont de Nemours and Co., Inc. We acknowledge support for T.A.M. from a NASA Graduate Research Fellowship and for M.T. from the Murata Overseas Scholarship Foundation.

References

1. F. S. Rowland, J. E. Spencer, and M. J. Molina, *J. Phys. Chem.*, 1976, **80**, 2711; *ibid.*, 2713.

2. P. O. Wennberg, R. C. Cohen, R. M. Stimpfle, J. P. Koplow, J. G. Anderson, R. J. Salawitch, D. W. Fahey, E. L. Woodbridge, E. R. Keim, R. S. Gao, C. R. Webster, R. D. May, D. W. Toohey, L. M. Avallone, M. H. Proffitt, M. Loewenstein, J. R. Podolske, K. R. Chan, and S. C. Wofsy, *Science*, 1994, **266**, 398.

3. M. Molina and L. T. Molina, *J. Photochem.*, 1979, **11**, 139.

4. W. S. Smith, C. C. Chou, and F. S. Rowland, *Geophys. Res. Lett.*, 1977, **4**, 517.

5. S. M. Adler-Golden and J. R. Wiesenfeld, *Chem. Phys. Lett.*, 1981, **82**, 281.

6. H. D. Knauth and R. N. Schindler, *Z. Naturfor.*, 1983, **38A**, 893.

7. J. J. Margitan, *J. Phys. Chem.*, 1983, **87**, 674.

8. J. P. Burrows, G. S. Tyndall, and G. K. Moortgat, *J. Phys. Chem.*, 1988, **92**, 4340. These authors proposed a hypothetical metastable state of $ClONO_2$ excited at 254 nm, because the $Cl + NO_3$ products could not account for all the photolysis yield. It is likely that the missing product is in the $ClO + NO_2$ channel, which they did not detect.

9. T. K. Minton, C. M. Nelson, T. A. Moore, and M. Okumura, *Science*, 1992, **258**, 1342.

10. A. R. Ravishankara, private communication.

11. J. J. Orlando, C. S. Kegley-Owen, G. S. Tyndall, and J. G. Calvert, *XXIst Informal Conference on Photochemistry,* Toronto, Ontario, Canada, May 1994.

12. S. L. Nickolaisen, S. P. Sander, R. R. Friedl, L. Jaegle, M. A. Allen, Y. L. Yung, C. R. Webster, R. D. May, G. C. Toon, B. Sen, and J.-F. Blavier, *XXIst Informal Conference on Photochemistry,* Toronto, Ontario, Canada, May 1994.

13. J. S. Chang, J. R. Barker, J. E. Davenport, and D. M. Golden, *Chem. Phys. Lett.*, 1979, **60**, 385.

14. R. Toumi, R. L. Jones, and J. A. Pyle, *Nature*, 1993, **365**, 37.

15. W. B. DeMore, S. P. Sander, D. M. Golden, R. F. Hampson, M. J. Kurylo, C. J. Howard, A. R. Ravishankara, C. E. Kolb, and M. J. Molina, *Chemical Kinetics and Photochemical Data for Use in Stratospheric Modeling, JPL Publication 92-20*, 1992.

16. A. Graña, T. J. Lee, and M. Head-Gordon, *J. Phys. Chem.*, 1995, **99**, 3493.

17. C. M. Nelson, T. A. Moore, M. Okumura, and T. K. Minton, *J. Chem. Phys.*, 1994, **100**, 8055.

18. Y. T. Lee, J. D. McDonald, P. R. LeBreton, and D. R. Herschbach, *Rev. Sci. Instrum.*, 1969, **40**, 1402.

19. T. K. Minton, P. Felder, R. J. Brudzynski, and Y. T. Lee, *J. Chem. Phys.*, 1984, **81**, 1759.

20. P. Felder, *Habilitationsschrift*, University of Zürich, Switzerland, 1993.

21. G. H. Cady, *Inorg. Synth.*, 1957, **5**, 156.

22. M. Schmeisser, *Inorg. Synth.*, 1967, **9**, 127.

23. G. E. Busch and K. R. Wilson, *J. Chem. Phys.*, 1972, **56**, 3626; *ibid.*, 3638.

24. T. K. Minton, G. M. Nathanson, and Y. T. Lee, *J. Chem. Phys.*, 1987, **86**, 1991.

25. A. M. Wodtke and Y. T. Lee, *J. Phys. Chem.*, 1985, **89**, 4744.

26. The 4 μs difference in peak positions of the ClO signals detected at $m/e = 51$ and $m/e = 35$ reflects the mass dependence on the ion flight time from the ionizer of the mass spectrometer to the Daly-type ion counter. The ion flight time was determined to be $t = 3.5\ (m/e)^{1/2}$ μs.

27. R. N. Zare, *Mol. Photochem.*, 1972, **4**, 1.

28. S. R. Langhoff, unpublished results.

29. P. J. Robinson and J. A. Holbrook, *Unimolecular Reactions*, Wiley-Interscience, 1972.

30. S.-C. Yang and R. Bersohn, *J. Chem. Phys.*, 1974, **61**, 4400.

Figure Captions

Fig. 1. Schematic diagram of the molecular beam photodissociation experiment. The numbers correspond to pressures in Torr for the various regions. Θ is the detector angle.

Fig. 2. TOF distributions *N(t)* collected at a detector angle of 30° for (**A**) Cl^+ and (**B**) ClO^+ fragments. The molecular beam velocity was 1580 m/s. Fits to the dominant product channels, Cl + NO_3 and ClO + NO_2, are calculated with optimized center-of-mass translational energy $P(E_T)$ and angular $w(\theta)$ distributions (see figs. 4 and 6). The long-dashed line at slow times in (**B**) is a hypothetical fit based on the assumption that ground electronic state ClO and NO_2 products are formed by a statistical (RRKM) process. The long-dashed line at slow times in (**A**) is also a hypothetical fit based on statistical (RRKM) decay that leads to ground electronic state products. This "fit" includes contributions to a Cl^+ signal from both ClO + NO_2 and Cl + NO_3 channels. The upper limit on the total yield from both channels is determined from the fits in (**A**) to be 0.07.

Fig. 3. TOF distributions collected at a detector angle of 15° for (**A**) Cl^+ and (**B**) ClO^+ fragments. The molecular beam velocity was 1350 m/s. Fits to the main peaks are calculated with the same $P(E_T)$ and $w(\theta)$ distributions used to achieve the analogous fits in fig. 2. Two kinds of hypothetical fits are shown at longer flight times. One is based on the assumption of statistical decay to ground state products, and the other is based on the assumption of statistical decay to excited state products. As in fig. 2, the hypothetical fits at m/e = 35 include dissociation along both ClO + NO_2 and Cl + NO_3 product channels. Statistical decay

to excited state products via channels (4) and (5) leads to low product translational energies and thus a smaller possible contribution to the signal than dissociation to ground state products. The upper limit on the total yield of ground state products is 0.07, while the upper limit on the total yield of excited state products at this detector angle is 0.03. The total yield of all slow products cannot exceed 0.07. At detector angles of 30° and larger, the excited state products cannot be detected because their center-of-mass velocities are too low.

Fig. 4. Optimized center-of-mass translational energy $P(E_T)$ distributions for the two dominant photodissociation channels. For the $Cl + NO_3$ channel, $\langle E_T \rangle$ = 32.9 kcal/mol, which is 62% of E_{avail}. For the $ClO + NO_2$ channel, $\langle E_T \rangle$ = 26.0 kcal/mol, which is 39% of E_{avail}.

Fig. 5. TOF distributions collected at 30° for (**A**) NO_2^+ and (**B**) NO^+ fragments. The peak in (**A**) is fit with the $P(E_T)$ and $w(\theta)$ distributions for the $Cl + NO_3$ channel under the assumption that all the signal at m/e = 46 arises from NO_3 which fragments to NO_2^+ in the ionizer. The bimodal distribution in (**B**) apparently contains signal from both NO_3 and NO_2 products which fragment to NO^+ in the ionizer; this distribution is fit with two components corresponding to both $Cl + NO_3$ and $ClO + NO_2$ channels.

Fig. 6. Semi-logarithm plot of the laboratory angular distributions for the two photodissociation channels observed. The circles are the experimental data, and the lines are the calculated distributions using values of the anisotropy parameter β shown. The solid lines are the best fit to the data; the dashed lines are calculated using upper and lower limits for the parameter β.

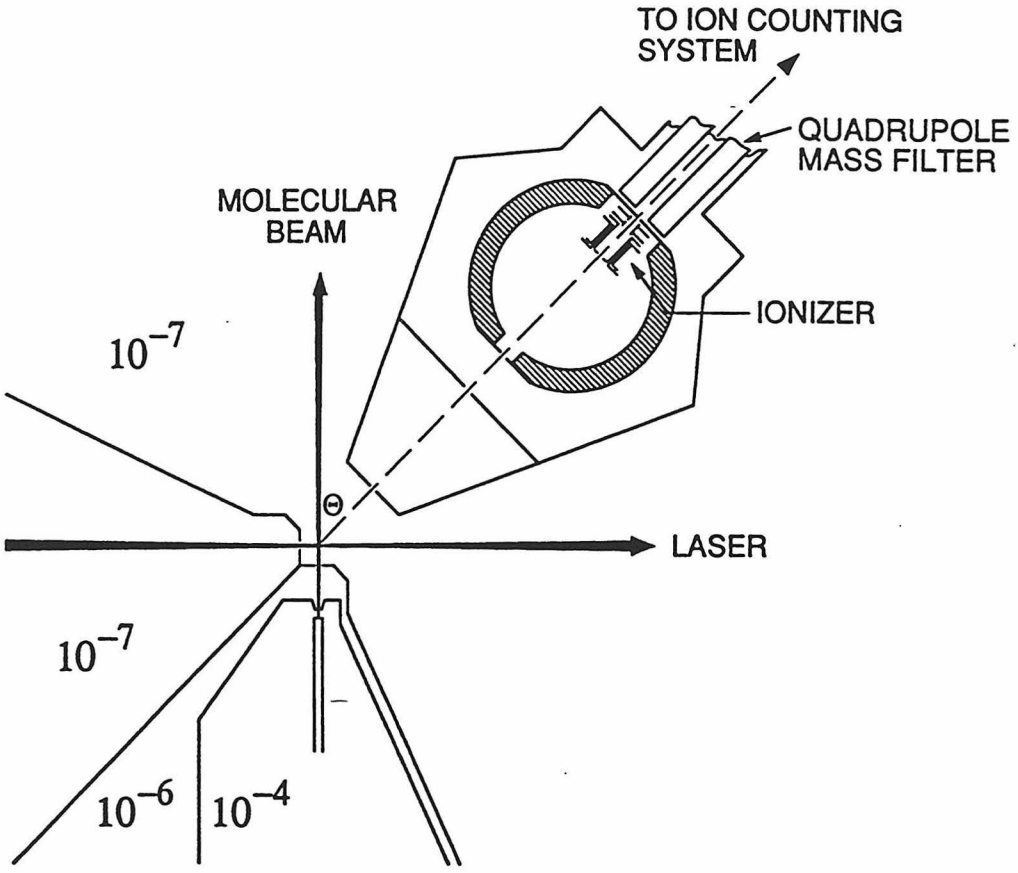
TO ION COUNTING SYSTEM
QUADRUPOLE MASS FILTER
MOLECULAR BEAM
IONIZER
10^{-7}
Θ
LASER
10^{-7}
10^{-6}
10^{-4}

Fig. 1

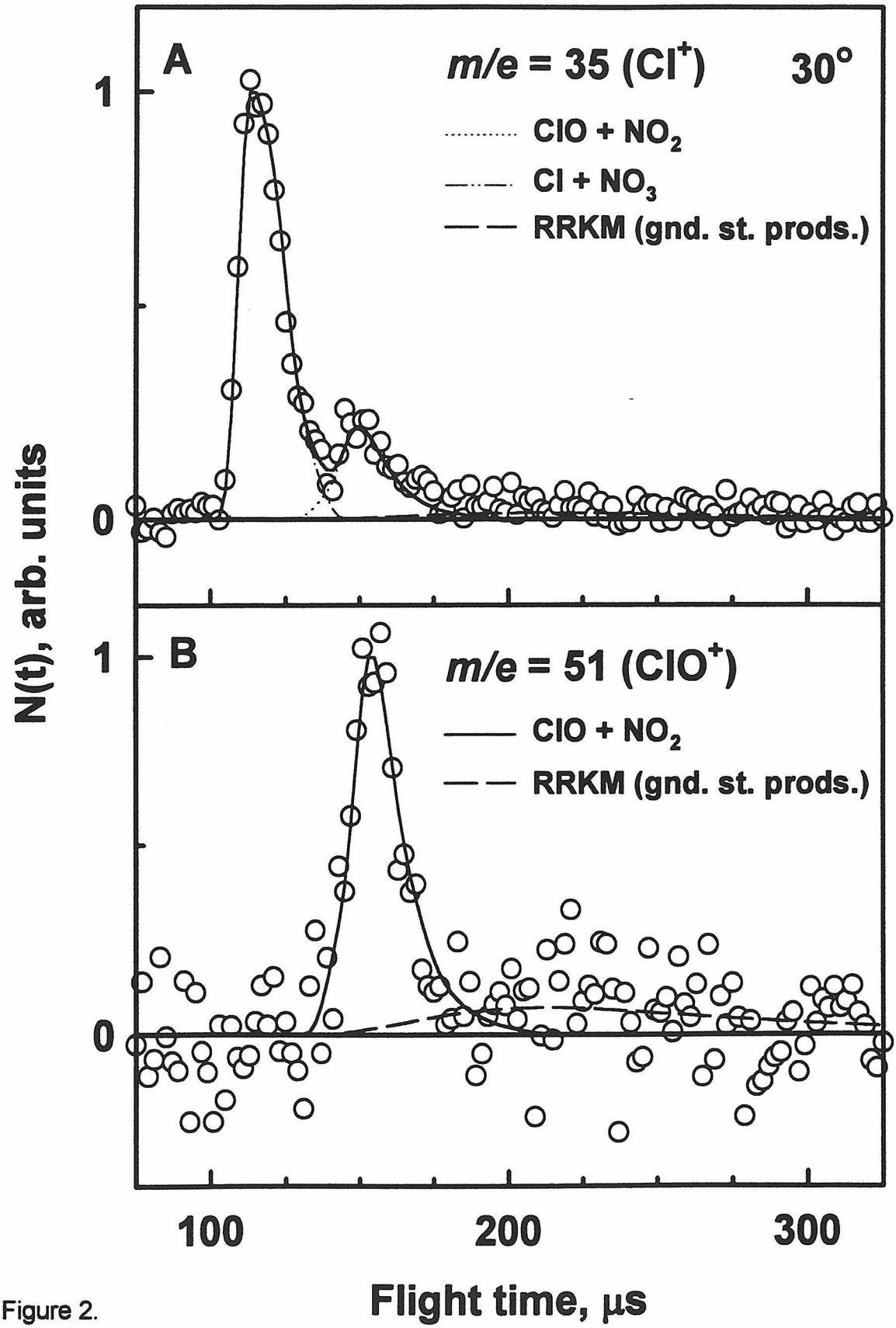
A
m/e = 35 (Cl+)
30°
ClO + NO2
Cl + NO3
RRKM (gnd. st. prods.)
1
0
B
m/e = 51 (ClO+)
ClO + NO2
RRKM (gnd. st. prods.)
1
0
N(t), arb. units
100
200
300
Flight time, μs

Figure 2.

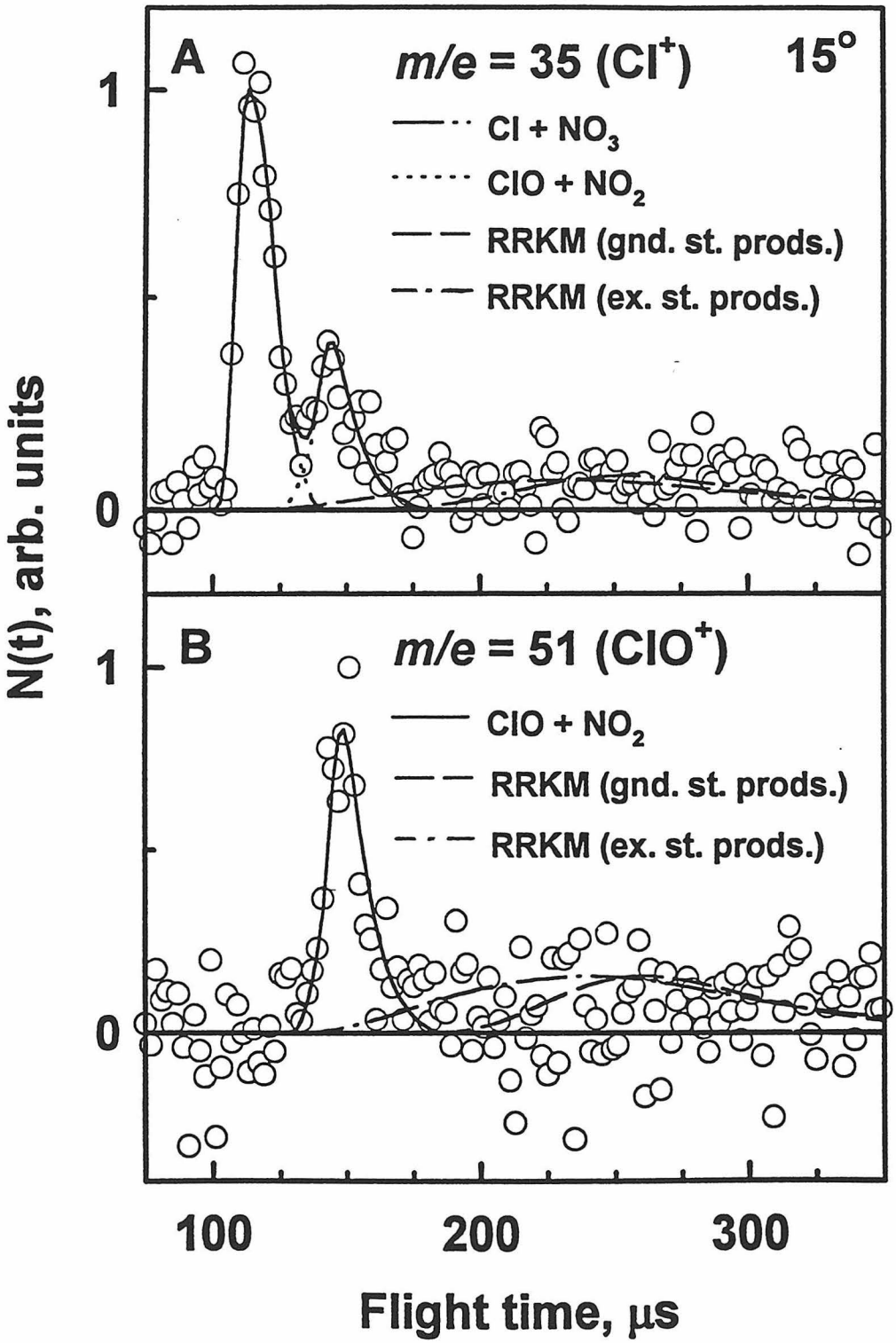
A
m/e = 35 (Cl+)
15°
Cl + NO3
ClO + NO2
RRKM (gnd. st. prods.)
RRKM (ex. st. prods.)
B
m/e = 51 (ClO+)
ClO + NO2
RRKM (gnd. st. prods.)
RRKM (ex. st. prods.)
1
0
1
0
N(t), arb. units
100
200
300
Flight time, μs

Fig. 3

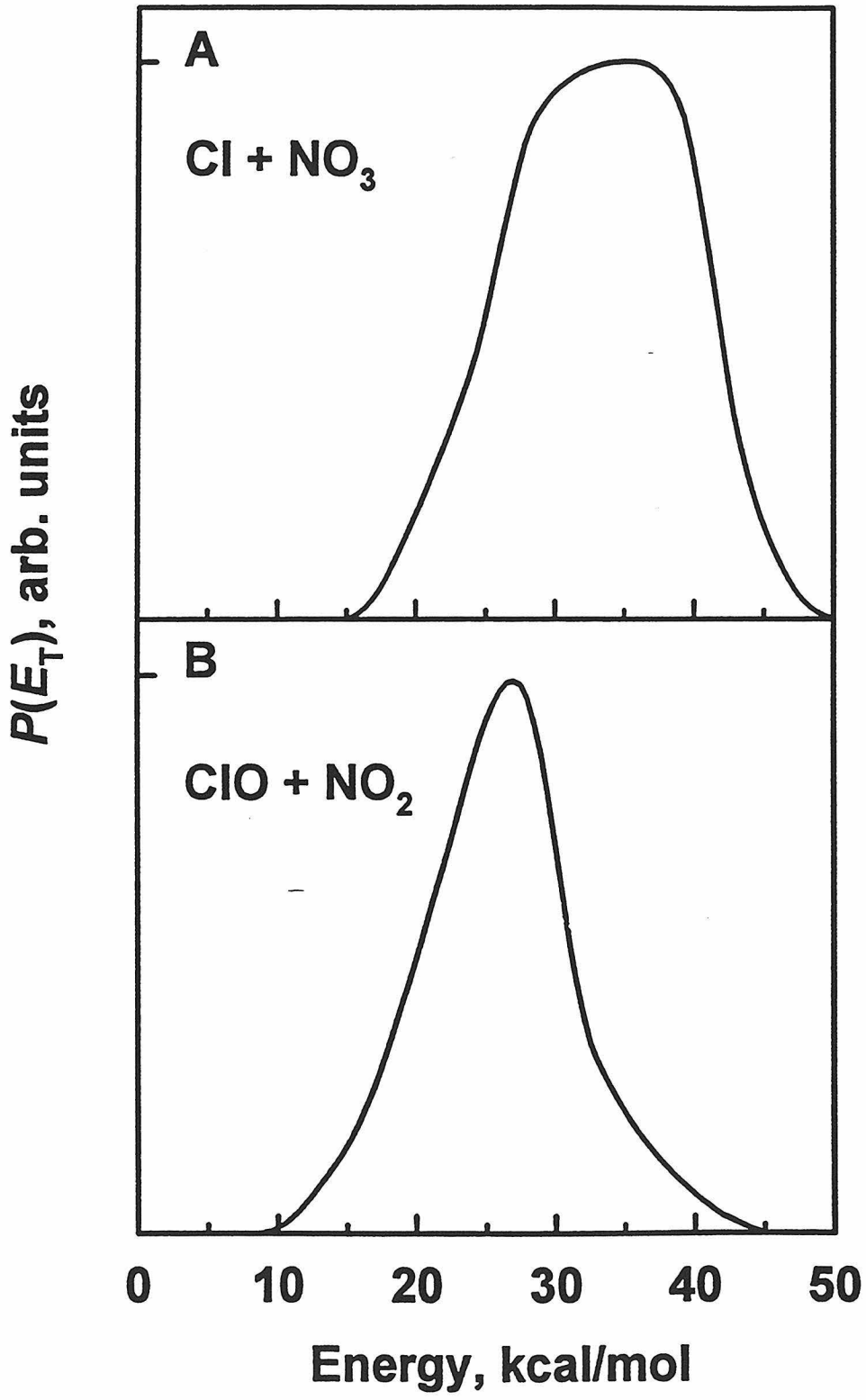

Fig. 4

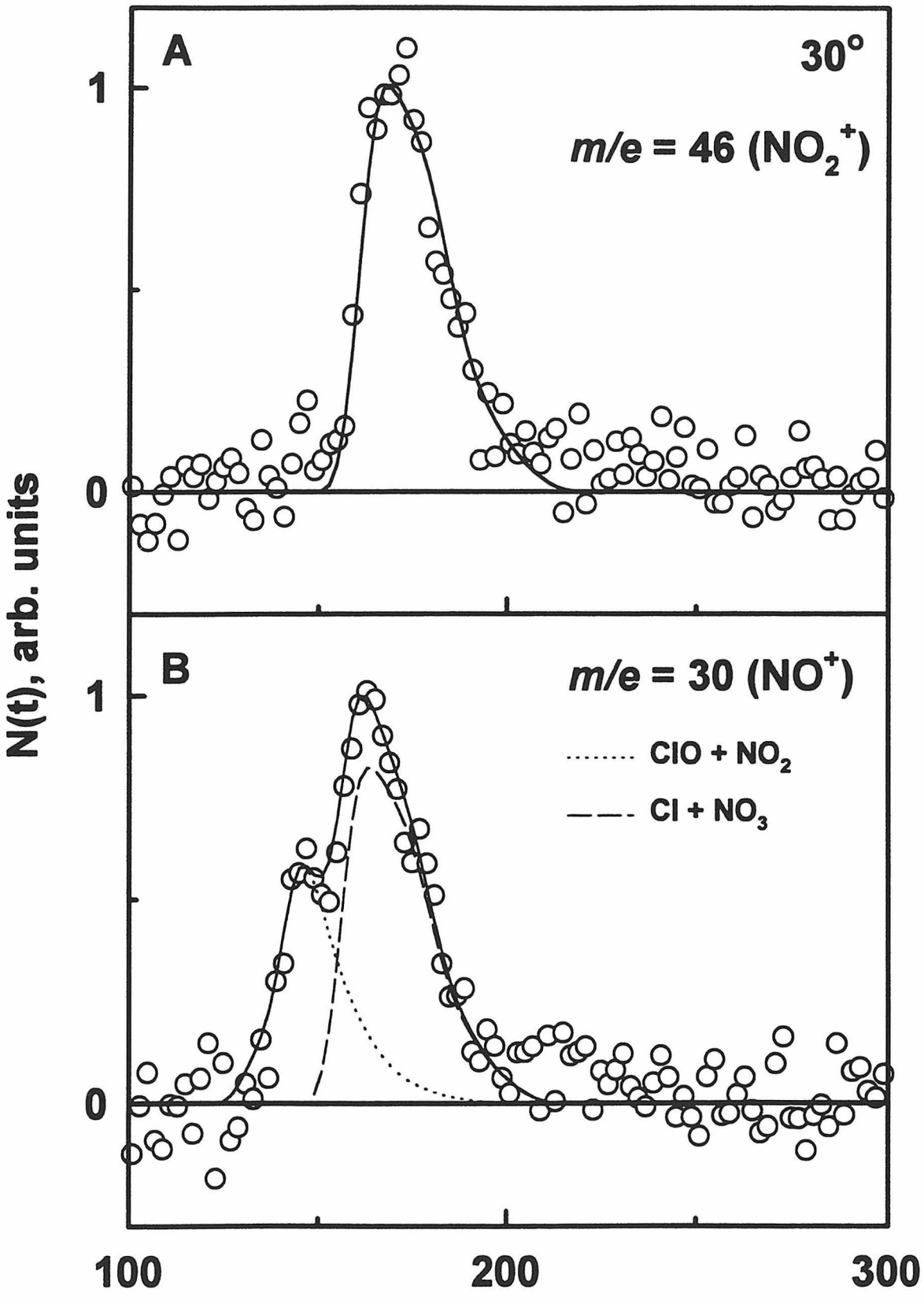
A
30°
m/e = 46 (NO2+)
1
0
B
m/e = 30 (NO+)
ClO + NO2
Cl + NO3
1
0
N(t), arb. units
100
200
300
Flight time, μs

Figure 5.

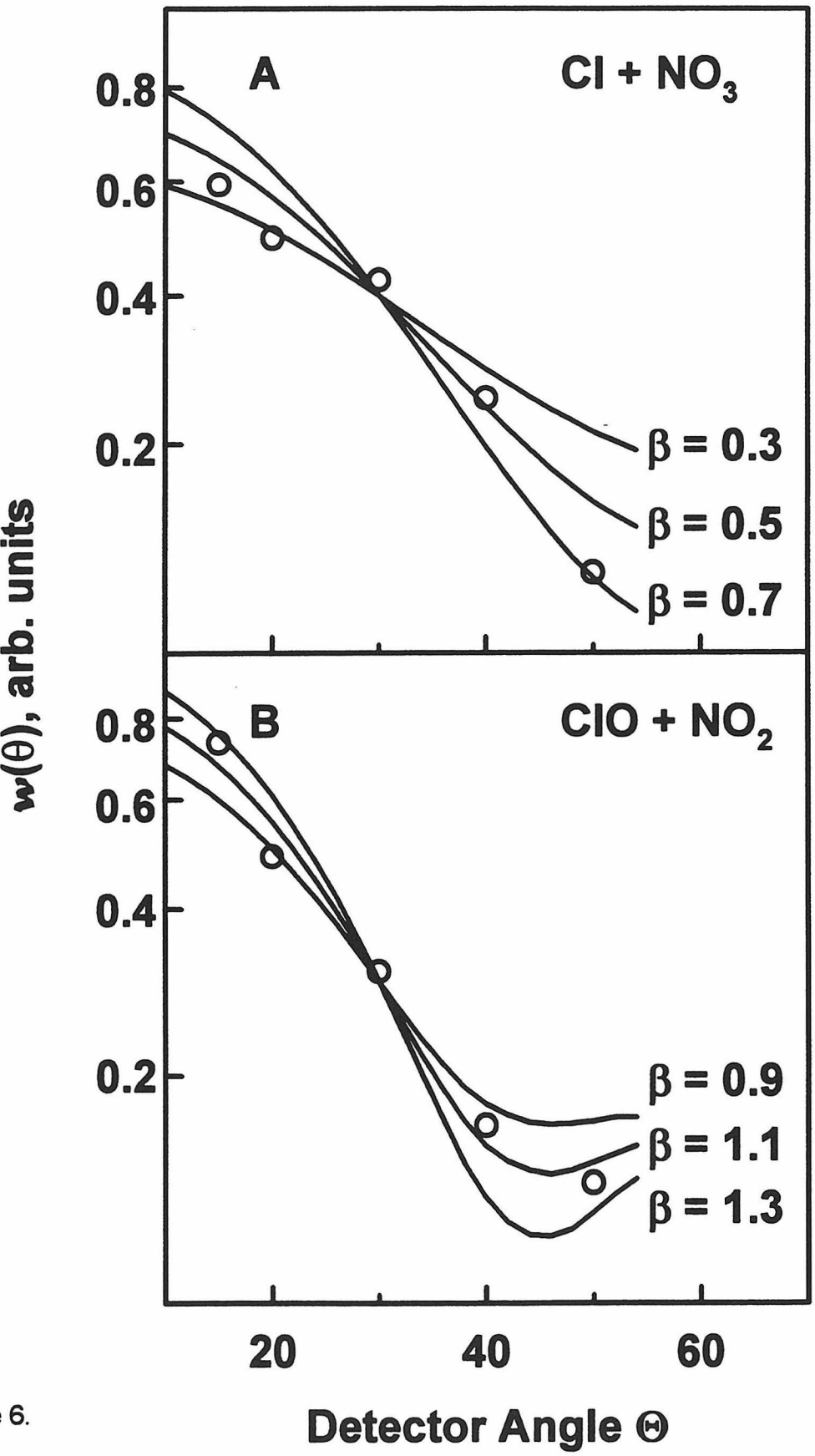
A
Cl + NO3
0.8
0.6
0.4
0.2
β = 0.3
β = 0.5
β = 0.7
B
ClO + NO2
0.8
0.6
0.4
0.2
β = 0.9
β = 1.1
β = 1.3
w(θ), arb. units
20
40
60
Detector Angle Θ

Figure 6.

Chapter 2.*

Photodissociation of Cl_2O at 248 and 308 nm

Molecular beam studies of Cl_2O photolysis at 248 and 308 nm have been repeated and the analysis refined. At 248 nm, three distinct dissociation pathways that led to Cl + ClO products were resolved. At 308 nm, the angular distribution was slightly more isotropic than previously reported, leaving open the possibility that Cl_2O excited at 308 nm lives longer than a rotational period.

---

* This chapter has been previously published. The reference is: Teresa A. Moore, Mitchio Okumura, and Timothy K. Minton, *J. Chem. Phys.* **107**, 3337 (1997).

Introduction

Studies of the photodissociation dynamics of Cl_2O (dichlorine monoxide) can aid in understanding the photochemistry of the more complex chlorine oxides which play a major role in stratospheric ozone depletion. As we reported in a previous publication,[1] formation of Cl + ClO products (ΔH_0° = 32.9 kcal/mol) is the only channel observed for Cl_2O photolysis at 308 nm and is the major channel at 248 nm. We have repeated the Cl_2O photolysis experiment at 248 and 308 nm and present here a refinement of the analysis for the Cl + ClO channel. At 248 nm, three distinct dissociation pathways that led to Cl + ClO products were resolved. At 308 nm, the angular distribution was slightly more isotropic than previously reported.

The experimental method and apparatus are described elsewhere.[2] Briefly, a molecular beam was crossed with an excimer laser beam at the center of rotation of a rotatable mass spectrometer detector. Collisionless conditions allowed for detection of primary dissociation products recoiling away from the beam direction. Photoproduct time-of-flight (TOF) distributions were measured as a function of detector angle.

The new data were recorded on the same apparatus under similar conditions and differed primarily in source conditions and laser polarization. For the new experiment, a continuous molecular beam of Cl_2O was formed by passing a gas mixture of 2% SF_6 in helium over the surface of liquid Cl_2O at −73 °C and expanding the mixture through a 0.1 mm quartz nozzle held at or below −60 °C with a stagnation pressure of 190 Torr. In all experiments, the laser beam was nearly randomly polarized in a plane perpendicular to the scattering plane and parallel to the molecular beam axis. In the current experiment, there was a slight net

polarization (~ 58%) perpendicular to the scattering plane, whereas previously there was a slight net polarization parallel to that plane. The differences in the beam conditions and the laser polarization were taken into account in the analysis. Analyses of product TOF and angular distributions were carried out by the forward convolution technique used previously. For each channel, center of mass (c.m.) translational energy $P(E_T)$ and angular $w(\theta)$ distributions were transformed to the LAB frame and adjusted iteratively until the predicted LAB TOF distributions agreed with the observed distributions at all LAB angles. The c.m. angular distributions were fit to $w(\theta) \propto 1 + \beta P_2(\cos\theta)$, where the anisotropy parameter β varies from −1 to 2 for dissociation with the recoil vector perpendicular and parallel to the transition dipole, respectively.

248 nm

Representative TOF distributions of products from 248 nm photolysis are shown in Figure 1. The m/z = 51 (ClO^+) data could not be fit at all angles with a single $P(E_T)$ distribution as was done in the previous work. Instead, the three observed peaks at m/z = 51 were fit with three separate components in the $P(E_T)$ distribution (Fig. 2), each with different anisotropy parameters. The fastest component had a large translational energy release with a maximum at 49 kcal/mol (E_{int} = 33 kcal/mol). The angular distribution was fit by $\beta = 0.7 \pm 0.2$, indicating a prompt, parallel dissociation. The middle component had an average translational energy release of $\langle E_T \rangle$ = 36 kcal/mol ($\langle E_{int} \rangle$ = 46 kcal/mol) and anisotropy of $\beta = 1.5 \pm 0.2$. A fit to the slowest component gave $\beta = 1.2 \pm 0.2$ and a $P(E_T)$ distribution with a sharp cutoff with a minimum E_T of 15 ± 1 kcal/mol. The cutoff was due to opening of the $Cl_2O \rightarrow Cl + Cl + O$ channel, because the internal energy of the ClO product exceeded the

bond dissociation energy (D_0 = 63.4 kcal/mol) for products with E_T < 19.9 kcal/mol. The 5 kcal/mol discrepancy could be attributed to a) spin-orbit excitation (2.5 kcal/mol) of one or both Cl atom products,[3] b) a centrifugal barrier to dissociation of rotationally excited ClO products (in the rigid radical approximation,[4] the ClO centrifugal barrier could be as high as 7.3 kcal/mol), or c) a combination of these causes.

The *m/z* = 35 signal (Fig. 1A, C) comprised direct Cl photoproducts, Cl atoms from secondary dissociation of ClO, ClO fragments which cracked in the ionizer, and background from cluster photolysis. In order to fit the Cl counterfragment, we extended the slowest $P(E_T)$ distribution to lower translational energies. We concluded that ≈ 4% of the ClO underwent spontaneous dissociation. The secondary Cl signal from this dissociation was modeled and included in the fit. Contributions from primary ClO products were fit assuming 32%, 37%, and 49% of the ClO fragmented to Cl^+ in the ionizer, increasing linearly with ClO internal energy. Photodissociation of ClO was also observed at higher laser power, but was minimized by keeping laser fluences low. A small underlying signal remained, which we assigned to products from photolysis of Cl_2O clusters.

In summary, we have now resolved three components in the $P(E_T)$ distribution with differing anisotropies, each leading to Cl + ClO products. These results support our conjecture that formation of Cl + ClO products involves several excited state potential energy surfaces.

308 nm

At 308 nm, the *m/z* = 51 (ClO^+) TOF spectra were fit by a $P(E_T)$ distribution very similar to the one published previously, with a peak at 33 kcal/mol and a slow shoulder

extending down to 6.5 kcal/mol. The angular distribution, fit with $\beta = 0.4 \pm 0.3$, was slightly less anisotropic than previously reported.

A long-lived excited state of Cl_2O was recently proposed by Nickolaisen *et al.*[5] to explain quenching at high pressures of the ClO yield from Cl_2O photolysis at $\lambda > 300$ nm in flow tube studies. They postulated a metastable excited state which must live longer than the mean collision time at 5 Torr of ~ 50 ns. Such a lifetime would lead to complete rotational averaging of the anisotropic angular distribution, resulting in $\beta \leq 0.19$ if Cl_2O dissociates from its ground state geometry.[6] This value of β is half of the observed value, but within our uncertainty. Our results thus indicate that $\tau < 9$ ps at 308 nm, but our uncertainties preclude us from ruling out a longer-lived state.

We acknowledge support of NASA grant NAGW-3893, and assistance from C. M. Nelson and J. W. Seale.

References

1. C. M. Nelson, T. A. Moore, M. Okumura, and T. K. Minton, J. Chem. Phys. **100**, 8055 (1994).

2. Y. T. Lee, J. D. McDonald, P. R. LeBreton, and D. R. Herschbach, Rev. Sci. Instrum. **40**, 1402 (1969); M. J. O'Laughlin, B. P. Reid, and R. K. Sparks, J. Chem. Phys. **83**, 5647 (1985).

3. Cl* products were observed with 18% yield from Cl_2O photolysis at 248 nm by A. J. Chichinin, Chem. Phys. Lett. **209**, 459 (1993).

4. G. E. Busch and K. R. Wilson, J. Chem. Phys. **56**, 3626 (1972).

5. S. L. Nickolaisen, C. E. Miller, S. P. Sander, M. R. Hand, I. H. Williams, and J. S. Francisco, J. Chem. Phys. **104**, 2857 (1996).

6. S.-C. Yang and R. Bersohn, J. Chem. Phys. **61**, 4400 (1974).

Figure Captions

1. TOF number density distributions $N(t)$ from Cl_2O photolysis at 248 nm for A) Cl^+ products collected at a detector angle of 30°, B) ClO^+ products at 30°, C) Cl^+ products at 50°, and D) ClO^+ products at 50°. The solid line is the overall fit to the data. The dashed, dotted, and dot-dashed lines correspond to the three components in the c.m. $P(E_T)$ distribution (Fig. 2). The long-dashed line in A) and C) is a hypothetical fit based on photolysis of Cl_2O clusters in the beam. The dot-dot-dashed line in A) and C) corresponds to the spontaneous secondary dissociation of ClO. Stimulated secondary dissociation of ClO is not included.

2. Optimized c.m. $P(E_T)$ distribution for the Cl + ClO channel from Cl_2O photolysis at 248 nm. The light-dashed line in the slowest component shows the cutoff from the $m/z = 51$ data, corresponding to internal energies beyond the ClO dissociation limit. The anisotropy parameters and average translational energies for each component are: dashed line, $\beta = 1.2 \pm 0.2$, $\langle E_T \rangle = 17.8$ kcal/mol; dotted line, $\beta = 1.5 \pm 0.2$, $\langle E_T \rangle = 35.9$ kcal/mol; and dot-dashed line, $\beta = 0.7 \pm 0.2$, $\langle E_T \rangle = 51.1$ kcal/mol. The scaling factor for each component is independent of angle.

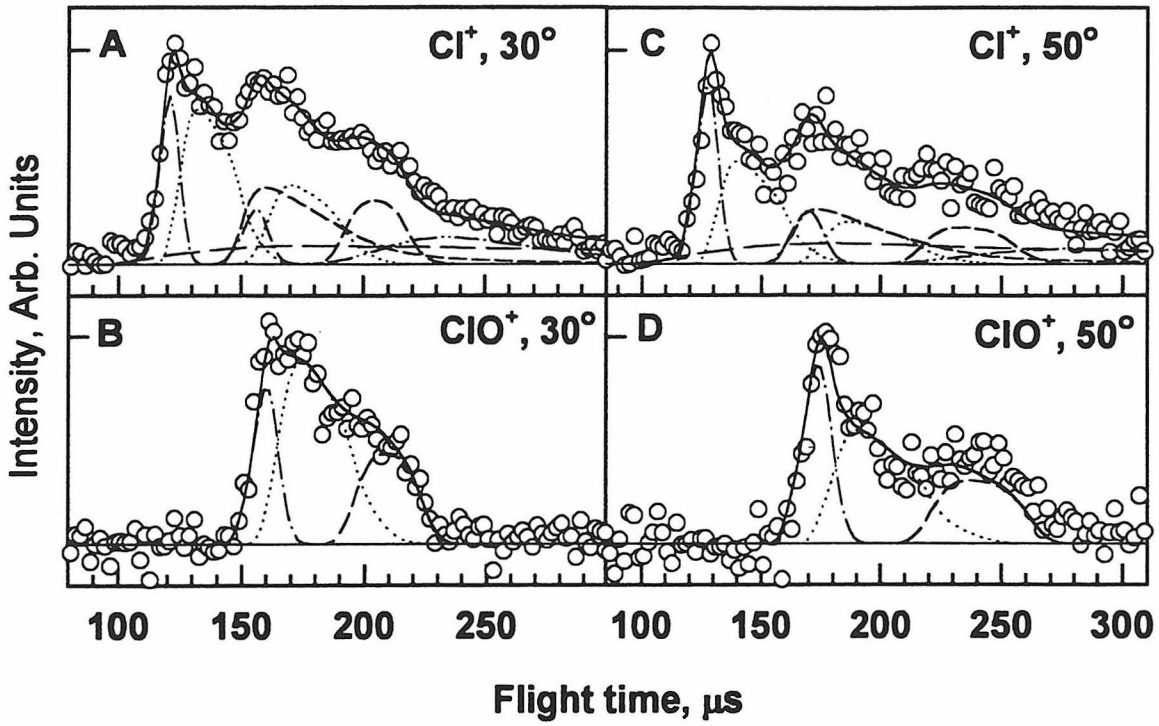
A
Cl+, 30°
C
Cl+, 50°
B
ClO+, 30°
D
ClO+, 50°
Intensity, Arb. Units
100
150
200
250
100
150
200
250
300
Flight time, μs

Figure 1

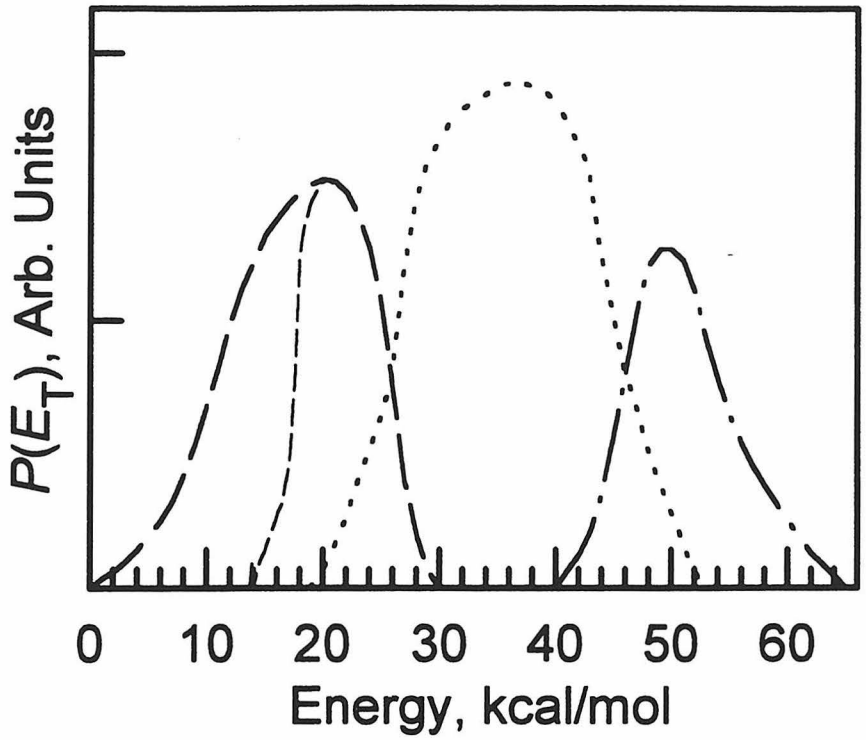

Figure 2

Chapter 3.

ClOOCl Molecular Beam Source

A molecular beam source of ClOOCl was designed in order to study ClOOCl photolysis using photofragment translational spectroscopy. We created a molecular beam of ClOOCl by photolyzing Cl_2O at 308 nm in the stagnation region and cooling the reaction cell to promote three body recombination to form ClOOCl. The main species in the beam were Cl_2, ClOOCl, and Cl_2O, with minor species O_2 and undimerized ClO also present.

A. Introduction

Knowledge of the branching ratio between Cl and ClO products from ClOOCl photolysis is crucial to our understanding of polar stratospheric ozone depletion. Because of the uncertainties in the previous measurements, we endeavored to study ClOOCl photolysis via photofragment translational spectroscopy, a powerful technique capable of direct detection of both Cl and ClO photolysis products that can provide an absorption cross-section independent method of determining the Cl:ClO branching ratio. Thus, we had to design a molecular beam source of ClOOCl.

Previous researchers have utilized different methods to produce ClOOCl, forming ClO either chemically or photolytically under conditions where three-body recombination is favored over the ClO self-reaction. These conditions usually included cooling to temperatures below 250 K, increasing the pressure, and selecting the buffer gas to increase the rate of dimer formation.[1] ClO has been formed by photolysis of Cl_2O,[2,3] by flash photolysis of Cl_2-Cl_2O, Cl_2-O_3, or Cl_2-O_2 mixtures,[4,5] by flash radiolysis of Cl_2O-Cl_2 mixtures,[6] by the chemical reaction of Cl with O_3,[7,8,9,10,11,12] Cl_2O,[7,10,11,12] or OClO,[7,10,11] or F + Cl_2O,[11] or by photolysis of OClO.[6] Static or flow cells were used in all previous experiments involving ClOOCl, in which typical concentrations of ClOOCl were on the order of 1-10 mTorr, with a maximum of a few hundred mTorr.[2,3]

In order to design a molecular beam source of ClOOCl that could be used for a photolysis experiment, several problems had to be overcome. The major design considerations are as follows:

- ClO source

ClO can be produced by any of the methods described above. The ClO source chosen determines what other species besides ClOOCl will be present. Table I lists other possible species that could be present in a ClOOCl source which could give rise to Cl or ClO photolysis signal, along with their absorption cross sections at 248 and 308 nm.

Table I. Absorption cross sections for various species that could be formed in a ClOOCl source. All cross sections are taken from the 1997 JPL evaluation,[13] except for the ClOOCl cross sections which are from ref. 3, with the values from ref. 13 in parentheses.

Species	σ(248 nm), cm^2	σ(308 nm), cm^2
Cl_2	1.1×10^{-21}	1.7×10^{-19}
ClO	3.2×10^{-18}	2.0×10^{-19}
Cl_2O	1.7×10^{-18}	4.6×10^{-19}
OClO	$\sim 10^{-19}$	$\sim 1.5 \times 10^{-18}$
ClOO	2.95×10^{-17}	
ClOOCl	$6.2\ (6.3) \times 10^{-18}$	$3.4\ (4.9) \times 10^{-19}$
Cl_2O_3	1.2×10^{-17}	2.4×10^{-18}

- ClO dimerization

The possible ClO + ClO reaction channels are

$$ClO + ClO + M \rightarrow ClOOCl + M$$
$$ClO + ClO \rightarrow ClOO + Cl \rightarrow Cl + Cl + O_2$$
$$\rightarrow Cl_2 + O_2$$
$$\rightarrow Cl + OClO.$$

At low temperature, below 250 K, ClOOCl formation is the dominant ClO reaction pathway. The identity of the third body is significant,[1] with reaction rates following the expected trend

for third body quenching efficiency except for O_2 and Cl_2. Oxygen results in a lower rate of ClOOCl formation, and chlorine in a higher rate. Thus, cooling the reaction cell and careful choice of the bath gas can encourage dimer formation.

- ClOOCl concentration

The kinetics experiments produced ClOOCl concentrations on the order of milliTorr, whereas for a beam experiment to be feasible, concentrations on the order of Torr are required. Major loss mechanisms for ClOOCl include 1) reaction with Cl or O in sources where these atoms are continuously present, 2) photolysis of ClOOCl in sources which employ continuous photolysis to produce ClO, and 3) thermal decomposition and the ClO self reaction in sources at temperatures above 250 K. The rate constant[13] for the three body association of ClO to form ClOOCl is

$$[2.2 \times 10^{-32} (T/300)^{-3.1}]cm^6/molec^2/s.$$

If a ClO concentration of 3×10^{16} molec/cm^3 (1 Torr) could be formed, for a background pressure of 6×10^{18} molec/cm^3 (200 Torr) and a temperature of 220 K, then 3×10^{20} molec ClOOCl/cm^3/s could be formed. In this case, to produce 1 Torr of ClOOCl, the residence time in the reaction chamber must be at least 100 μs (not accounting for loss processes). Thus, high production of ClO, long residence times, and minimization of loss processes are necessary to obtain the high ClOOCl concentration required.

We chose Cl_2O photolysis at 308 nm as our ClO source, because the other species likely to be present besides ClOOCl are residual Cl_2O, ClO, and Cl_2, with little or no OClO or Cl_2O_3. Cl_2 and ClO are diatomics, and will produce sharp well-defined peaks at $m/z = 35$ in a photolysis experiment. We have extensively studied Cl_2O photolysis,[14] which produces

signal at Cl^+ and ClO^+, and can model that in our photodissociation experiment. With the exception of a small concentration of clusters, no species likely to be present in the beam besides ClOOCl and Cl_2O can produce ClO photolysis signal. We wanted to avoid ClO sources that would have significant concentrations of OClO and Cl_2O_3 to minimize the number of species that could contribute to the ClO^+ photolysis signal so that we could obtain a more accurate ClO/Cl branching ratio. Also, the absorption cross sections of OClO and Cl_2O_3 at 308 nm and of Cl_2O_3 at 248 nm are significantly higher than that for ClOOCl, so that the photolysis signal from these components could mask the ClOOCl photolysis signal.

A molecular beam of ClOOCl was formed by photolyzing Cl_2O in a quartz cell and expanding the reaction mixture through a 0.1 mm nozzle. At 308 nm, the only Cl_2O photolysis products formed are Cl and ClO. The Cl atoms produced also reacted with Cl_2O, producing ClO and Cl_2:

$$Cl_2O + h\nu \rightarrow Cl + ClO$$

$$Cl + Cl_2O \rightarrow Cl_2 + ClO$$

$$\underline{ClO + ClO + M \rightarrow ClOOCl + M}$$

$$\text{net: } 2Cl_2O \rightarrow ClOOCl + Cl_2$$

A pulse of $ClOOCl/Cl_2O/Cl_2$ and other reaction products exited the nozzle, effectively creating a pulsed ClOOCl source with a continuous background of Cl_2O.

Given our choice of ClO source, our solutions to the problems posed in the previous section are as follows:

- **Continuous gas flow** allowed for long residence times, on the order of milliseconds.
- **Pulsed laser photolysis in the stagnation region** allowed for high pressures, but avoided

steady state effects like ClOOCl photolysis and attack by Cl.

- **Cooling the source** to T < 240K minimized the ClO self reaction and ClOOCl thermal decomposition.

- **High stagnation pressure** promoted rapid three body recombination, but could be kept low enough to avoid significant formation of clusters in the beam.

- **Minimization of** a) **back diffusion** of photolyzed gas and b) **mixing** of cooled gas with incoming warm gas keeps the ClOOCl concentration from being diluted by the Cl_2O and buffer gas.

The chemistry of this source was modeled using the reactions and photochemistry shown in Table II, including the species Cl_2O, Cl, ClO, O, ClOOCl, Cl_2, O_2, OClO, ClOO, and Cl_2O_3. All rate constants, branching ratios, and photodissociation cross sections were taken from the 1994 JPL report,[13] except the branching ratio for ClOOCl photolysis, for which we used an adjustable parameter for the ClO + ClO yield. Model calculations were carried out using values of 0.0 to 0.5 for this parameter. The model predicted that for pressures on the order of 100T, temperatures around 220K, and initial Cl_2O concentrations of ~ 10 T, the output from this source would be primarily Cl_2, Cl_2O, and ClOOCl, with some ClO and O_2, and negligible amounts of OClO and Cl_2O_3. Figure 1 shows the results of a model calculation for the initial conditions P_{stag} = 200T, P_{Cl2O} = 10T, T = 200K, residence time t_{res} = 50 μs, laser spot size = 0.09 cm^2, and laser energy = 0.5 mJ/pulse, with the ClO + ClO yield set to 0.2.

B. Source Design Parameters

Preliminary source development was carried out in a test chamber at Caltech, and optimization of the operating parameters was completed on the 35" rotating detector Crossed

Molecular Beams Apparatus at Montana State University. A schematic diagram of the source

Table II. Chemistry and photochemistry modeled for the ClOOCl source.

Chemistry	Photochemistry
$ClO + ClO + M \rightarrow ClOOCl + M$	$Cl_2O + h\nu \rightarrow Cl + ClO$
$ClO + OClO + M \rightarrow Cl_2O_3 + M$	$Cl_2 + h\nu \rightarrow Cl + Cl$
$Cl + ClOOCl \rightarrow Cl_2 + ClOO$	$OClO + h\nu \rightarrow O + ClO$
$Cl + Cl_2O \rightarrow Cl_2 + ClO$	$ClOO + h\nu \rightarrow O + ClO$
$Cl + OClO \rightarrow ClO + ClO$	$Cl_2O_3 + h\nu \rightarrow ClO + OClO$
$Cl + ClOO \rightarrow Cl_2 + O_2$	
$\rightarrow ClO + ClO$	$ClOOCl + h\nu \rightarrow Cl + ClOO$
$O + ClOOCl \rightarrow ClO + OClO$	$\rightarrow ClO + ClO$
	$ClO + h\nu \rightarrow Cl + O$
$O + Cl_2O \rightarrow ClO + ClO$	
$O + ClO \rightarrow Cl + O_2$	
$O + OClO \rightarrow ClO + O_2$	
$ClO + ClO \rightarrow ClOO + Cl$	
$\rightarrow Cl_2 + O_2$	
$\rightarrow Cl + OClO$	
$ClOO + M \rightarrow Cl + O_2$	
$ClOOCl + M \rightarrow ClO + ClO$	

is shown in Figure 2. The shape and dimensions of the reaction chamber were very important to the beam composition. The chamber diameter helped define the reaction volume, and the shape helped control the mixing of the laser processed gas with the unprocessed gas. Several

reaction chamber configurations were tested. The best configuration was a tapered cell starting from an ID of 3 mm and tapering down to about 0.1 mm over a length of about 1 cm, with a 0.1 mm nozzle at the tip. The cell protruded 1 cm from the cooling jacket, with a constriction of the inner diameter to ~ 1mm at the point where the cell left the cooling jacket. This constriction was quite important because it reduced back diffusion of the ClOOCl into the unprocessed Cl_2O, which would result in a dilution of the ClOOCl signal and thus a reduction of the peak ClOOCl concentration. Another constriction was placed at the entrance to the cooling jacket, to reduce mixing of the cold Cl_2O with the warm incoming Cl_2O.

The 3 inches of the 1/4 inch OD quartz tubing immediately prior to the cell tip was encased in a cooling jacket held at 205-220 K to facilitate ClO dimer formation and reduce side reactions. At temperatures below 205 K, condensation of Cl_2O in the cell and the formation of clusters in the molecular beam occurred. At higher temperatures, the absolute concentrations of ClOOCl were reduced. Cold pentane was circulated through the cooling jacket to maintain the temperature. Pentane was used as the cooling fluid because its low viscosity allows it to be easily pumped at these low temperatures. After every experiment, the pentane bath was allowed to warm up, and the water separated out. The pentane was stored in metal containers until the next experiment. The cell was mounted using two sets of three point Vespel contacts set in a Nema G-10 base in order to minimize movement when cooled and thus keep the nozzle aligned with the plane of the detector. Great care had to be taken to tighten the contacts enough to hold the cell in place but not so much that the cell cracked. The temperature was measured by thermocouples epoxied to the stainless steel Swagelock nuts of the input and output ports on the vacuum jacketed liquid feedthrough

through which the cold pentane flowed. Helium was kept flowing through the nozzle after the beam was turned off until the nozzle reached room temperature, in order to prevent condensation of pump oil on the cold nozzle which could lead to clogging.

C. Time-of-flight Mass Spectrometric Analysis

The beam passed through two regions of differential pumping before entering the main chamber. The source chamber pressure was ~ 2×10^{-4} Torr with the beam on. The beam exited the source chamber through a 0.5 mm skimmer which was located 6 mm downstream from the nozzle. The beam passed through a second differentially pumped chamber, with a pressure of < 10^{-5} Torr, and exited through a slit aperture (1.66 mm horizontal by 2.2 mm vertical) which defined a molecular beam cross section of 1.92 mm by 2.55 mm at the interaction region (the intersection point of the ClOOCl molecular beam and the photolysis laser or scattering molecular beam, and the point around which the detector rotates). This aperture also reduced the effusive background entering the detector at small viewing angles. The pressure in the main chamber was ~10^{-7} Torr.

The rotatable mass spectrometer detector had three regions of differential pumping, with pressures in the third region, which housed the ionizer, reaching ~10^{-10} Torr. Time-of-flight (TOF) mass spectra of the source output were obtained by rotating the mass spectrometer to look directly at the beam. From the interaction region, the beam traveled 34.5 cm to a Brink electron bombardment ionizer. The nominal electron energy used for examining the beam was lowered to 30 eV in order to reduce fragmentation of the ClOOCl in the ionizer. Ions were mass analyzed with an Extranuclear quadrupole mass filter, and detected with a Daly-type ion detector. Table III lists the ionizer conditions used to obtain

all of the source TOF spectra shown. The firing of the source laser was used to trigger the multi-channel scaler, so that the measured flight time of the ClOOCl signal was the sum of the residence time of the gas in the nozzle after the laser fired, the flight time from the nozzle to the ionizer, and the time for the resulting ion to travel through the mass filter to the ion detector (ion flight time). The ion flight time for an ion with mass-to-charge ratio *m/z* was empirically determined to be 3.14 $(m/z)^{1/2}$ μs for these ionizer conditions. The source TOF signal consisted of the background signal from the pure Cl_2O beam before and after the laser processed pulse and the processed region (Cl_2O depletion and ClOOCl peak).

Table III. Low electron energy ionizer conditions for examining the source beam.

Ionizer Component	Voltage
Aluminum coated cathode	- 30 kV
Photomultiplier tube	-2000 to-2200 V
First and second exit lenses	-900 V
Electron energy	30 eV
Filament emission current	2.1 mA
Mass spectrometer resolution	$\Delta m \sim 2.2$ amu (at $m/z = 51$)
Extractor	-10 V
Lens	-400V
Ion energy	35 eV

TOF spectra of the molecular beam were obtained at $m/z = 35$ (Cl^+), 51(ClO^+), 67 ($ClOO^+$), 70 (Cl_2^+), 86(Cl_2O^+), 102 ($ClOOCl^+$), 118($Cl_2O_3^+$), 121($Cl_2O{\bullet}Cl^+$), and 137 ($Cl_2O{\bullet}ClO^+$, $ClOOCl{\bullet}Cl^+$). Typical source data are shown in Figure 3. No signal was observed for cluster masses above $m/z = 137$, up to the mass spectrometer limit of $m/z = 200$.

Although ClOOCl is the lowest energy isomer of Cl_2O_2,[15,16,17,18] two other isomers, $ClClO_2$ and ClOClO, exist. These isomers do not form stable parent cations when ionized,[19] so that the signal at $m/z = 102$ was not from ionization of these isomers, which would appear at $m/z = 67$. ClOOCl is the dominant reaction product in flow tube experiments,[19] although there is some evidence that $ClClO_2$ can be formed heterogeneously, especially if the walls of the flow tube are coated with ice.[20] In our experiment, the walls of the reaction cell were dry; furthermore, the shape and arrival time (after accounting for the ion flight time) of the $m/z = 67$ peak was very similar to that of the $m/z = 102$ peak, indicating that the two peaks arose from the same species. Thus, we assumed that the only Cl_2O_2 isomer formed in our experiment was ClOOCl. It is possible that some ClOClO was formed by clustering of ClO in the expansion, but the low concentration of ClO (< 30 mTorr) remaining at the nozzle suggests that if ClOClO is present in our experiment, the concentration must be small compared to the ClOOCl concentration.

Even with the low electron energy used, the ClOOCl still fragmented in the ionizer, with major cracks at $m/z = 67$ ($ClOO^+$) and $m/z = 51$ (ClO^+). Cl_2O contributed some signal at ClO^+, but the cracking pattern of Cl_2O was measured separately with the source laser turned off, and Cl_2O was accounted for at $m/z = 51$ based on the $m/z = 86$ signal. While it is possible that OClO could contribute signal to the $m/z = 67$ peak, this is unlikely because 1) the peaks at $m/z = 67$ and 102 have the same shape and arrival time after accounting for ion flight time, 2) the model of the source chemistry indicates that the OClO concentration in the source is very low, 3) an elastic scattering experiment (described later in this chapter) showed no evidence of OClO present in the beam, and 4) no photolysis signal corresponding to OClO

was observed for photolysis at 308 nm.[21] The mass spectrometer resolution was set such that the large Cl_2 signal observed at $m/z = 70$ contributed < 5% to the signal at $m/z = 67$. Thus, we assumed that all of the signal at $m/z = 67$ arises from ClOOCl that has fragmented in the ionizer.

Table IV shows the fragmentation pattern for Cl_2, Cl_2O, and ClOOCl for the ionizer conditions used. The background signal at $m/z = 51$ and 86 was assumed to be entirely from the Cl_2O background and was used to determine the relative amounts of the ClO^+ and Cl_2O^+ ion fragments of Cl_2O. The remaining signal at the bottom of the depletion at $m/z = 86$ was assumed to be undissociated Cl_2O, and the remaining signal at $m/z = 51$ was assumed to be ClO, Cl_2O, and ClOOCl, with the Cl_2O contribution scaled by the Cl_2O fragmentation pattern. The ClO accounted for ~ 6% of the $m/z = 51$ signal, based on subsequent analysis of the ratio of the ClO : Cl_2O photolysis signal at 248 nm. The $m/z = 70$ background was attributed to residual Cl_2 impurities in the Cl_2O, and the peak signal to Cl_2 formed in the beam. The SF^+ and SF_2^+ cracks from SF_6 (also present in the buffer gas) contributed negligible signal to the $m/z = 51$ and $m/z = 70$ TOF spectra for this electron energy and were neglected. Almost every species present in the beam contributed signal to $m/z = 35$, so the contributions are difficult to sort out, but at this electron energy the $m/z = 35$ signal is very small compared to the other fragment masses.

Table IV. Fragmentation pattern for Cl_2, Cl_2O, and ClOOCl.

Species	$m/z = 35$	$m/z = 51$	$m/z = 67$	$m/z = 70$	$m/z = 86$	$m/z = 102$
Cl_2	1			14		
Cl_2O	~.05	1			1.1	
ClOOCl	~.1	3.4	4.5			1

A peak at $m/z = 118$, which could correspond to $Cl_2O_3^+$ or to cluster peaks including $Cl_2O{\bullet}O_2^+$ or $ClOOCl{\bullet}O^+$, was observed, rising and reaching a maximum at slower times than the ClOOCl peak. This peak was at least an order of magnitude smaller than the ClOOCl parent peak. The observation that this peak was slower and shaped differently than the ClOOCl peak indicated that the signal at $m/z = 102$ did not arise from Cl_2O_3 fragmenting in the ionizer. A depletion in the signal at $m/z = 121$ ($Cl_2O{\bullet}Cl^+$) was observed, corresponding to the depletion in the Cl_2O. At $m/z = 137$ ($Cl_2O{\bullet}ClO^+$, $ClOOCl{\bullet}Cl^+$), a small peak was observed, indicating the formation of some ClOOCl-containing clusters. This peak did not start rising until after the maximum ClOOCl signal. The cluster signals were small compared to the Cl_2O and ClOOCl signals, and we attempted to minimize them in spite of the need for a cold nozzle which is conducive to cluster formation. Figure 4 shows $m/z = 102$ and the higher mass peaks 118, 121, and 137. The photolysis laser delay was set to sample only the maximum ClOOCl signal, where the cluster peaks (including $Cl_2O_3^+$) were small or negligible.

An estimate of the relative amounts of each species in the molecular beam could be made by examining the source TOF spectra. The background signal arose only from Cl_2O, any residual Cl_2 impurities, and Cl_2O clusters (which were a small fraction of the total signal and can be ignored in this estimate). At the flight time corresponding to the ClOOCl peak, the signal arose from all the species formed from the photolysis and ensuing reactions: Cl_2, Cl_2O, ClOOCl, and ClO. From the background signal and the fragmentation patterns, the relative contributions at each mass could be sorted out. Then we added up the signal at all of the ion fragments for each species to get the total signal arising from that species. We estimated the relative detection efficiencies for each species by estimating the ionization cross

sections from the polarizability.[22] Based on the total signal for each species and the relative detection efficiencies, we obtained the ratio

$$ClO : Cl_2 : Cl_2O : ClOOCl \sim 0.14 : 14 : 1.0 : 2.4$$

for the relative amounts of the major species formed in the source. Based on these amounts and the absorption cross sections (using Huder and DeMore[3] for ClOOCl), we could predict the relative contributions to the photolysis signals expected at 248 and 308 nm:

$$248\ nm:\ Cl_2 : Cl_2O : ClOOCl \sim 0.008 : 1.0 : 8.8$$

$$308\ nm:\ ClO : Cl_2 : Cl_2O : ClOOCl \sim 0.3 : 5.2 : 1.0 : 1.8.$$

These predictions were based on average values for the relative amounts of each species in the beam over all of the experiments performed; however, each experiment was carried out under slightly different conditions, so the photolysis signal contributions can vary depending on the actual ratios of the species for that given beam. No estimate for the ClO photolysis contribution at 248 nm is provided, because the observed photolysis contribution was used to obtain the relative ClO concentration in the beam.

D. Optimization of Source Conditions

A carrier gas swept over liquid Cl_2O to produce a continuous beam of Cl_2O which was then photolyzed at 308 nm. The Cl_2O synthesis, purification, and Cl_2:Cl_2O ratio are discussed in Appendix 1. The photolytically produced ClO had an average internal energy of 28 kcal/mol, and the dimer bond dissociation energy is 17.1 kcal/mol, so the excess internal energy needed to be quenched in order for dimerization to occur. Different buffer gases were tested, including pure helium and nitrogen buffer gases, as well as CH_4, CH_3F, CH_2F_2, CHF_3, and SF_6 mixtures in helium. Figure 5 shows TOF spectra for a pure helium beam, He + 2%

CF_3H, and He + 2% SF_6. A mixture of 2% SF_6 in helium was chosen as the best mixture, as it allowed for the highest absolute amounts of $ClOOCl^+$ signal for the desired $ClOOCl^+$:Cl_2O^+ ratio. Increasing the amount of SF_6 led to a slower beam velocity and lower absolute ClOOCl concentrations for the same $ClOOCl^+$:Cl_2O^+ ratio. We tested to be sure that the SF_6 did not cause any spurious signal by carrying out a photolysis experiment using pure helium as the buffer gas.

The absolute stagnation pressure used was ~190 Torr, ranging from 180 to 200 T. Higher stagnation pressures led to formation of clusters, and lower stagnation pressures led to a weaker expansion and poorer beam quality (lower speed ratio). The Cl_2O was held at -73° to -74° (vapor pressure 10-12 Torr). Higher Cl_2O concentrations caused an increase in cluster formation, and lower concentrations led to reduced ClOOCl concentrations.

The 308 nm output from a pulsed Lambda Physik EMG103 MSC excimer laser was focussed with a 1 m focal length lens and sent into the source chamber through a fused silica window and then directed onto the tip of the reaction cell by a 90° prism. The laser spot size was varied by changing the position of the lens, with the best results obtained for a spot size ~ 8mm wide by 2 mm high, so that a section of the cell 2mm long by the cell diameter at the laser spot position was illuminated. The laser spot could be moved along the cell closer to or further from the tip to vary the reaction time between when the laser fired and when the reaction mixture exited the cell. The spot position was changed by raising or lowering the rear legs of the laser, which could be done in a reproducible manner. The laser was aligned to the cell by removing the top flange of the source chamber, inserting a white business card under the cell, and firing the laser for 10-20 shots until the card showed a burn mark. The

outside diameter of the cell was 5 mm, so 3 mm of the laser spot overlapped the edges of the cell. The laser position was adjusted until the "shadow" made by the cell was centered on the burn mark on the business card. The laser position from the tip of the cell was determined by moving the laser spot along the cell until it passed the tip and the cell no longer caused a shadow to form in the burn mark. A typical experiment was run with the center of the laser spot about 5 mm from the tip of the cell. During the experiment, care was taken to not move the spot within 1 mm of the tip to avoid blowing the tip off the cell. The laser power was varied by attenuating the laser beam with quartz plates to change the extent of Cl_2O dissociation, with typical laser energies of 130-170 mJ/pulse. Ninety to ninety-five percent depletion of the Cl_2O signal gave the highest $ClOOCl^+$:Cl_2O^+ ratio. At laser powers causing > 95% Cl_2O depletion, the ClOOCl parent signal was also reduced, because of secondary photodissociation of ClO and attack of ClOOCl by Cl atoms. At lower laser powers, the amount of Cl_2O remaining undissociated (>10%) was much greater than the amount of ClOOCl formed. Figure 6 shows the *m/z* = 86 and 102 spectra for laser energies of 130 mJ/pulse (**A**, **B**) and 160 mJ/pulse (**C**, **D**).

The source laser was operated at 40 Hz, as that was the maximum repetition rate of the photolysis laser used to do the photolysis experiments. Some data was also obtained at a repetition rate of 20 Hz. The absolute ClOOCl signal did seem to increase at the lower repetition rate, possibly because the reaction cell could maintain a lower temperature. The increase in signal at 20 Hz was not enough to compensate for the reduction in counting time obtained by going to the higher repetition rate.

The laser power and position were optimized before each set of experiments while the

other operating conditions remained consistent from experiment to experiment. The laser parameters were adjusted until the ClOOCl peak observed at m/z = 102 was 0.1 to 1.0 times the Cl_2O signal remaining at m/z = 86. For the conditions described, the pulse of ClOOCl, Cl_2O, Cl_2, and undimerized ClO that exited the nozzle was about 1-3 ms wide, with the ClOOCl pulse maximum spanning ~200 μs. Typical residence times in the cell after the laser pulse were 100 - 500μs.

E. Elastic Scattering

In order to further characterize the source beam, we performed an elastic scattering experiment in which we scattered the ClOOCl beam off a neon beam and measured the angular distribution of the deflected products. Angular distributions were measured for a given m/z to determine what masses contributed to the signal. This technique provides a measure of mass that is independent of m/z and fragmentation patterns.

A neon beam produced by expanding neon at a stagnation pressure of 1250 Torr through a 0.1 mm nozzle at 22° C was crossed by a ClOOCl beam at an angle of 90° in the interaction region. The beam velocity of the ClOOCl beam could not be measured directly or inferred from diatomic photolysis signal. However, the beam velocity for all of the photolysis experiments as well as that measured separately with a chopper wheel remained fairly consistent, ranging from 9.0 to 9.5 × 10^4 cm/s. The source conditions for the scattering experiment were closest to those for the preceding few experiments, for which the beam velocity was 9.05× 10^4 cm/s; thus, we used this value as the ClOOCl beam velocity. Because we did not measure the velocity directly, this value may have some error, which would slightly change the angles corresponding to the edges of the elastic Newton circle. The

deflected molecules were detected by rotating the detector off the ClOOCl beam axis. Distributions were obtained both with the beams crossing and with the neon beam blocked by a beam flag. The background distributions (beam flagged) were subtracted from the total signal (beam unflagged) to obtain the scattered signal, which consisted of signal from the Cl_2O background as well as the Cl_2O depleted, ClOOCl rich portion of the beam. The distributions were obtained with a resolution of 100 μs/point, so different ranges could be taken to characterize the ClOOCl portion of the beam. Ranges of 100, 200, 400, and 600 μs were used. Data for the ClOOCl beam scattering off neon were obtained for m/z = 51 (ClO^+), 67 ($OClO^+$), 86 (Cl_2O^+), and 102 ($ClOOCl^+$), with angular ranges of 19° - 49°, 20° - 36°, 25° - 31°, and 13° - 25°, respectively. Experiments were also done for a pure Cl_2O beam from a cooled nozzle (ClOOCl source laser turned off) crossed with neon and for argon crossed with helium.

For the Ar + He case, there are no vibrations or rotations for the collision energy to be partitioned into. The Ar beam velocity was 5.54×10^4 cm/s and the He beam velocity was 1.75×10^5 cm/s. From the Newton diagram (Fig. 7), the Ar signal can not be scattered beyond the edge of the Newton circle, or a lab angle of 37°. The angular distribution shown in Figure 8 shows this sharp cutoff in signal as expected, centered about the laboratory velocity corresponding to the edge of the elastic Newton circle.

In the pure Cl_2O + Ne case, the Cl_2O beam velocity was 7.7×10^4 cm/s and the Ne beam velocity was 7.8×10^4 cm/s. From the Newton diagram (Fig. 9), the maximum lab angle at which scattered Cl_2O can be observed is 32.4°. However, unlike the pure elastic Ar + He scattering data, the angular distribution (Fig. 10) shows that the scattered signal has

essentially disappeared before this angle, and the drop in signal occurs over a longer angular range, 10° instead of ~ 6°. These differences indicate that the scattering is inelastic, with some of the energy partitioned into Cl_2O internal modes.

If we took the midpoint of the portion where the signal is rapidly falling (i.e. the region which would correspond to the edge of the elastic Newton circle if the scattering was elastic), we obtained an angle of 26.5°. Assuming that this angle corresponded to the edge of the inelastic Newton circle, we obtained a new c.m. velocity (and thus translational energy) of the scattered Cl_2O and, using conservation of energy, determined the amount of the collision energy partitioned into Cl_2O internal energy. The initial total c.m. translational energy E_T was 9.8 kJ/mol. Using 26.5° as the edge of the inelastic Newton circle, the final E_T becomes 5.0 kJ/mol, indicating that 4.8 kJ/mol was partitioned into internal energy (E_{int}). Thus, the change in translational energy was 49% of the initial translational energy, or $\Delta E_T/E_T = 0.49$.

With the source laser turned on, we examined the Cl_2O background at both $m/z = 51$ and 86 well after the ClOOCl portion of the distribution. The beam velocity in this region was 8.4×10^4 cm/s, as measured previously with a chopper wheel, and the edge of the elastic Newton circle (see Newton diagram, Fig. 11) corresponded to a laboratory angle of 30.4°. Again, the scattered signal is already gone by this angle. At $m/z = 86$, we did not collect data at small enough angles to see where the drop in signal begins, but at $m/z = 51$ we were able to obtain this information (Fig. 12 A,B). The midpoint of the drop, as explained before, came at 24°, which we then took as the edge of the inelastic Newton circle. Using this value, the amount of energy partitioned into Cl_2O internal energy was $\langle E_{int} \rangle = 6.2$ kJ/mol. The initial

E_T was 10.75 kJ/mol, so $\Delta E_T/E_T = 0.58$. This value is higher than that for the pure Cl_2O beam. However, the collision energy was higher because the Cl_2O beam velocity was higher, so the fraction partitioned into internal energy would not be expected to remain the same.

For the ClOOCl beam scattering experiment, all ClOOCl beam components will contribute to the scattered signal. The ClOOCl beam velocity was 9.05×10^4 cm/s, and the Newton diagram including elastic Newton circles for ClO, OClO, Cl_2O, ClOOCl, and Cl_2O_3 is shown in Fig. 13.

The m/z = 86 signal can have contributions from Cl_2O_3, ClOOCl, or Cl_2O. Unfortunately, we did not take data at small enough angles to observe the Cl_2O_3 or ClOOCl contributions, or to observe the portion of the angular distribution before the signal started to drop. The angular distribution is shown in Fig 14 A, where it is apparent that 1) there is signal after the ClOOCl elastic Newton circle cutoff, and 2) there is a small shoulder (~ 10% of the peak signal before the drop) at 29°, just before the edge of the Cl_2O elastic Newton circle. We can obtain information on the Cl_2O internal energy partitioning from the m/z = 51 angular distribution, shown in Fig. 14 B. The Cl_2O^+ : $ClOOCl^+$ ratio was high for this experiment, so the m/z = 51 signal arose mainly from Cl_2O. Also, the signal drop observed occurs near the ClOOCl elastic Newton circle; however, the ClOOCl scattering would be expected to also be inelastic and thus be observed at smaller angles, where no data was taken. If we assumed the scattered signal observed at m/z = 51 arises solely from Cl_2O, and that the same fraction of the collision energy was partitioned into internal energy as in the background Cl_2O distribution ($\Delta E_T/E_T$), then we predicted that the edge of the inelastic Newton circle would be at 23°. From the m/z = 51 angular distribution, the edge of the Newton circle

should be at ~ 23.5°, which would lead to a $\Delta E_T/E_T$ of 0.63. The beam velocity was higher in the ClOOCl-rich region than in the Cl_2O background, which could account for the higher fraction of collision energy partitioned into internal energy.

The *m/z* = 51 angular distribution also shows a small fraction of scattered signal remaining out to 43°, well beyond the elastic Newton circle of every species in the beam except for ClO. This signal was small compared to the Cl_2O signal (~ 5%) and indicated the presence of a small concentration of ClO in the beam.

The *m/z* = 102 signal can consist of contributions from ClOOCl, Cl_2O_3, and any higher cluster masses. The edge of the elastic Newton circle is at 24.8° for ClOOCl and 21.3° for Cl_2O_3. Like the Cl_2O signal, the *m/z* = 102 angular distribution (Fig 14 C) showed a gradual drop in signal which was gone by 25° (but not 21°). There was a slight shoulder peaking at 22°, just before the edge of the elastic ClOOCl Newton circle, similar in width and magnitude to the shoulder near the Cl_2O Newton circle in the *m/z* = 86 angular distribution. The midpoint of the sharp drop in signal occurred around the laboratory angle 19° - 19.5°. If we assumed that the *m/z* = 102 signal arose from ClOOCl, the resulting collision energy was 11.8 kJ/mol, and the amount partitioned into internal energy was 6.7 kJ/mol, indicating that $\Delta E_T/E_T = 0.56$. If we instead assumed that the signal arose from Cl_2O_3, the collision energy was 13.1 kJ/mol, and the amount partitioned into internal energy was 4.5 kJ/mol, indicating that $\Delta E_T/E_T = 0.34$. Because Cl_2O_3 has more internal degrees of freedom than Cl_2O, we would expect that the fraction of the collision energy partitioned into internal energy would be greater, not less, than that for the Cl_2O case. The Cl_2O_3 parent signal was too weak to obtain scattering data. The amount of energy partitioned into the ClOOCl internal energy was

comparable to the Cl_2O case if we assumed that the m/z = 102 signal was from ClOOCl. From the energy partitioning results, we inferred that the m/z = 102 signal arises from ClOOCl.

The m/z = 67 angular distribution, shown in Fig 14 D, only includes angles from the last 4° of the portion where the signal was dropping rapidly out to the edge of the OClO elastic Newton circle, but not the portion showing the beginning of the drop in signal. The drop in the angular distribution occurs before the edge of the ClOOCl elastic Newton circle. The average angular range over which the signal drops is ~ 8°, so we assumed that the edge of the inelastic Newton circle was ~ 20°. If the signal arose from OClO, then the $\Delta E_T/E_T$ would be 0.94, with nearly all of the collision energy being partitioned into OClO internal energy. The edge of the inelastic Newton circle for the m/z = 102 scattered signal was ~ 19.5°, which strongly indicates that the m/z = 67 and m/z = 102 signal arise from the same species. A very small shoulder (≤ 6% of the highest signal observed, or ≈ 3% of the estimated peak) was observed right at the edge of the ClOOCl elastic Newton circle, and no signal was observed beyond this shoulder. If shoulder arose from OClO scattering, most of the collision energy would again be partitioned into internal energy, with $\Delta E_T/E_T$ = 0.72. These considerations indicate that the m/z = 67 signal does not arise from OClO, which provides indirect evidence that its reaction product Cl_2O_3 is also unimportant in our source.

The other two isomers of Cl_2O_2 could contribute to the m/z = 67 scattered signal; however, we did not obtain data at small enough angles to observe much of the angular range where these species could contribute signal. It is possible that the different Cl_2O_2 isomers might result in different fractions of the collision energy partitioned into internal energy. In

this case, a careful study of $m/z = 67$ angular distributions and comparison to $m/z = 102$ data (to which only ClOOCl contributes) could give some information on the relative concentrations of each isomer in the beam.

In conclusion, the scattering experiment showed that the components of the ClOOCl beam scattered inelastically off of the neon beam, with over half of the collision energy being partitioned into internal energy. Evidence was observed for ClOOCl, Cl_2O, and ClO in the laser processed portion of the beam, with OClO and Cl_2O_3 unlikely to be major components in the beam. No scattering data for Cl_2 was obtained, although it is a major component in the beam. More data was needed to be able to make more firm conclusions on the species present in the beam and their relative concentrations.

F. References

1. S. L. Nickolaisen, R. R. Friedl, and S. P. Sander, *J. Phys. Chem.* **98**, 155 (1994).

2. R. A. Cox and G. D. Hayman, *Nature* **332**, 796 (1988).

3. K. J. Huder and W. B. DeMore, *J. Phys. Chem.* **99**, 3905 (1995).

4. S. P. Sander, R. R. Friedl, and Y. L. Yung, *Science* **245**, 1095 (1989).

5. N. Basco and J. E. Hunt, *Int. J. of Chem. Kinetics* **Vol XI**, 649 (1979).

6. T. Ellermann, K. Johnsson, A. Lund, and P. Pagsberg, *Acta Chemica Scandinavica* **49**, 28 (1995).

7. L. T. Molina and M. J. Molina, *J. Phys. Chem.* **91**, 433 (1987).

8. M. J. Molina, A. J. Colussi, L. T. Molina, R. N. Schindler, and T.-L. Tso, *Chem. Phys. Lett.* **173**, 310 (1990).

9. M. Schwell, H.-W. Jochims, B. Wassermann, U. Rockland, R. Flesch, and E. Rühl, *J. Phys. Chem.* **100**, 10070 (1996).

10. J. B. Burkholder, J. J. Orlando, and C. J. Howard, *J. Phys. Chem* **94**, 687 (1990).

11. M. Birk, R. R. Friedl, E. A. Cohen, H. M. Pickett, and S. P. Sander, *J. Chem. Phys.* **91**, 6588 (1989).

12. M. Trolier, R. L. Mauldin III, and A. R. Ravishankara, *J. Phys. Chem.* **94**, 4896 (1990).

13. W. B. DeMore, S. P. Sander, D. M. Golden, R. F. Hampson, M. J. Kurylo, C. J. Howard, A. R. Ravishankara, C. E. Kolb, and M. J. Molina, *Chemical Kinetics and Photochemical Data for Use in Stratospheric Modeling, Evaluation Number 12*, 1997, also Evaluation Number 11, 1994.

14. C. M. Nelson, T. A. Moore, M. Okumura, and T. K. Minton, *J. Chem. Phys.* **100**, 8055 (1994), and T. A. Moore, M. Okumura, and T. K. Minton, *J. Chem. Phys.* **107**, 3337 (1997).

15. T. J. Lee, C. M. Rohlfing, and J. E. Rice, *J. Chem. Phys.* **97**, 6593 (1992).

16. J. F. Stanton, C. M. L. Rittby, R. J. Bartlett, and D. W. Toohey, *J. Phys. Chem.***95**, 2107 (1991).

17. M. P. McGrath, K. C. Clemitshaw, F. S. Rowland, and W. H. Hehre, *Geophys. Res. Lett.* **15**, 883 (1988).

18. F. Jensen and J. Oddershede, *J. Phys. Chem.* **94**, 2235 (1990).

19. M. Schwell, H.-W. Jochims, B. Wassermann, U. Rockland, R. Flesch, and E. Rühl, *J. Phys. Chem.* **100**, 10700 (1996).

20. R. N. Schindler, *Proceedings of the 4. Statusseminar des Ozonforschungsprogramms*, Bonn, 1994, as reported in Ref. 19.

21. The OClO photochemistry at 308 nm was modeled using translational energy distribution and angular distributions obtained from Floyd Davis, unpublished data.

22. R. E. Center and A. Mandl, *J. Chem. Phys.* **57**, 4104 (1972).

G. Figure Captions

Figure 1. Model prediction of the concentrations of the species in the ClOOCl beam for the initial conditions P_{stag} = 200T, P_{Cl2O} = 10T, T = 200K, t_{res} = 50 μs, laser spot size 0.09 cm^2, laser energy 0.5 mJ/pulse, and ClO + ClO yield 0.2.

Figure 2. Schematic of the ClOOCl source cell.

Figure 3. Typical TOF spectra of the molecular beam at *m/z* = 35 (Cl^+), 51(ClO^+), 67 ($ClOO^+$), 70 (Cl_2^+), 86(Cl_2O^+), 102 ($ClOOCl^+$), 118($Cl_2O_3^+$), 121($Cl_2O{\bullet}Cl^+$), and 137 ($Cl_2O{\bullet}ClO^+$, $ClOOCl{\bullet}Cl^+$).

Figure 4. Source TOF spectra of the ClOOCl parent mass and the higher cluster masses. The solid vertical line indicates the time where the photolysis laser was fired for the photodissociation experiments.

Figure 5. Comparison of the ClOOCl parent TOF spectra for different buffer gas compositions. A) Pure helium; B) He + CF_3H; C) He + SF_6.

Figure 6. TOF spectra for the ClOOCl and Cl_2O parent masses showing the effect of laser power on the ClOOCl concentration and the Cl_2O:ClOOCl ratio. A) *m/z* = 102, 130 mJ/pulse; B) *m/z* = 86, 130 mJ/pulse; C) *m/z* = 102, 160 mJ/pulse; D) *m/z* = 86, 160 mJ/pulse. The lines show the region of the pulse where the Cl_2O^+ : $ClOOCl^+$ ratio is the greatest.

Figure 7. Newton diagram for argon scattering off of helium. The edge of the Newton circle for Ar scattering corresponds to a laboratory angle of 37.0°.

Figure 8. Angular distribution for argon scattered off of helium. The line indicates the laboratory angle (37.0°) corresponding to the edge of the elastic Newton circle.

Figure 9. Newton diagram for a pure Cl_2O beam scattering off of neon. The edge of the Newton circle for Cl_2O corresponds to a laboratory angle of 32.4°.

Figure 10. Angular distribution for Cl_2O scattered off of neon. The solid line (32.4°) corresponds to the edge of the elastic Newton circle. The dotted line indicates the angle (26.5°) which we took to correspond to the edge of the inelastic Newton circle.

Figure 11. Newton diagram for Cl_2O in the background region of the ClOOCl beam scattering off of neon. The edge of the Newton circle for Cl_2O scattering corresponds to a laboratory angle of 30.4°.

Figure 12. Angular distribution for $m/z = 86$ (A) and $m/z = 51$ (B) for Cl_2O in the background region of the ClOOCl beam scattered off of neon. The solid line (30.4°) indicates the edge of the elastic Newton circle; the dotted line indicates the angle (24°) which we took to correspond to the edge of the inelastic Newton circle.

Figure 13. Newton diagram for the ClOOCl beam scattering off of neon. Newton circles for ClO (48.8°), OClO (37.5°), Cl_2O (29.6°), ClOOCl (24.8°), and Cl_2O_3 (21.3°) are shown.

Figure 14. Angular distributions for m/z = 86 (A), m/z = 51 (B), m/z = 102 (C), and m/z = 67 (D) from the ClOOCl beam scattering off of neon. The solid lines indicate the edges of the elastic Newton circles as marked, and the dotted lines indicate the angles we took as the edges for the inelastic Newton circles.

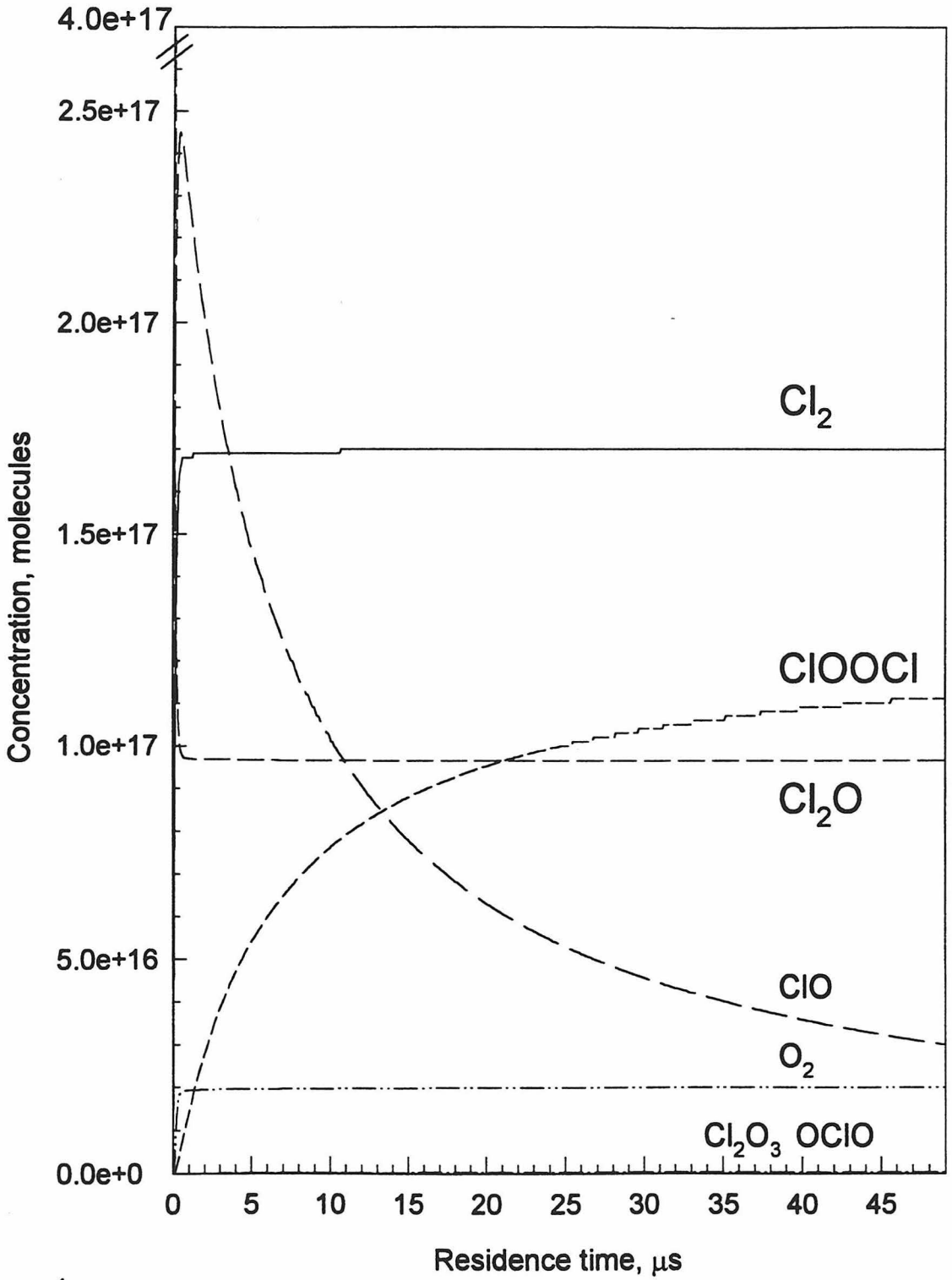
4.0e+17
2.5e+17
2.0e+17
1.5e+17
1.0e+17
5.0e+16
0.0e+0
Concentration, molecules
0
5
10
15
20
25
30
35
40
45
Residence time, μs
Cl2
ClOOCl
Cl2O
ClO
O2
Cl2O3 OClO

Figure 1.

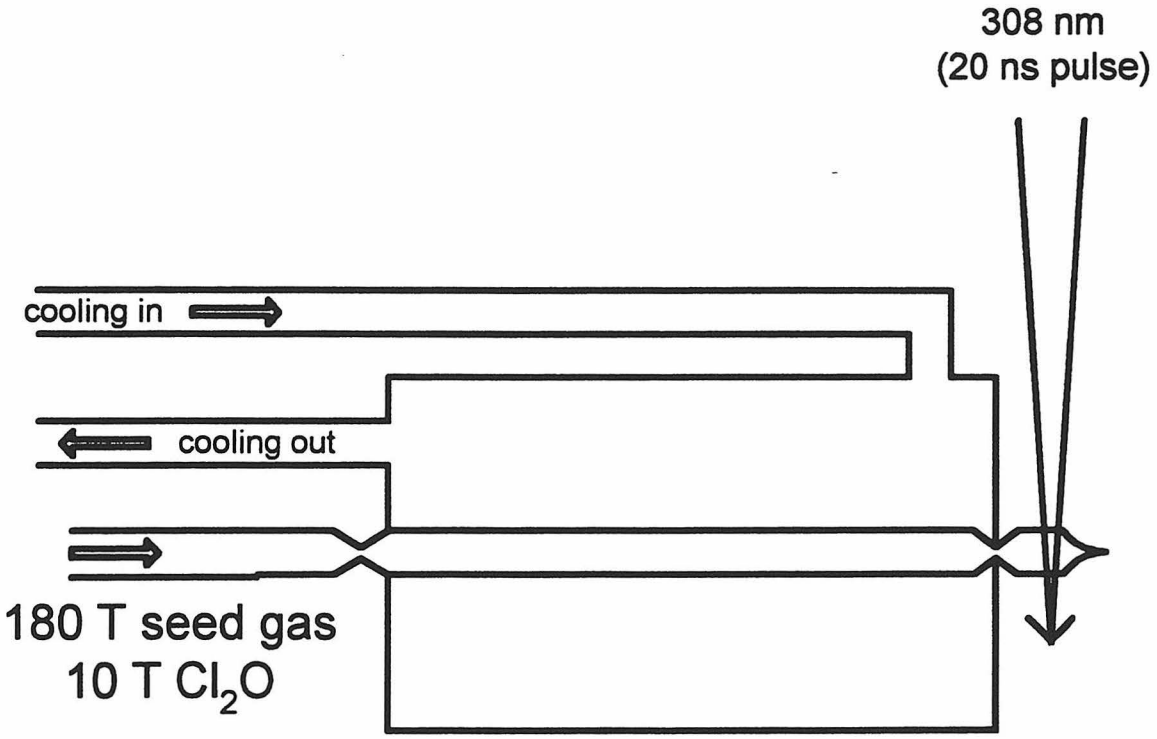
308 nm
(20 ns pulse)
cooling in
cooling out
180 T seed gas
10 T Cl_2O

Figure 2.

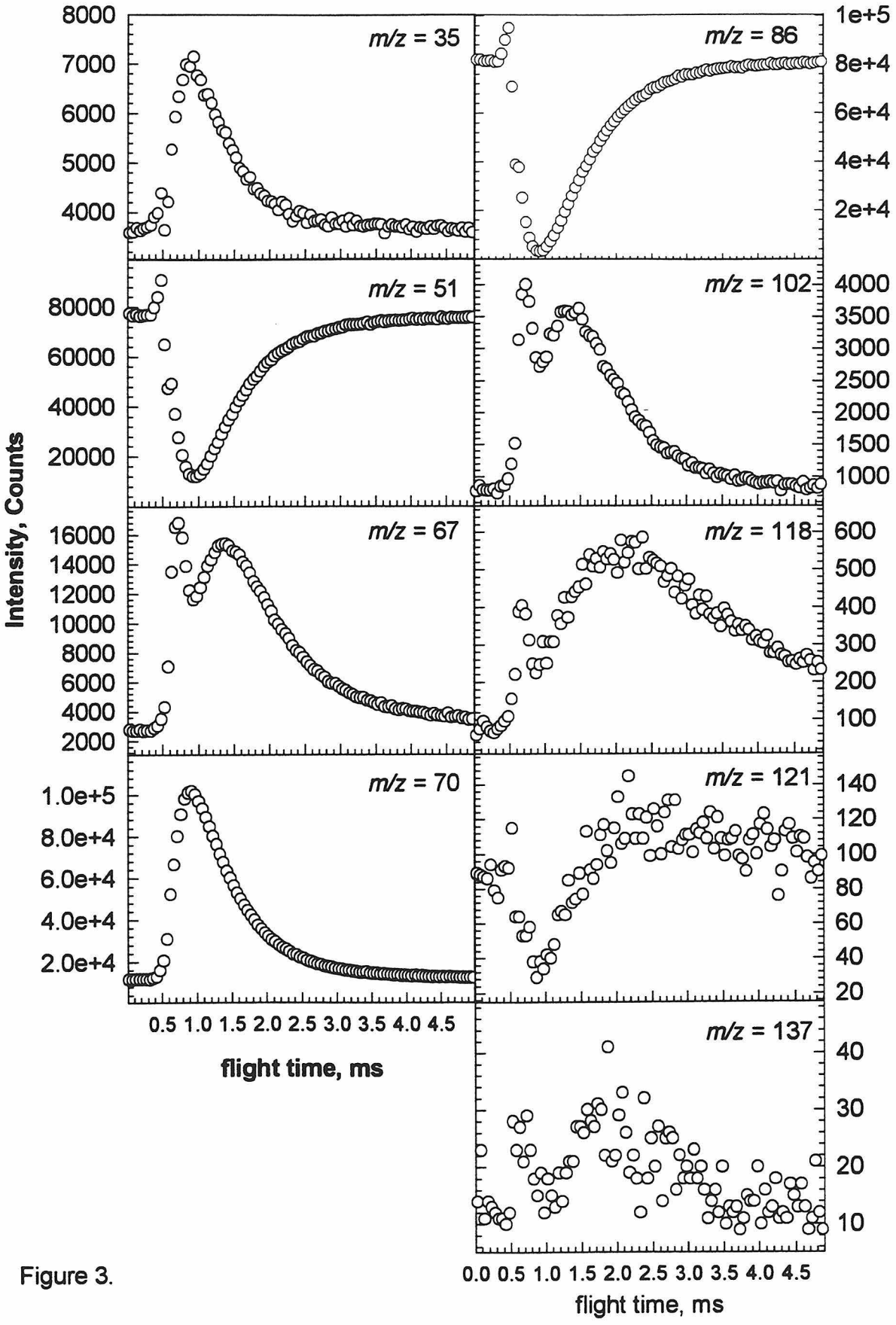
m/z = 35
m/z = 86
m/z = 51
m/z = 102
m/z = 67
m/z = 118
m/z = 70
m/z = 121
m/z = 137
Intensity, Counts
flight time, ms
flight time, ms

Figure 3.

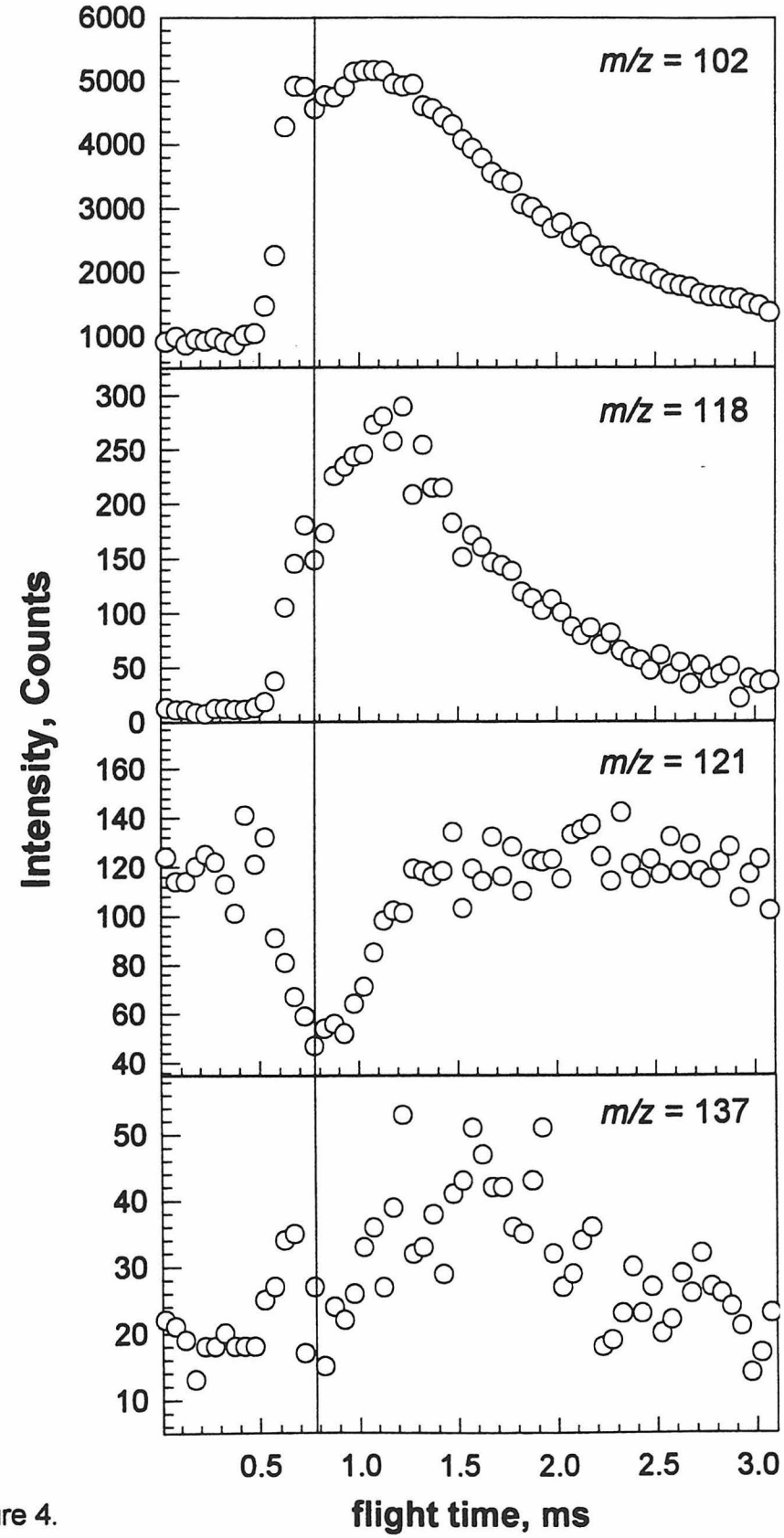
m/z = 102
m/z = 118
m/z = 121
m/z = 137
Intensity, Counts
flight time, ms
6000
5000
4000
3000
2000
1000
300
250
200
150
100
50
0
160
140
120
100
80
60
40
50
40
30
20
10
0.5
1.0
1.5
2.0
2.5
3.0

Figure 4.

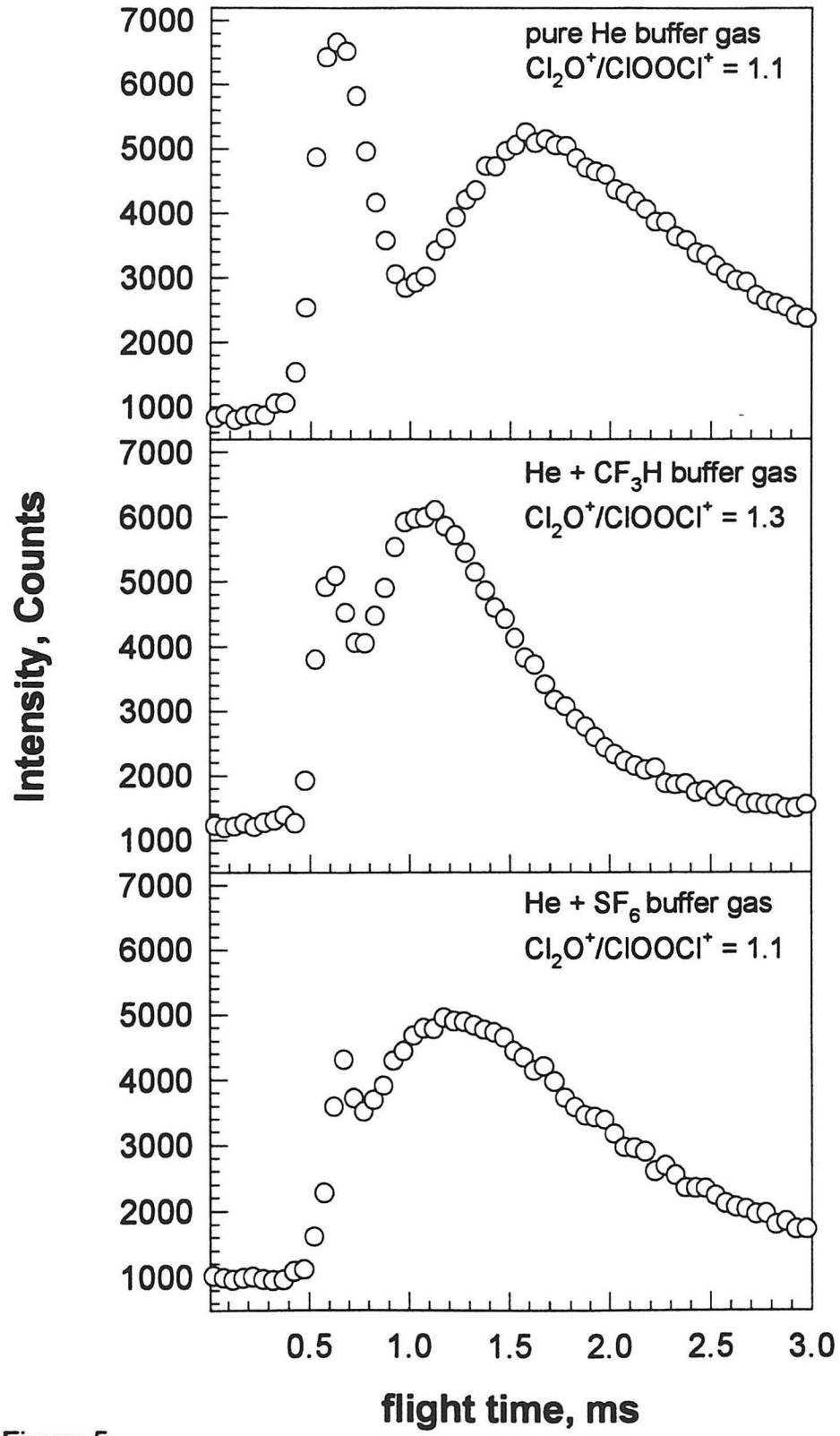
pure He buffer gas
$Cl_2O^+/ClOOCl^+$ = 1.1
He + CF_3H buffer gas
$Cl_2O^+/ClOOCl^+$ = 1.3
He + SF_6 buffer gas
$Cl_2O^+/ClOOCl^+$ = 1.1
Intensity, Counts
flight time, ms
7000
6000
5000
4000
3000
2000
1000
0.5
1.0
1.5
2.0
2.5
3.0

Figure 5.

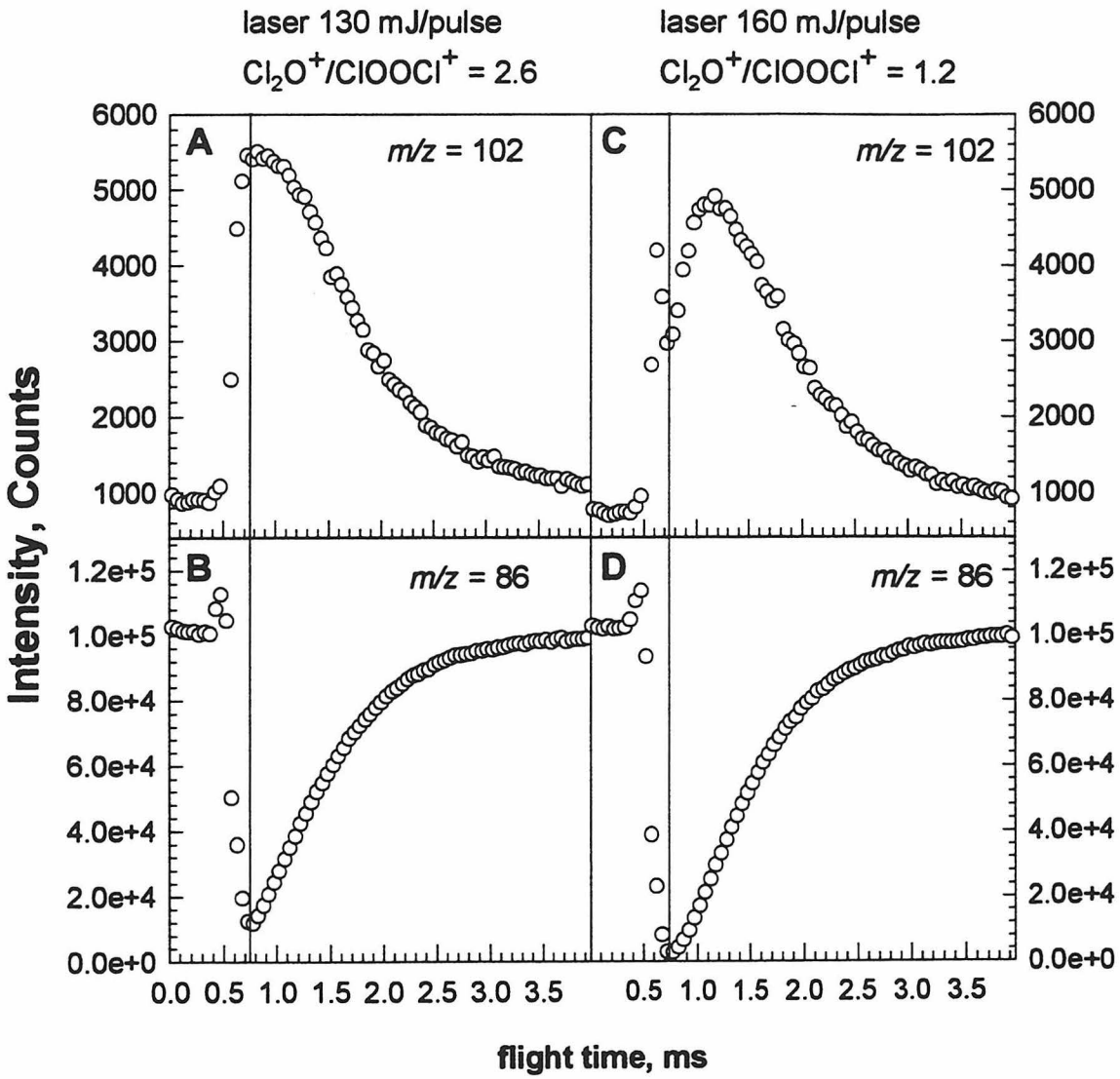
laser 130 mJ/pulse
$Cl_2O^+/ClOOCl^+$ = 2.6
laser 160 mJ/pulse
$Cl_2O^+/ClOOCl^+$ = 1.2
A
m/z = 102
C
m/z = 102
B
m/z = 86
D
m/z = 86
Intensity, Counts
flight time, ms
6000
5000
4000
3000
2000
1000
1.2e+5
1.0e+5
8.0e+4
6.0e+4
4.0e+4
2.0e+4
0.0e+0
0.0 0.5 1.0 1.5 2.0 2.5 3.0 3.5
0.5 1.0 1.5 2.0 2.5 3.0 3.5

Figure 6.

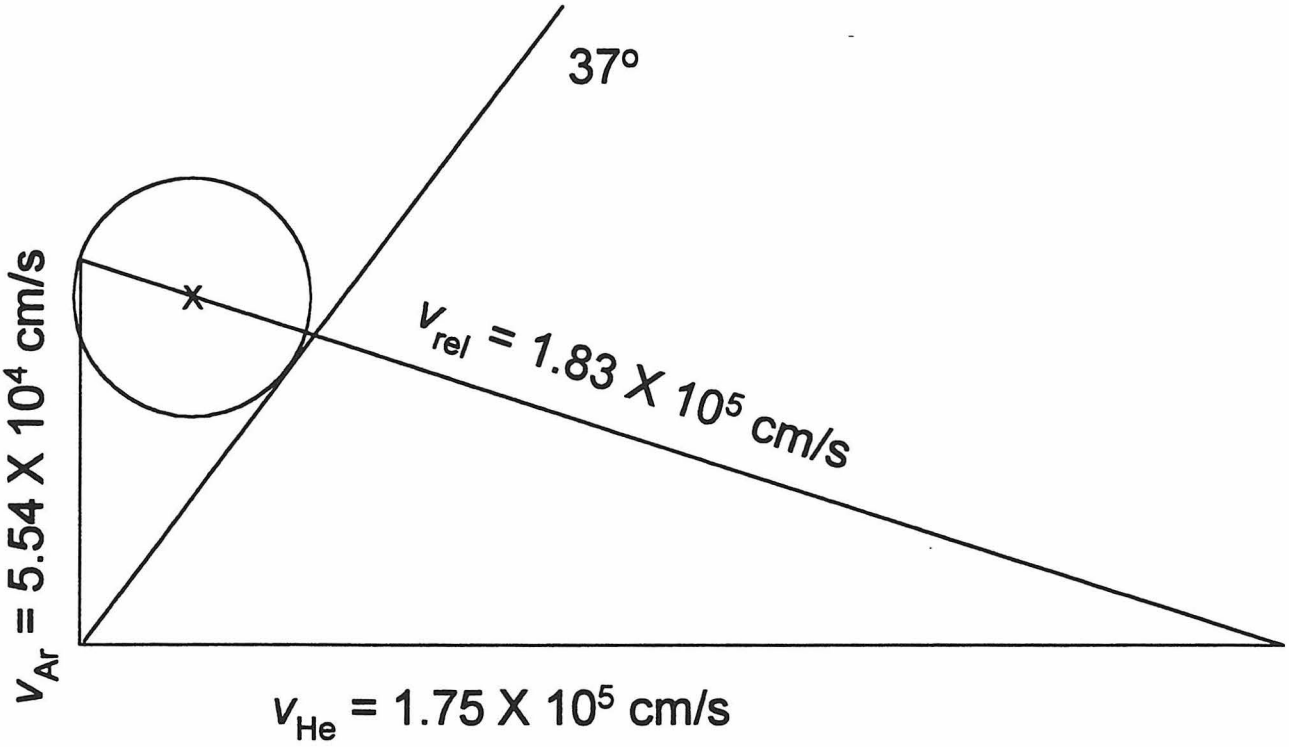

Figure 7.

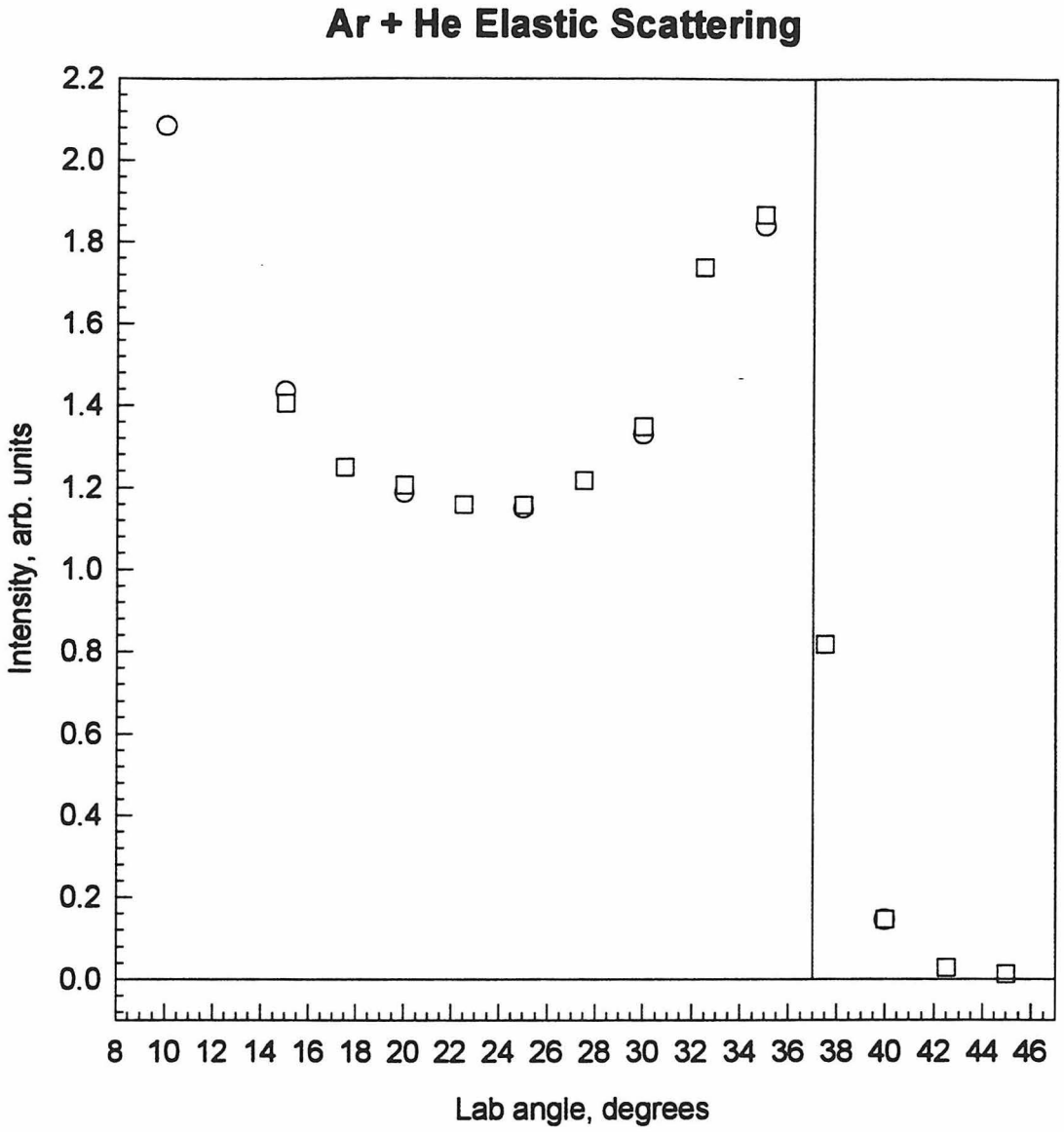
Ar + He Elastic Scattering
Intensity, arb. units
2.2
2.0
1.8
1.6
1.4
1.2
1.0
0.8
0.6
0.4
0.2
0.0
8 10 12 14 16 18 20 22 24 26 28 30 32 34 36 38 40 42 44 46
Lab angle, degrees

Figure 8.

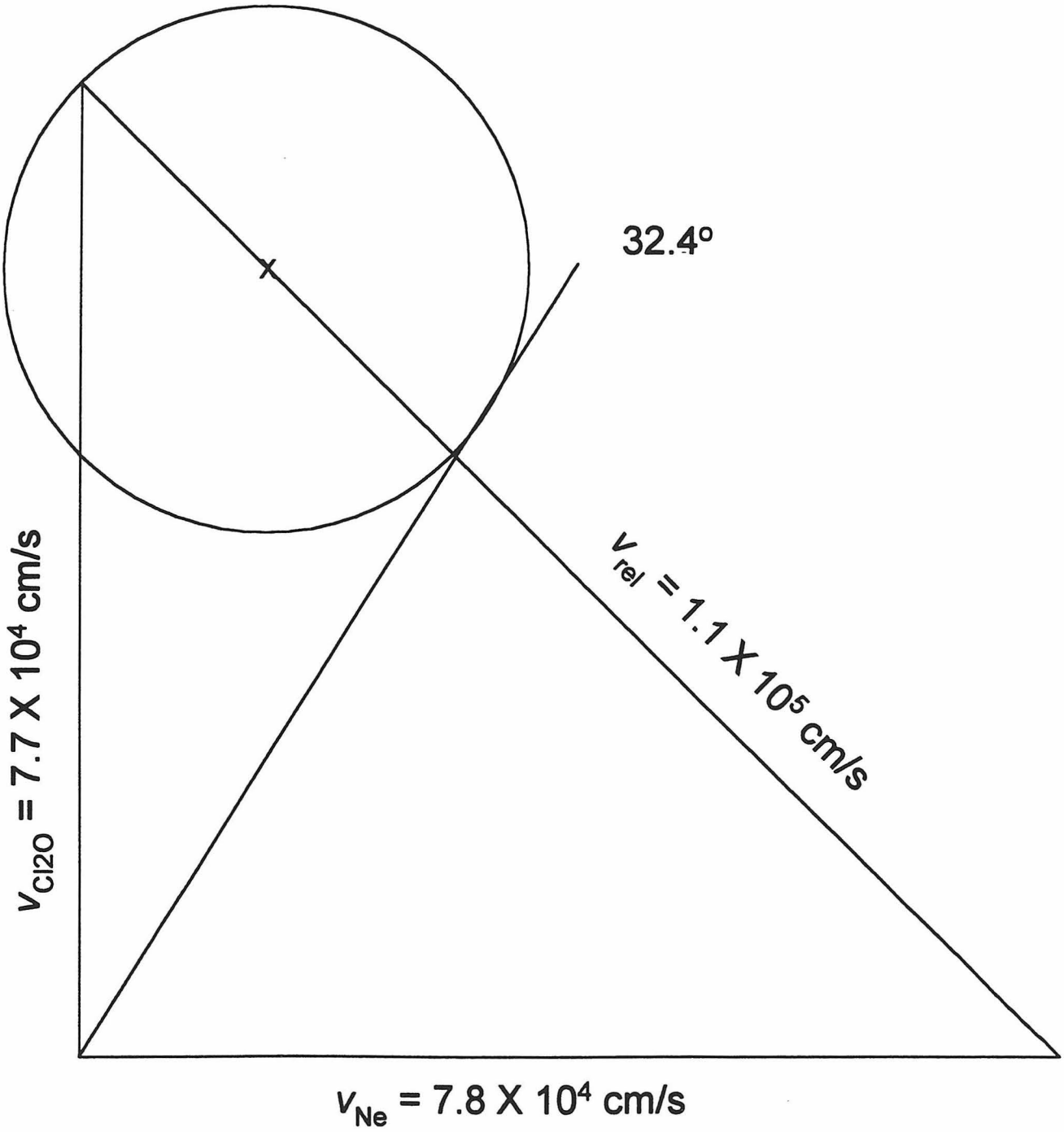

Figure 9.

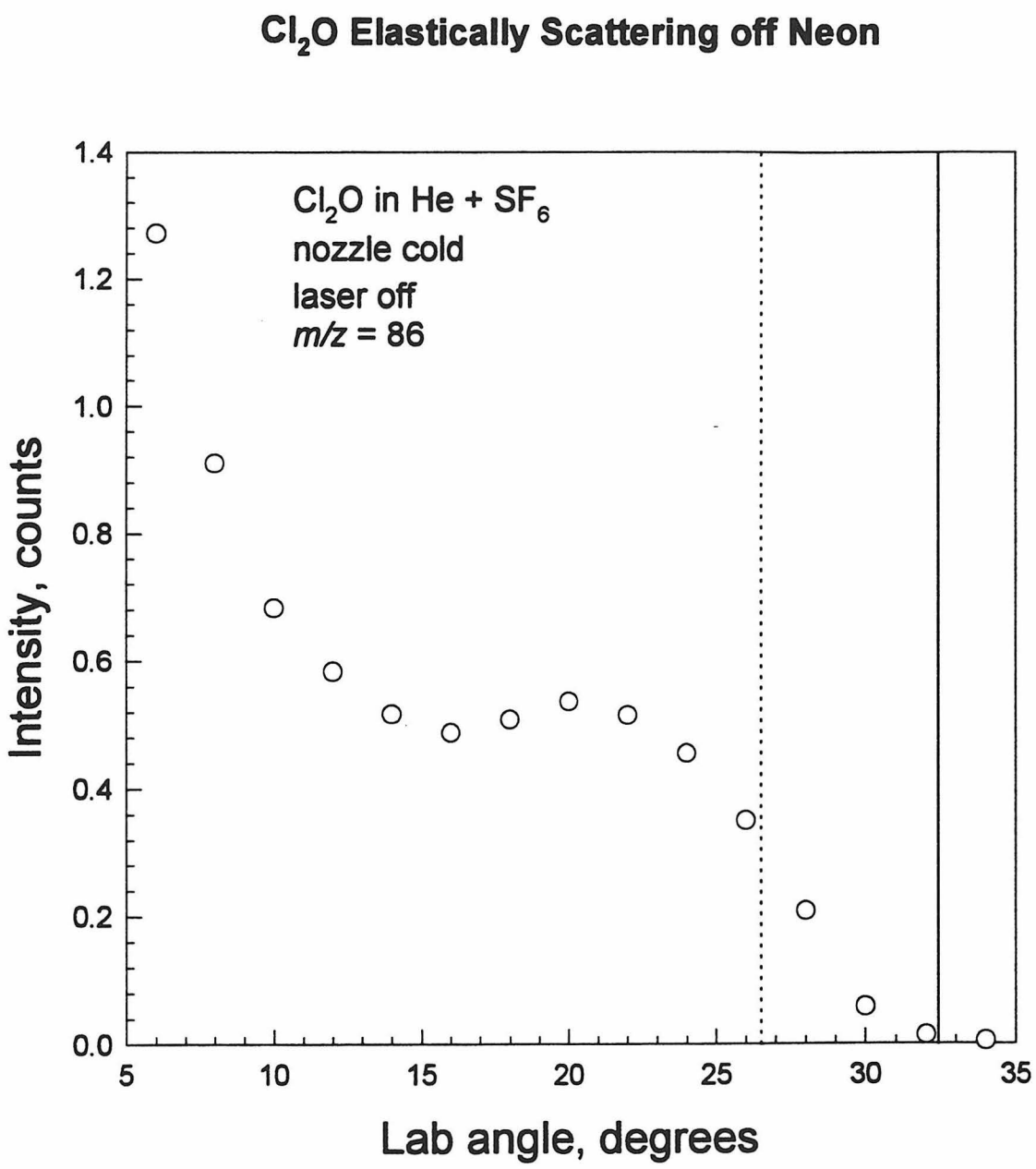
Cl2O Elastically Scattering off Neon
Cl2O in He + SF6
nozzle cold
laser off
m/z = 86
Intensity, counts
Lab angle, degrees
0.0
0.2
0.4
0.6
0.8
1.0
1.2
1.4
5
10
15
20
25
30
35

Figure 10.

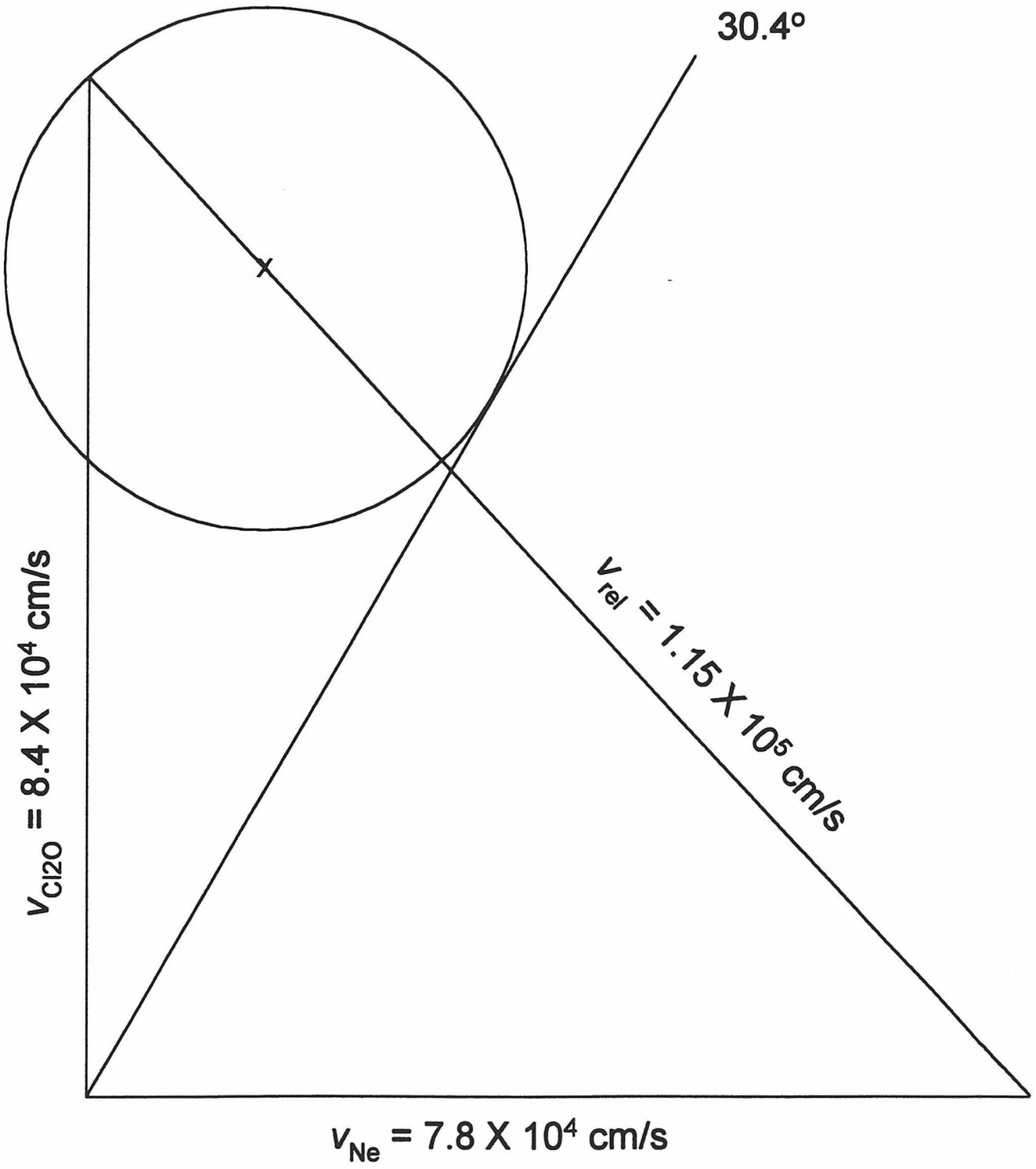

Figure 11.

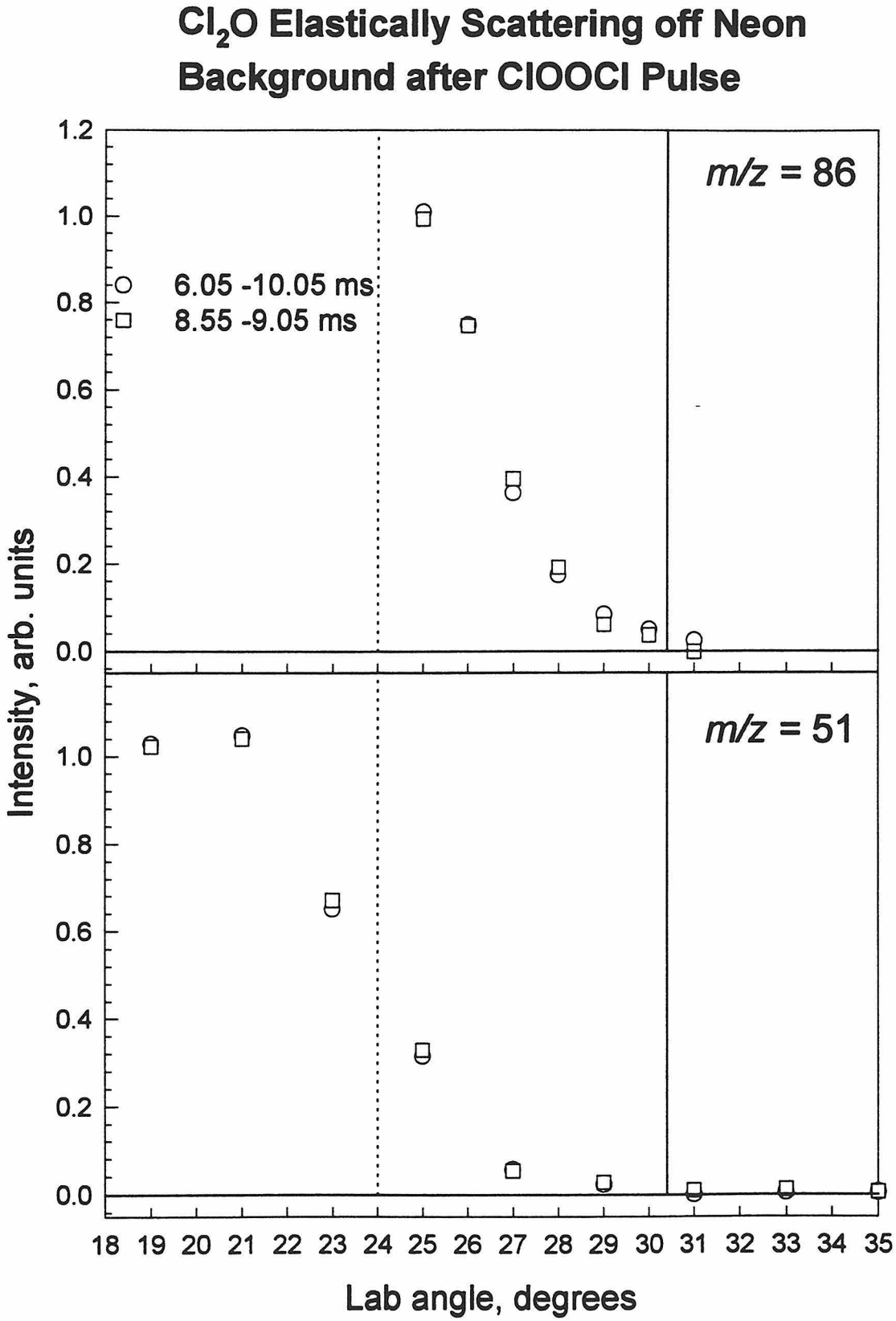
Cl2O Elastically Scattering off Neon Background after ClOOCl Pulse
m/z = 86
6.05 -10.05 ms
8.55 -9.05 ms
m/z = 51
Intensity, arb. units
Lab angle, degrees
1.2
1.0
0.8
0.6
0.4
0.2
0.0
18 19 20 21 22 23 24 25 26 27 28 29 30 31 32 33 34 35

Figure 12.

ClOOCl + Neon Elastic Scattering

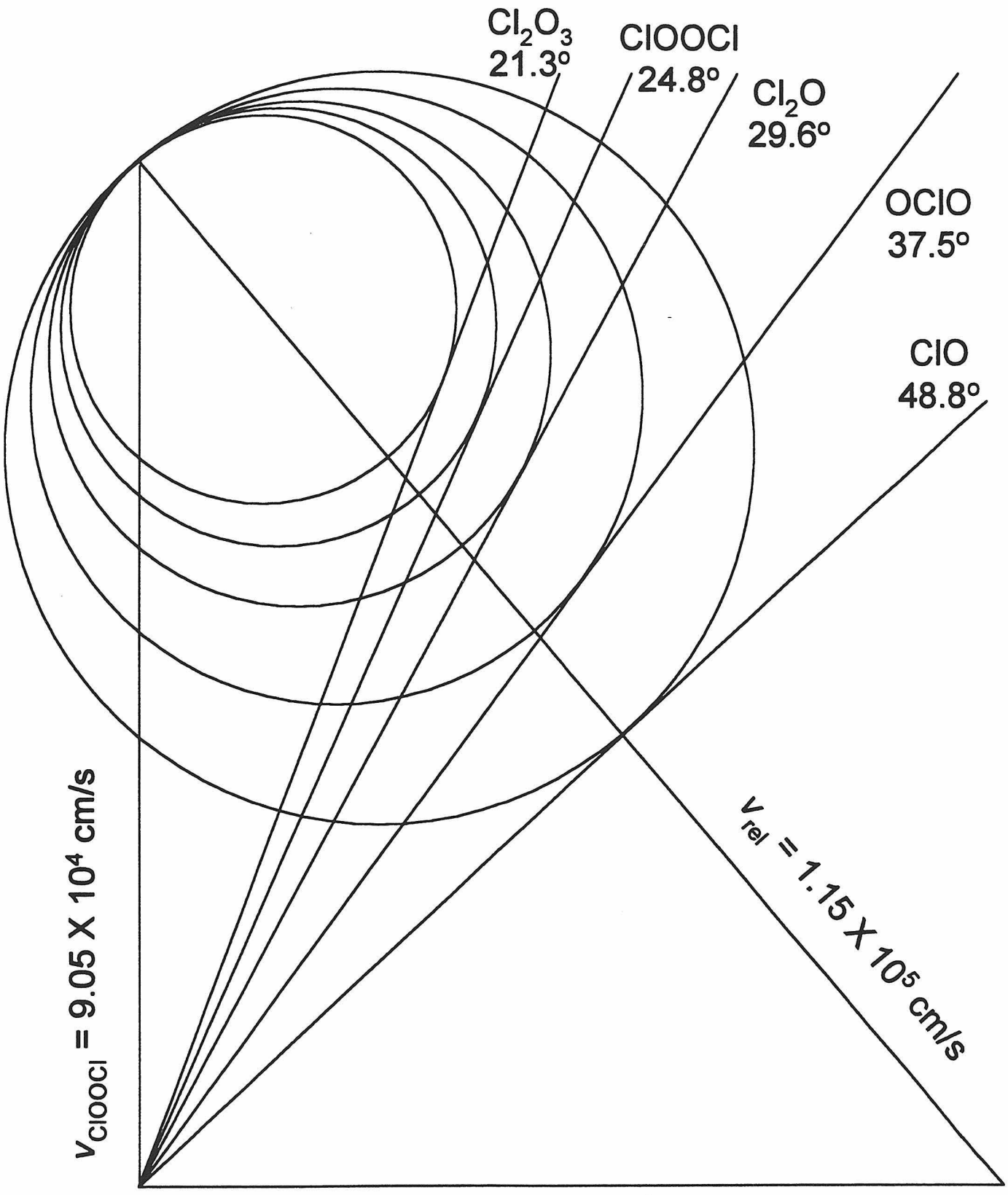

Figure 13.

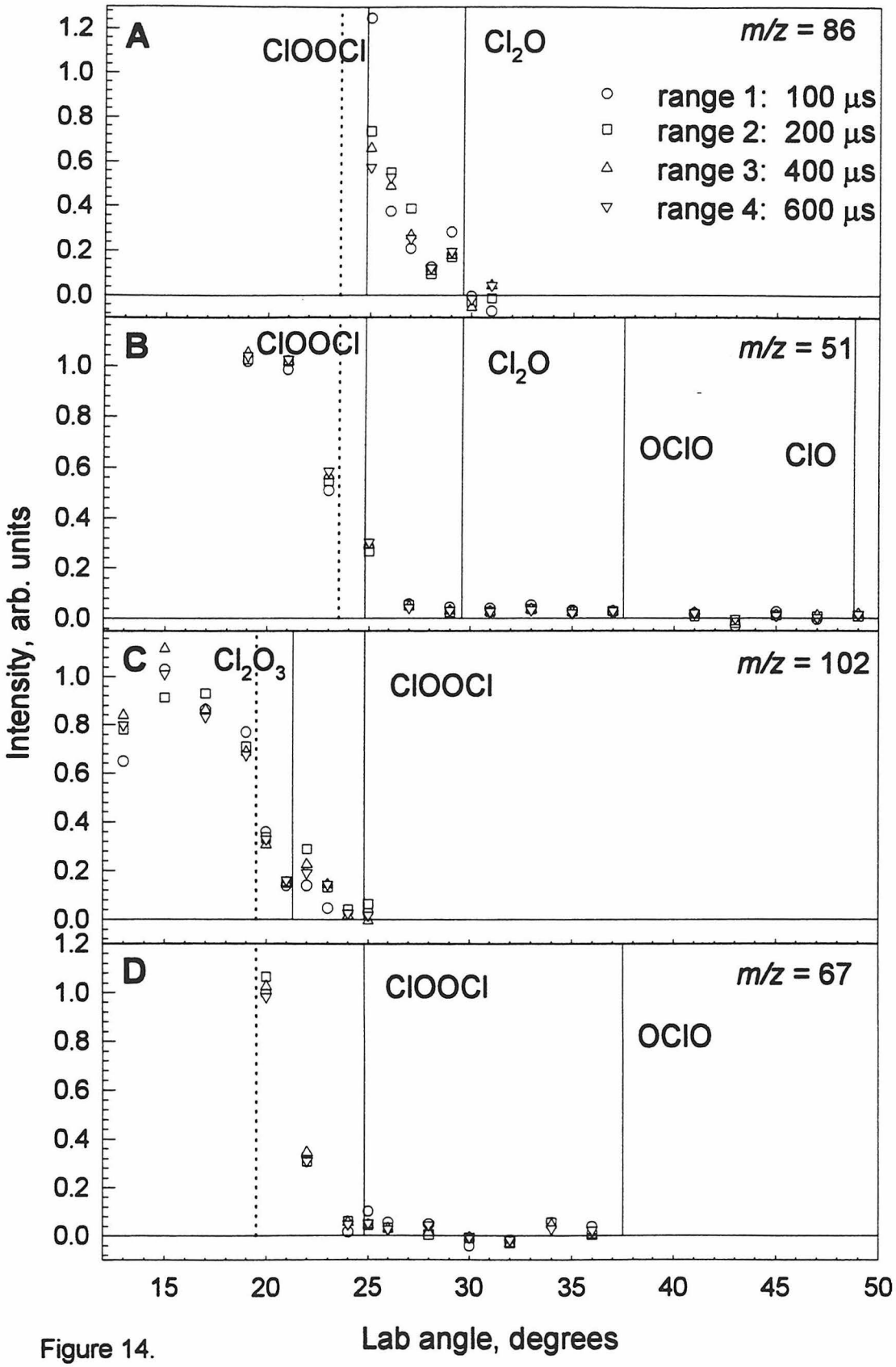
A
ClOOCl
Cl_2O
m/z = 86
range 1: 100 μs
range 2: 200 μs
range 3: 400 μs
range 4: 600 μs
B
ClOOCl
Cl_2O
m/z = 51
OClO
ClO
C
Cl_2O_3
ClOOCl
m/z = 102
D
ClOOCl
m/z = 67
OClO
Intensity, arb. units
Lab angle, degrees

Figure 14.

Chapter 4.

ClOOCl Photolysis at 248 and 308 nm

We investigated the photodissociation of ClOOCl at 248 and 308 nm using photofragment translational spectroscopy, with mass spectrometric detection of products. Time-of-flight and angular distributions of all observed products were collected in order to determine the primary and secondary photolysis channels and their relative yields. At 248 nm, Cl, ClO, and O_2 products were observed from the photodissociation of ClOOCl (after subtracting out signal arising from Cl_2O photolysis). Both ClO and Cl products were produced from multiple competing channels. At 308 nm, the data was more difficult to interpret because of extensive interference from Cl_2 and Cl_2O byproducts, but there was evidence for both Cl and ClO products from ClOOCl photolysis. The upper limit for the relative yield for ClO products is 31% at 308 nm and 19% at 248 nm.

Introduction

ClOOCl photolysis is a key step in the catalytic ozone-depleting cycle[1]

$$ClO + ClO + M \rightarrow ClOOCl + M \quad (1)$$

$$ClOOCl + h\nu \rightarrow ClOO + Cl \quad (2)$$

$$ClOO + M \rightarrow Cl + O_2 + M \quad (3)$$

$$2[\, Cl + O_3 \rightarrow ClO + O_2 \,] \quad (4)$$

$$\text{net:} \quad 2O_3 \rightarrow 3O_2.$$

This cycle is thought to be responsible for a majority of Antarctic springtime ozone depletion. Current models assume that only Cl-atom products are formed from ClOOCl photolysis. Photodissociation of ClOOCl to form ClO products would result in a null cycle, which would not deplete ozone. The branching ratio of ClOOCl photolysis into Cl and ClO products is critical in determining the effectiveness of this mechanism for destroying ozone.

Recent theoretical work[2,3,4,5] has shown that there are three thermodynamically stable isomers of Cl_2O_2, with dichlorine peroxide (ClOOCl) being the most stable, and chloryl chloride ($ClClO_2$) and chlorine chlorite (ClOClO) ~1 and ~ 10 kcal/mol less stable.[2] The ClOOCl isomer is thought to be the main dimerization product in flow tube experiments, although there is some evidence for formation of the $ClClO_2$ isomer if the walls of the flow tube are coated with water ice.[6] The ground state structural parameters[7] of the ClOOCl molecule are r_{OO} = 1.42 Å, r_{ClO} = 1.70 Å, $\angle_{ClOO}$ = 110.1°, and dihedral angle = 81.0°, as shown in Figure 1.

Possible photolysis channels for ClOOCl are[8]

$$ClOOCl + h\nu \rightarrow ClO + ClO \quad \Delta H_0^\circ = 17.1 \text{ kcal/mol} \qquad (5)$$

$$\rightarrow ClOO + Cl \qquad = 21.2 \text{ kcal/mol} \qquad (6)$$

$$\rightarrow 2Cl + O_2(^3\Sigma^-_g) \qquad = 25.9 \text{ kcal/mol} \qquad (7)$$

$$\rightarrow 2Cl + O_2(^1\Delta_g) \qquad = 48.4 \text{ kcal/mol} \qquad (8)$$

$$\rightarrow Cl + O + ClO \qquad = 80.5 \text{ kcal/mol} \qquad (9)$$

$$\rightarrow Cl_2 + O_2 \qquad = -31.2 \text{ kcal/mol.} \qquad (10)$$

Two experiments have found that the quantum yield for Cl atom production from ClOOCl photolysis is unity or greater, but large uncertainties remain in both measurements. Cox and Hayman[9] examined steady-state photolysis of Cl_2O at 254 nm and modeled the disappearance of Cl_2O and the appearance of ClOOCl in a static photolysis cell held at 203-233K. They reported a yield of 3.8 ± 1.6, which is unphysically high. In a more direct study, Molina *et al.*[10] reported a Cl atom quantum yield of 1.03 ± 0.12 from ClOOCl photolysis at 308 nm in a flow cell. They used resonance fluorescence to detect Cl atoms and calibrated the Cl signals relative to Cl_2 photolysis. No ClO was inferred from titration with NO. Their value for the quantum yield depends on the ratio of the ClOOCl absorption cross section at 245 and 308 nm, for which they used a value of 22, which is larger than more recent literature values. If the cross section ratio of 13 from the 1997 JPL evaluation of photochemical data[11] were used, the recalculated Cl atom yield would be reduced to 0.6. The absorption spectrum has also been recently measured by Huder and DeMore,[12] who observed a smaller cross section in the long-wavelength tail. Using their 245/308 nm ratio of 18.7, Molina's quantum yield for Cl would become 0.88.

A recent experiment[13] by Schmidt, Benter, and Schindler examined ClOOCl photolysis in the wavelength range 240-260 nm as well as at 308 nm. They photolyzed a ClOOCl beam produced by OClO photolysis and recombination of ClO in the ion source of a reflectron equipped with a time-of-flight mass analyzer. Products were ionized by Resonant Enhanced Multi-Photon Ionization (REMPI). Cl products were detected, but no ClO(v = 0-5) products were observed. ClO (v>5) states can not be detected via REMPI. They reported a quantum yield for the Cl + ClOO channel of $\Phi = 0.65 \pm 0.15$ at 250 nm, and an average Cl translational energy of 0.42 ± 0.05 eV.

We have examined the photodissociation of ClOOCl at 248 and 308 nm in a molecular beam experiment with mass spectrometric detection. Direct detection of both Cl and ClO photoproducts provides a cross-section independent means of determining the branching ratio between Cl and ClO products. The relative detection efficiencies for Cl and ClO were calibrated by performing Cl_2O photolysis experiments at 308 nm, where the only photolysis products are Cl and ClO in a 1:1 ratio.

Experiment

The experiments were performed on a crossed molecular beams apparatus[14] modified for laser photodissociation.[15,16,17] The ClOOCl beam, described in the previous chapter, was crossed at right angles with the focused UV radiation from a pulsed excimer laser in the main vacuum chamber. The photodissociation products were detected off the beam axis by a mass spectrometer that is rotatable in the plane of the laser and molecular beams. Only photofragments which scatter out of the molecular beam are detected; undissociated

molecules do not contribute to the scattered signal. Product time-of-flight (TOF) distributions were collected at various detector angles by monitoring the signal from the mass spectrometer at a single mass as a function of time and accumulating the signal over many laser pulses at each angle.

Photofragments traveled 33.3 or 33.5 cm from the intersection of the two beams to the Brink electron bombardment ionizer. The shape and position of the electron cloud for this type of ionizer depend on the ionizer conditions used. Two ionizer settings were used to obtain data. The initial setting, with which almost all of the 308 nm data and the preliminary 248 nm data were taken, was optimized on axis with an argon beam using the small detector aperture. The other setting was obtained by optimizing the $m/z = 51$ signal from Cl_2O photolysis using the large aperture for off-axis detection. The electron energies were nominally 80 and 160 eV for the first and second settings, respectively. The mass resolution of the mass spectrometer was set so that $\Delta m \geq 2$ amu, in order to increase the signal. Pulses from the Daly-type ion counter were sent to a LeCroy 8818 discriminator and then recorded by an EG&G Ortec ACE-MCS multichannel scaler with a dwell time of 2 μs per channel.

We determined the velocity distributions of the parent ClOOCl molecules by several methods. The beam was chopped with a slotted disk which was synchronized with the source laser pulse and then delayed to sample the ClOOCl pulse. TOF distributions were collected at various ion fragment masses and then converted to a velocity distribution $N(v)$ which was fit with an assumed functional form, $N(v) \propto v^2 \exp[-(v/\alpha - S)^2]$, where $N(v)$ is the number density of molecules with speeds in the range v to $v + dv$, α is the width of the speed distribution, and S is the ratio of the stream velocity v_s to the width α.[18] The TOF wheel was

only used for beam velocity measurements are was removed for source optimization and the photodissociation experiments. Since the beam velocity depended on the section of the ClOOCl pulse sampled and the ClOOCl beam conditions, the actual beam velocity was determined independently for each experiment by examining the diatomic Cl_2 photolysis signal at $m/z = 35$ for the 308 nm experiments and the diatomic ClO photolysis signal at $m/z = 35$ for the 248 nm experiments. The beam velocities obtained in this manner agreed very well with each other, with an average beam velocity of 9.1×10^4 cm/s (α = 0.83-0.86, S = 10.6-10.9).

The measured flight time was the sum of the time for the photofragment to travel to the ionizer and the ion flight time from the ionizer to the detector. The ion flight times were determined to be $4.68(m/z)^{1/2}$ μs and $3.2(m/z)^{1/2}$ μs for the first and second ionizer settings, respectively. Corrections for ion flight time were made in the fitting routine, so the abscissa of all TOF spectra shown are total flight times.

The ultraviolet radiation source for the ClOOCl photolysis was a Lambda Physik EMG 150 excimer laser operating in oscillator only mode, which was used to provide 248 nm (KrF) or 308 nm (XeCl) radiation. Typical pulse energies used were ~ 70 mJ/pulse at 248 nm and 20-100 mJ/pulse at 308 nm at a repetition rate of 40 Hz. The laser light was partially preferentially polarized (~56%) in the plane perpendicular to the scattering plane and parallel to the molecular beam. The rectangular-shaped laser beam was focused with a combination of a CaF_2 cylindrical lens (focal length f = +600 mm) and a UV grade fused silica plano-convex lens (f = +300 mm) to a ~ 1.5 mm wide × 3mm high spot at the interaction region.

At 308 nm, the delay between the firing of the source laser and the photolysis laser

was set by maximizing the photodissociation signal at $m/z = 35$ from Cl_2. Since the maximum Cl_2O depletion and the Cl_2 and ClOOCl peak positions in the source TOF spectra coincide, maximizing the Cl signal from Cl_2 photolysis should coincide with the maximum Cl_2O depletion and thus the highest ClOOCl:Cl_2O ratio. At 248 nm, the photolysis laser delay was based on the beam shape and timing, and checked for consistency by comparing with delays set for similar beam profiles at 308 nm. Since the maximum ClOOCl signal spanned several hundred microseconds, the delay only had to be within ± 100 μs of the actual peak center.

TOF distributions of the photoproducts from photolysis at both wavelengths were collected at $m/z =$ 16, 32, 35, 51, 67, and 70, corresponding to O^+, O_2^+, Cl^+, ClO^+, $ClOO^+$, and Cl_2^+, respectively. These distributions were recorded at detector angles from 15° to 50° and were averaged for 100,000 to 2,000,000 laser pulses, depending on signal level. No significant signal was observed at m/z = 16 (O^+), 67 ($ClOO^+$), or 70 (Cl_2^+) for either wavelength, or at $m/z = 32$ (O_2^+) at 308 nm. The $m/z = 32$ signal-to-noise ratio was low because of the large background O_2 signal, and the lower ClOOCl absorption cross section at 308 nm made it impossible to observe any O_2^+ signal.

Laboratory angular distributions for $m/z = 35$ and 51 were recorded at detector angles 15°, 30°, 40°, and 50° in both the 248 and 308 nm experiments, and for $m/z = 32$ over the same angular range in the 248 nm experiment. In order to eliminate systematic error resulting from possible long-term drifts, the detector was rotated back and forth over this angular range, and TOF distributions were collected for 50,000 or 100,000 laser pulses at each increment. The resulting TOF distributions at each angle were averaged for a total of 330,000 pulses for $m/z = 32$ and 250,000 pulses for $m/z = 35$ and 51 at 248 nm, and 500,000

pulses at $m/z = 51$ and 600,000 pulses at $m/z = 35$ at 308 nm. In the 248 nm experiment, we continued recording 50,000 pulse scans at a detector angle of 30° for $m/z = 35$ and 51 for a total of 500,000 pulses at each mass. In the 308 nm experiment, 20 sets of 50,000 pulse scans were obtained separately from the angular distribution experiments at 15° and 40° for a total of 1,000,000 pulses at each angle, and 5 sets of 100,000 pulse scans were obtained at 30° for a total of 500,000 pulses. These back-and-forth scans were obtained in order to accurately measure the relative signal intensities for determination of the branching ratio between the Cl and ClO products. The peak counts per pulse at $m/z = 32$, 35, and 51 at 248 nm for a detector angle of 30° were 0.0048, 0.0137, and 0.0035 cts/pulse, respectively. At 308 nm, the counts per pulse at the peak channel at 30° were $m/z = 35$, 0.034 cts/pulse and $m/z = 51$, 0.002 cts/pulse.

Other species in the molecular beam besides ClOOCl contributed to the photolysis signal. These included ClO and Cl_2O at 248 nm and Cl_2, ClO, and Cl_2O at 308 nm. Photolysis experiments of Cl_2 and Cl_2O were performed at both wavelengths, although the Cl_2 photolysis signal was negligible at 248 nm. A molecular beam of Cl_2 was formed by flowing the He/SF_6 buffer gas mixture over liquid Cl_2 at -95° C and expanding through the nozzle, which was held at the same temperature as in the ClOOCl photolysis experiments. Data was collected at $m/z = 35$ at 10°, 20°, 30°, 40°, and 50° for 5 scans of 20,000 pulses each, rotating the detector back and forth among the angles. The analysis of the Cl_2 photolysis data provided a check on the input parameters for our fitting routine. Cl_2O photolysis experiments were performed before or after each ClOOCl data taking session. The Cl_2O beam was formed by turning off the source laser used to make the ClOOCl. The results

of the Cl_2O photolysis experiments have been published elsewhere.[19,20]

The relative detector sensitivity for detecting Cl and ClO was required for determination of the Cl/ClO branching ratio. The Cl_2O photolysis experiment at 308 nm also allowed for calibration of the relative detector sensitivities for Cl and ClO, since the only photolysis products at this wavelength are Cl and ClO in a 1:1 ratio.

Results and Analysis

Analysis Overview

A forward convolution technique was utilized in the analysis of TOF and angular distributions. For each two-body dissociation channel, trial center-of-mass (c.m.) translational energy $P(E_T)$ and angular $w(\theta)$ distributions were transformed to the lab frame of reference to obtain a predicted number density TOF distribution $N(t)$. The predicted $N(t)$ distributions were compared with the experimental data, and the $P(E_T)$ and $w(\theta)$ distributions were adjusted iteratively until the predicted TOF distributions agreed with the observed distributions at all angles.

An extension of this procedure[21] was needed to model three-body dissociation. Spontaneous three-body dissociation can occur via a concerted or a stepwise mechanism. We will use the terms defined by Maul and Gericke,[22] based on terms originally developed by Dewar[23] for the three body decay of a molecule ABC. A concerted decay takes place in a single kinetic event, whereas a sequential decay is characterized by two independent dissociation steps in which the decay of the primary fragment AB is not influenced by forces from the first fragment C. The kinetic event is taken to be a rotational period. Thus, a three

body dissociation is called *sequential* if the time span Δt between the first and second bond cleavage steps is greater than a rotational period τ_{rot} of the primary fragment AB. As Δt becomes smaller than τ_{rot}, the two decay processes are no longer independent of each other, and the dissociation is called *concerted*. As Δt approaches zero, all bond breaking processes take place simultaneously, and the dissociation occurs by the *synchronous concerted* mechanism, as opposed to the *asynchronous concerted* mechanism in which $0 < \Delta t \leq \tau_{rot}$.

The sequential dissociation of ClOOCl

$$ClOOCl + h\nu \rightarrow Cl + ClOO \rightarrow Cl + Cl + O_2$$

was modeled by separating the dissociation into two independent center-of-mass reference frames in which linear momentum is conserved. Thus, a primary dissociation step Cl + ClOO was modelled, followed by secondary dissociation of the ClOO to Cl + O_2. The secondary angular distribution $P(\Omega)$ is referenced relative to the primary c.m. dissociation direction (i.e. along the Cl–O bond, assuming the geometry doesn't change from the ground state) and not the electric vector of the laser. Since the rotational excitation of the intermediate ClOO may be broad, the secondary angular distribution is likely to be highly averaged. If the secondary angular distribution is asymmetric about $\Omega = 90°$, then the dissociation occurs within a rotational period, and is considered asynchronous concerted rather than stepwise.[24]

The synchronous concerted dissociation channel

$$ClOOCl + h\nu \rightarrow Cl + O_2 + Cl$$

was modeled with a separate analysis routine.[25] An overall translational energy distribution for the total energy released by all three fragments was determined by a forward convolution technique. The angles between the relative c.m. velocity vectors were determined for a given

dissociation geometry by assuming that dissociation occurs along the Cl–O bonds, and angle width parameters were chosen which determined the width of the assumed Gaussian distribution of geometries about the most probable dissociation geometry. Given the $P(E_T)$ and the angles between the c.m. velocity vectors, conservation of linear momentum and energy were applied to give a predicted TOF spectra. The parameters were adjusted until the predicted TOF matched the observed O_2 and Cl data at all angles.

Stimulated secondary dissociation, in which a primary photofragment absorbs a second photon during the laser pulse and dissociates, was not modeled in this work. The laser power was kept low so that secondary photodissociation was minimized.

Relative Scaling of Primary and Secondary Distributions

The scaling for the secondary products relative to the primary products when both only contributed signal to a single mass was determined by modeling a single primary channel and the corresponding secondary dissociation in the analysis routine. The ratio of the primary to secondary scaling factors was then set to be 1:1, in which case the analysis routine rigorously enforces the relative scaling. The ratio between the integrals of the primary and secondary products at each angle obtained by this method was then used to determine the secondary contribution from each channel when adding in all of the other channels that contribute signal to that mass. Where the primary or secondary channel contributes signal to multiple masses, but at least one of the masses has a contribution from both primary and secondary dissociations, the scaling for a given channel was more difficult to determine but a good approximation could be made. For instance, for the $ClOOCl + h\nu \rightarrow ClO(X) + ClO(A) \rightarrow ClO(X) + Cl + O(^3P)$ channel, the scaling for the secondary Cl products was first

approximated by modeling only the primary and secondary dissociations from this channel at $m/z = 35$. Because 1) 13% of the ClO (X) fragments in the ionizer to $m/z = 35$ and 2) the relative detector efficiency for ClO is approximately equal to that for Cl, the ratio of the primary to secondary scaling factor was set to 0.13:1.

Relative Yields

The total c.m. flux distribution for a given channel was assumed to be proportional to the product of the $P(E_T)$ and $w(\theta)$ distributions, which were determined for each channel by simultaneously fitting of all the laboratory TOF distributions for all observed channels. The relative proportionality of the product fluxes for two channels which contributed to the signal at $m/z = 35$ was determined by fitting both primary components of the $m/z = 35$ TOF distributions. The relative detection efficiencies of ClO and Cl at $m/z = 35$ were calibrated using information from an analogous study of Cl_2O photolysis. The flux of ClO for a given channel detected at $m/z = 35$ is equal to the product of the total flux of ClO (I_{ClO}) for that channel, the total ionization cross section of ClO (σ_{ClO}), and the fraction of ClO that fragments to $m/z = 35$ in the ionizer [$f_{ClO}(35)$]:

$$I^{+}_{ClO}(35) = I_{ClO} \cdot \sigma_{ClO} \cdot f_{ClO}(35) \qquad (1)$$

When two photolysis channels can lead either to ClO or Cl photoproducts, the ratio of the relative yield for the two channels is given by:

$$\frac{I_{ClO}}{I_{Cl}} = \frac{I^{+}_{ClO}(35)}{I^{+}_{Cl}(35)} \cdot \frac{\sigma_{Cl}}{\sigma_{ClO}} \cdot \frac{f_{Cl}(35)}{f_{ClO}(35)} \qquad (2)$$

where $f_{Cl}(35) = 1$. For Cl_2O photolysis at 308 nm ($Cl_2O + h\nu \rightarrow ClO + Cl$), this ratio must be 1, and the relative ionization cross sections for Cl and ClO can be obtained. The first factor on the right-hand side of this equation is determined from the primary c.m. flux distribution scaling factors obtained by simultaneously fitting all of the lab TOF distributions at $m/z = 35$. The scaling factors between the primary flux distributions remained constant for all angles. The third factor in eq. 2 depends on the fragmentation pattern of ClO, which depends on the internal energy of the ClO. Eq. (2) implicitly assumes that σ_{ClO} does not vary with internal excitation of ClO for a given ionizer condition. Because we used the Cl_2O photolysis experiment for calibration, no assumptions about absolute detection efficiencies or the mass-dependent transmission of the quadrupole mass filter were required.

248 nm

Overview of Results

Photolysis signal was observed at ClO^+, O_2^+, and Cl^+ masses. The signal at $m/z = 51$ (see figure 2) comprised a fast bimodal peak and a slow broad peak. The signal at $m/z = 32$, shown in figure 3, was sharp and fast, with the leading edge arriving at ≤ 100 μs for a detector angle of 15°. This arrival time was faster than any of the observed signal at the other two masses. The largest amount of signal was observed at $m/z = 35$ (see figure 4), where the data consisted of a fast peak with multiple unresolved components and a slow sharp peak and a slow broad peak that were prominent at smaller angles.

ClO Contribution

The sharp peak in the $m/z = 35$ TOF distribution arriving at ≈ 235 μs that was prominent at smaller detector angles was assigned to Cl products from photolysis of diatomic

ClO radicals which remained in the beam. At 248 nm, ClO photolyzes to produce $Cl(^2P_{3/2})$ + $O(^1D)$ products.[26] The bond dissociation energy[27] for this channel is 108.78 kcal/mol. Vibrations are not efficiently cooled in a supersonic expansion, so the vibrational temperature of the ClO will be ~ 200K, at which temperature greater than 99% of the ClO is in the ground vibrational state. The 248 nm photon energy is 115.01 kcal/mol. Since ClO is a diatomic, all of the energy left after breaking the ClO bond must appear as fragment translational energy. Thus, the translational energy distribution used to fit the ClO consisted of a spike ~ 0.1 kcal/mol wide at 6.22 kcal/mol and another spike 0.91 kcal/mol higher in energy and 19.9 times weaker corresponding to dissociation of spin-orbit excited ClO, assuming a thermal distribution at 200 K for the excited ClO. The beam velocity was adjusted until the fit to the ClO peak matched the observed data. The resulting beam velocity was then fixed and used in all subsequent analysis for that experimental run. The angular distribution for this channel was fit by an anisotropy parameter of 2.0.

<u>Cl_2O Contribution</u>

Because the beam contains Cl_2O as well as ClOOCl, some Cl_2O contribution to the m/z = 51 data is expected. The translational energy and angular distribution for Cl_2O photolysis were obtained from the Cl_2O photolysis experiments. If we assumed that the m/z = 51 signal from the ClOOCl beam photolysis arose solely from Cl_2O for a given angle, the other angles could be scaled to the Cl_2O angular distribution as shown in Figure 5. The leading edge of the resulting predicted TOF spectra rose faster than the observed data, especially at the smaller angles, and fell off too quickly with increasing angle. The leading edge discrepancy is evident in Figure 6, which compares the best Cl_2O fit to the data at Θ_{LAB}

= 30°. Furthermore, the two peaks in the TOF spectrum do not correspond well to the three components in the predicted Cl_2O spectrum. Since the beam velocity is constrained by the ClO bond energy (which is well known) in order to fit the ClO photolysis signal at $m/z = 35$, the discrepancy with the rising edge can not be explained by an incorrect beam velocity. Thus, it seems reasonable to conclude that the signal at $m/z = 51$ does not all arise from Cl_2O photolysis. The maximum reasonable contribution to the $m/z = 51$ signal from Cl_2O photolysis products was determined by scaling the Cl_2O contribution as high as possible without causing the rising edge of the predicted TOF to become faster than the observed data. This scaling was carried out at 15° (see Figure 7), where the rising edge of the TOF is the most sensitive, and the remaining angles were scaled according to the Cl_2O angular distribution.

The Cl_2O contribution at $m/z = 35$, including both Cl photofragments and ClO that fragmented in the ionizer to form Cl^+, was obtained based on the Cl_2O contribution determined at $m/z = 51$ and scaled based on the pure Cl_2O experiments. From the Cl_2O experiments, the extent of ClO fragmentation in the ionizer was observed to depend approximately linearly on the ClO internal energy.

ClO + ClO Channels

We assigned the remaining fast signal at $m/z = 51$ to ClO from ClOOCl photolysis. The resulting $P(E_T)$ distribution, shown in Figure 8, was bimodal. The $w(\theta)$ distribution was fit with an anisotropy parameter of $\beta = 0.5$. The data is clearly bimodal, with the two peaks becoming better resolved as more scans were averaged. The dip between the two peaks occurs at approximately the same time as the prominent middle component in the Cl_2O

distribution, and reducing the Cl_2O contribution could not eliminate the bimodality of the ClO + ClO translational energy distribution. The average energy released in translation was $\langle E_T \rangle$ = 26 kcal/mol, or ~ 26% of E_{avail}, indicating that most of the energy ($\langle E_{int} \rangle$ = 73.5 kcal/mol) tended to go into internal excitation of the ClO products. The ClO bond dissociation energy is 63.4 kcal/mol and the maximum internal energy in the ClO products is E_{int} = 93.5 kcal/mol, so the energy would have to be unequally distributed between the two ClO fragments for spontaneous ClO bond breakage to occur. The signal at m/z = 51 is unlikely to have any contribution from a ClO^+ crack from ClOO because 1) the Cl-O bond in ClOO is very weak, and any ClOO from the primary dissociation is unlikely to survive intact, and 2) the ClOO equilibrium structure resembles a Cl loosely associated with an O_2 molecule.

Slow signal, which was more prominent at the smaller angles, was also observed at m/z = 51. We assigned this slow ClO signal to the channel

$$ClOOCl + h\nu \rightarrow ClO(X) + ClO(A) \rightarrow ClO(X) + Cl + O(^3P).$$

The $P(E_T)$ distribution fell more rapidly with increasing energy than calculated for statistical RRKM dissociation to ground state products. The ClO $A\ ^2\Pi$ state is 90.5 kcal/mol above the ground state, leaving 9 kcal/mol available to be partitioned into translational and internal energy. If one of the ClO fragments was formed in the $A\ ^2\Pi$ state (and the other in the ground state $X\ ^2\Pi$) then the resulting statistical translational energy distribution (see Figure 6) predicted TOF spectra which matched the observed data. The ClO $A\ ^2\Pi$ state predissociates rapidly to give Cl + $O(^3P)$, so the slow signal observed at m/z = 51 consists only of the ground state counterfragment. The angular distribution for this slow peak was fit by $\beta = 0$, indicating that the excited ClOOCl may live longer than a rotational period.

The slow signal was not present when the source laser was off (that is, for pure Cl_2O photolysis); thus, it was correlated with the ClOOCl beam. The signal could also arise from photodissociation of clusters containing ClOOCl. However, when looking at the ClOOCl beam TOF spectra, the ClOOCl-correlated cluster peaks rose much more slowly than the ClOOCl peak, so at the photolysis laser delay we chose (sampling the ClOOCl peak), the cluster concentration should be small.

The contribution at m/z = 35 from the ClO products from ClOOCl photolysis fragmenting in the ionizer was determined by assuming that the internal energy in the two ClO products was distributed evenly and calculating the extent of fragmentation based on the average internal energy of the ClO. The percent of signal fragmenting to m/z = 35 vs. internal energy was plotted for the three Cl_2O components, and the ClOOCl fragmentation values were inferred from this plot. The average internal energy for the fast peak was 37 kcal/mol, resulting in 32% of the ClO fragmenting to m/z = 35, and the average internal energy of the slow peak was ~ 3 kcal/mol, which was extrapolated to give 13% of the slow ClO fragmenting to Cl^+. Spontaneous secondary dissociation of the ClO $A^2\Pi$ state was also modeled. The ClO A state energy is 90.5 kcal/mol above the ground state, and the ClO bond dissociation energy is 63.4 kcal/mol, so that the minimum translational energy of the secondary Cl products will be 27.1 kcal/mol. Up to 9 kcal/mol from the primary dissociation can be partitioned into the ClO(A) internal energy, which would go into translational energy of the secondary products; the statistical translational energy distribution ranging from 27.1 to 36.1 kcal/mol shown in Figure 8 was used to model the secondary dissociation. The secondary angular distribution was assumed to be isotropic. The signal from the secondary

dissociation of ClO (*A*) contributed to the slow shoulder of the fast peak in the $m/z = 35$ TOF spectra.

Concerted Cl + O_2 + Cl Channel

A sharp, fast signal was observed at $m/z = 32$, shown in figure 3. Because this signal was faster than the observed Cl^+ signal, we assigned it to O_2 recoiling from both Cl atoms from the concerted synchronous dissociation of ClOOCl to Cl + O_2 + Cl. The translational energy distribution, dissociation geometry, and the width of the Gaussian distribution of angles about the equilibrium geometry were determined by iterating between the O_2 peak and the corresponding Cl peak to achieve the best fit. For a concerted synchronous dissociation, the two Cl atoms will be identical and give rise to a single peak. The predicted Cl peak position was very sensitive to the assumed dissociation geometry. Since the dissociation geometry is not known, we started with the ground state geometry and then adjusted the dihedral angle. The Cl position was predicted to be around the main peak in the $m/z = 35$ TOF spectra, and the best fit was obtained for a dissociation geometry with a smaller dihedral angle of 65° (instead of 81°) and angle width parameters of 4°. The translational energy distribution (Fig. 9) indicated that on average 65 kcal/mol, or 72% of E_{avail} ,went into translation, leaving an average of 25.7 kcal/mol in internal energy, most of which must go into the O_2. The maximum translational energy for this dissociation was 87 kcal/mol, leaving ~4 kcal/mol in internal energy of the products. The angular distribution for the $m/z = 32$ peak indicated a perpendicular transition with an anisotropy parameter of $-1.0 \leq \beta \leq -0.5$ if the O_2 signal was modeled as arising from a two-body process; the Cl angular distribution corresponded to $0.0 \leq \beta \leq 0.4$.

Because the O_2 and Cl products are detected at different masses with no contributions from both products at the same mass, the relative scaling of the Cl to the O_2 signal could not be done exactly; however, an estimate can be made. Two Cl atoms are produced for each O_2, and the relative ionization cross section for Cl is about 1.3 times that for O_2 ($\sigma_{O2} = 2.7 \times 10^{-15}$ cm^2 for an electron energy of 100 eV, $\sigma_{Cl} = 3.5 \times 10^{-15}$ cm^2 at 75 eV).[28,29] The Cl signal should thus be about a factor of 2.6 larger than the O_2 signal. The integrals of the O_2 peaks were on the order of 10,000 counts, while the integrals of the corresponding Cl products were around 42,000 if scaled to the same number of shots. However, the angular distribution of the Cl products is not the same as that of the O_2, and a direct comparison of integrals can only provide a rough estimate of the relative amounts of Cl and O_2.

If we were to instead assign the fast O_2 to products from the secondary dissociation of ClOO following primary dissociation of ClOOCl to Cl + ClOO, no more than 14 kcal/mol (15% of E_{avail}) could be partitioned into translation in the primary dissociation step, with the remainder going into ClOO internal excitation. The ClOO internal excitation must then all become translational energy in the secondary dissociation to Cl + O_2, with very little or no energy remaining in the O_2 molecule. Such a dissociation mechanism seems very unlikely. Furthermore, the existence of a peak at $m/z = 35$ that corresponds to the Cl counterfragment from the concerted dissociation lends credence to our assignment of the O_2 peak as arising from the concerted dissociation mechanism. No other peaks were observed at $m/z = 32$, but the signal-to-noise ratio was very low due to the high O_2 background, so that the slower, broader signal from the secondary dissociation of any ClOO was lost in the noise.

Another possibility is that the O_2 arises from the Cl_2 + O_2 channel. However, no peak

was observed at m/z = 70, and the average background was 4.6 times lower than the background at m/z = 32. The ionization cross section[27] for Cl_2 is $\sigma_{Cl2} = 7.0 \times 10^{-16}$ cm^2, a factor of 2.6 times the O_2 ionization cross section, and the fragmentation pattern for Cl_2 was measured to be $Cl^+:Cl_2^+ = 1.0 : 1.9$ for similar ionizer conditions. Therefore, if the O_2 were from the $Cl_2 + O_2$ channel, we should have observed the Cl_2 counterfragment at m/z = 70.

Cl + ClOO Channels

The remaining signal at m/z = 35 consisted of a fast shoulder, a slow shoulder, and a very slow peak. The fast shoulder was assigned to primary Cl products from the Cl + ClOO channel and fit with the translational energy distribution shown in figure 10. The angular distribution was fit with an anisotropy parameter of 0.6. The average energy in translation for this channel was $\langle E_T \rangle$ = 25 kcal/mol, or ~ 26 % of E_{avail}, leaving on average 66 kcal/mol of internal energy primarily in the ClOO fragment. The minimum internal energy in the ClOO fragment was 37.4 kcal/mol. This is significantly greater than the bond dissociation energy of ClOO, which is only 4.7 kcal/mol; thus, the ClOO must undergo spontaneous secondary dissociation if it is formed in the ground state. Calculations[30] on the four lowest energy doublet states of both A' and A" symmetry indicate that only the ground state is bound; all excited doublet states investigated were repulsive with respect to dissociation to $Cl + O_2$. Table I shows the relative energies of the eight calculated doublet states of ClOO. Even if the ClOO were formed in an excited electronic state, dissociation would still occur. Thus, the lack of signal at m/z = 67 ($ClOO^+$) is not surprising.

We modeled the spontaneous secondary dissociation of ClOO assuming formation of

ground state Cl + O_2 products. The average energy in translation was 6.4 kcal/mol, with a maximum translational energy of 19 kcal/mol. The secondary angular distribution $P(\Omega)$ was estimated by assuming that the ClOO dissociated promptly from the ground state ClOOCl geometry. The reference direction for the secondary angular distribution is the c.m. primary dissociation direction, i.e. the first Cl-O bond axis. In the ground state geometry the vectors along the two Cl-O bonds make an angle of 89°, so the secondary angular distribution was assumed to be sideways-peaked about 89°. A sideways peaked angular distribution gave the best fit to the slow shoulder of the fast peak; however, the fact that this signal consisted of multiple unresolved components precluded us from unambiguously determining the secondary angular distribution. Even if the true angular distribution is sideways-peaked, because it is symmetric about $\Omega = 90°$ we can not rule out the possibility that the ClOO* lives longer than a rotational period.

Table 1. The eight lowest doublet states calculated for ClOO. Taken from Ref. 29.

state	relative energy (kcal/mol)	correlates to ground or excited state products
4 ^{2}A'	65.6	e.s.
4 ^{2}A"	61.3	e.s.
3 ^{2}A'	58.9	g.s.
3 ^{2}A"	52.0	e.s.
2 ^{2}A"	47.3	g.s.
2 ^{2}A'	45.0	g.s.
1 ^{2}A'	36.1	g.s.
1 ^{2}A"	0.0	

Slow Signal at $m/z = 35$

The $m/z = 35$ TOF distributions also exhibited a broad, slow component that was more prominent at the smaller angles. This signal could arise from several sources: 1) dissociation of ClOOCl to form Cl + ClOO* which then dissociates to Cl + O_2*, 2) dissociation of ClOOCl- or Cl_2-containing clusters, 3) secondary photodissociation of ClO photoproducts or other secondary processes, or 4) a combination of the above. Some of the low-lying excited states[29] predicted for ClOO correlate to formation of electronically excited O_2* products (see Table I). If we modeled the slow signal at $m/z = 35$ as a statistical dissociation to Cl + ClOO* followed by a statistical dissociation of ClOO* to Cl + O_2*, a satisfactory fit at all angles could not be achieved unless the translational energy fell more rapidly than the predicted RRKM $P(E_T)$ distribution, as shown in figure 11. This was so even for the highest calculated excited state of ClOO* that correlates to excited state products, the 4 ^{2}A' state at 65.6 kcal/mol above the ground state, and for subsequent dissociation of the ClOO* to Cl + O_2 ($^1\Sigma_g$) 39.0 kcal/mol above the ground state. The primary angular distribution was fit with $\beta = 0$, and the secondary dissociation was fit assuming an isotropic secondary angular distribution; thus, both dissociations may occur after a rotational period. As with the slow signal at $m/z = 51$, the slow signal at $m/z = 35$ is not observed in the pure Cl_2O photolysis experiments, indicating that if the signal arises from cluster dissociation, the clusters must be correlated with the ClOOCl beam. The slow signal is not likely to arise exclusively from secondary photolysis of primary ClO, again because the signal was not observed for Cl_2O photolysis at the same laser power. Some slow signal was observed at $m/z = 35$ for pure Cl_2O photolysis. This slow signal was small compared to the fast peak and

broader than the slow signal observed in the ClOOCl photolysis. For Cl_2O, the slow signal was modeled as cluster dissociation, and was included when modeling the Cl_2O contribution to the ClOOCl photolysis signal.

308 nm

Overview of Results

Photolysis signal was observed for ClO^+ and Cl^+ fragments (Figure 12). A single ClO^+ peak was observed, with no discernable "slow" signal. The Cl^+ TOF spectrum consisted of three peaks, dominated by a sharp, fast peak which had faster and slower weak shoulders followed by two slower peaks. The signal-to-noise (S/N) ratio was worse than at 248 nm because of the decreased absorption cross section.

Contributions from other components in the beam

We observed contributions to the photolysis signal from ClO, Cl_2, Cl_2O, and ClOOCl. Of these, dissociation of Cl_2 (the major component in the beam) dominated the Cl^+ TOF spectrum. A separate Cl_2 photolysis experiment was performed to obtain the $P(E_T)$ and β needed to fit the Cl_2 contribution to the photolysis signal. The Cl_2 experiment also allowed us to test our input file for the analysis routine, fixing the length of the ionizer and providing a double check on the other parameters. Figure 13 shows the Cl_2 photolysis data at $m/z = 35$. We modeled the signal with a $P(E_T)$ that reflected dissociation to 94% $Cl(^2P_{3/2}) + Cl(^2P_{3/2})$, 2% $Cl(^2P_{3/2}) + Cl(^2P_{1/2})$, and 4% $Cl(^2P_{1/2}) + Cl(^2P_{1/2})$. The angular distribution was fit with $\beta = -1$ for the $Cl(^2P_{3/2}) + Cl(^2P_{3/2})$ channel; the other two channels were too small to be able to determine β values. Matsumi *et al.*[31,32] observed a lower yield of 0.0095 for $Cl(^2P_{1/2})$ from

Cl_2 photolysis at 308 nm, and anisotropy parameters $\beta = -1$ for $Cl(^2P_{3/2})$ and $\beta = -0.7$ for $Cl(^2P_{1/2})$. Samartzis *et al.*[33] observed a slightly higher yield of Cl* than Matsumi *et al.* for photolysis at 351 nm, 0.08 as opposed to 0.016.

The magnitudes of the ClO and Cl_2O contributions could not be determined from the TOF data alone. We therefore scaled the ClO (dot-dot-dashed lines, Fig. 12) and Cl_2O (dashed line, Fig. 12) contributions to the Cl^+ signal relative to the Cl_2 contribution using relative abundances determined by mass spectrometer measurements of the source, as discussed in Chapter 3, using the absorption cross sections at 308 nm. Knowledge of the ClOOCl absorption cross sections or the amount of signal arising from ClOOCl was not needed for this calculation. The ClO contribution was modeled as a combination of photolysis to $Cl(^2P_{1/2}) + O(^3P)$ and $Cl(^2P_{3/2}) + O(^3P)$ and was observed in the middle peak of the Cl^+ TOF spectrum. The anisotropy parameter was assumed to be $\beta = 0$. The Cl_2O $P(E_T)$ and β as well as the relative scaling for Cl and ClO photofragments were obtained from separate Cl_2O photolysis experiments. With this information we could model the Cl_2O contribution for both Cl^+ and ClO^+ products.

ClOOCl photolysis

The only contributions to the $m/z = 51$ signal were from Cl_2O and ClOOCl. Once the Cl_2O contribution was determined, the remaining signal was assigned to the ClO + ClO channel from ClOOCl photolysis (dotted line, Fig. 12) and fit with the translational energy distribution shown in Fig. 14. The angular distribution was fit with an anisotropy parameter of $\beta = 2.0$. The average energy in translation was 27 kcal/mol, or ~ 35% of Eavail, indicating that the ClO fragments were highly vibrationally excited, with $\langle E_{int} \rangle = 50$ kcal/mol distributed

between the two fragments. The maximum amount of energy in ClO internal energy was 65.3 kcal/mol, which is barely enough energy for spontaneous dissociation of the ClO if all the internal energy were partitioned into one of the ClO fragments. Thus, spontaneous secondary dissociation of ClO is unlikely. We also modeled the ClO signal as only arising from ClO + ClO (no Cl_2O contribution) in order to determine the upper limit for the ClO branching ratio from ClOOCl photolysis.

A fast shoulder, slow shoulder, and a very slow peak remained after taking into account Cl^+ signal from the Cl_2, Cl_2O, and ClO photolysis contributions and from ClO fragmenting in the ionizer. The fast shoulder was assigned to primary Cl from the Cl + ClOO channel and fit with the $P(E_T)$ shown in Figure 15. The angular distribution was modeled with an anisotropy parameter of $\beta = 1.5$. The average energy in translation was $\langle E_T \rangle = 27$ kcal/mol (37% of E_{avail}), leaving on average 46 kcal/mol in the ClOO fragment, well above its dissociation energy ($D_o = 4.7$ kcal/mol). As at 248 nm, no ClO_2^+ signal was observed. The secondary dissociation of ClOO to Cl + O_2 was modeled with an impulsive $P(E_T)$ and an isotropic angular distribution. The secondary Cl^+ signal appeared in the slow shoulder of the fast peak. Because the Cl_2 photolysis signal obscured the signal from ClOOCl, and because the signal-to-noise ratio was low, and because no O_2 signal was observed, it was impossible to determine the dynamics (sequential or concerted) of the dissociation.

Very slow Cl^+ signal remained, which we modeled as arising from a statistical dissociation to Cl + ClOO* → 2Cl + $O_2(^1\Sigma_g^+)$. This signal is larger in proportion to the Cl^+ ClOOCl photolysis signal than it was at 248 nm, and could also arise from dissociation of clusters in the beam.

Relative Yields

To obtain the overall relative yields for ClOOCl photodissociation at 248 nm, we had to assume that ClOOCl only dissociates via the channels considered. Relative yields could be calculated assuming that 1) all slow signal, 2) only the slow signal at $m/z = 35$ or 51, or 3) none of the slow signal arises from ClOOCl photolysis. Including the slow signal did not greatly change the overall relative yields. Only the primary dissociation channels were used to calculate the relative yields, with the secondary contributions scaled so that the primary and secondary dissociation processes had a 1:1 ratio for a given channel. The relative yield for the concerted channel was determined by modeling the Cl products as arising from a primary two-body channel to get a primary c.m. flux distribution.

All of the calculated yields depended somewhat on the choice we made for the contribution from Cl_2O photolysis. At 248 nm, we determined the Cl_2O contribution from the Cl^+ product TOF spectrum as discussed in the Results and Analysis section. This method gave a Cl_2O contribution that was comparable to that predicted from source TOF measurements, as described in Chapter 3. The ratio of Cl_2O to ClOOCl photolysis signal was predicted to be Cl_2O : ClOOCl = 1.0 : 5.6 for this experiment. After the final analysis of all the photolysis signal using the ClO^+ "rising edge" method to determine the Cl_2O contribution, the Cl_2O : ClOOCl photolysis signal ratio was 1.0 : 4.6 if the very slow Cl^+ and ClO^+ signal was attributed to clusters and 1.0 : 6.8 if this signal was attributed to ClOOCl photolysis. Because the ClO channel for ClOOCl photolysis is minor, changing the Cl_2O contribution over this range does not greatly affect the Cl : ClO branching ratio for ClOOCl photolysis. We could obtain an absolute upper limit on the relative yield of the ClO + ClO channel by

assuming that all of the ClO signal was from ClOOCl photolysis with no contribution from Cl_2O. This upper limit on the relative yield is $\Phi_{ClO + ClO} = 0.19$ for ClOOCl excited at 248 nm. The upper limit we measured would be too low if any of the primary ClO photofragments absorbed a photon. However, secondary dissociation of ClO was minimal for all of these experiments, as verified by the corresponding Cl_2O photolysis experiments.

At 308 nm, we observed two main product channels, ClO + ClO and Cl + ClOO → 2Cl + O_2, as well as some slow Cl^+ signal. The slow signal was much higher with respect to the ClOOCl signal in the fast peak than it was at 248 nm, and thus makes more of a difference in the relative Cl and ClO yields from ClOOCl photolysis. We calculated the relative yields for both the case where with slow signal was attributed to clusters as well as the case where it arose from ClOOCl photolysis. The Cl_2O contribution was determined relative to the Cl_2 contribution from TOF measurements of the source and did not rely on any assumptions involving ClOOCl. We can again obtain an upper limit for the relative yield of the ClO + ClO channel by assuming that all the signal arises from ClOOCl; this upper limit for ClOOCl photoexcited at 308 nm is $\Phi_{ClO + ClO} = 0.31$.

Table II indicates the observed channels and their relative yields, as well as the relative Cl : ClO product yields for ClOOCl photolysis at 248 and 308 nm. The values given were calculated assuming that the slow signal can all be attributed to cluster photolysis; the values in parentheses were calculated assuming that the slow signal arises from ClOOCl photolysis. For these calculations, all of the Cl_2O_2 photolysis signal was attributed to the ClOOCl isomer. The other possible isomers, ClOClO and $ClClO_2$, were discussed in Chapter 3. ClOOCl is the major product from the three-body recombination of ClO, on which we based our source

design; however, we can not preclude the presence of the other isomers in our source. In particular, it is possible (although unlikely) that some of the ClO signal came from the ClOClO isomer.

Table II. Relative yields* for the ClOOCl photolysis channels observed at 248 and 308 nm.

	relative yield	
	248 nm	308 nm
Dynamical Channels		
$Cl + ClOO \rightarrow Cl + Cl + O_2$	0.67 (0.55)	0.83 (0.50)
$Cl + O_2 + Cl$ (concerted)	0.22 (0.18)	
$ClO + ClO$	0.12 (0.09)	0.17 (0.10)
$Cl + ClOO^* \rightarrow Cl + Cl + O_2^*$	0.00 (0.15)	0.00 (0.40)
$ClO + ClO^* \rightarrow ClO + Cl + O$	0.00 (0.04)	
Relative Product Yields		
$2Cl + O_2$	0.89 (0.88)	0.83 (0.90)
$ClO + ClO$	0.12 (0.13)	0.17 (0.10)

*The numbers listed assume that products with low c.m. translational energies arise from some other process such as cluster dissociation; the numbers in parentheses include those products as arising from ClOOCl dissociation.

Discussion

At 248 nm, we observed three primary dissociation channels: ClO + ClO, a concerted channel in which both Cl–O bonds break simultaneously to form $2Cl + O_2$, and a sequential dissociation to $2Cl + O_2$ via Cl + ClOO. In addition, slow signal was observed for both ClO^+ and Cl^+ photofragments that could correspond to ClO(X) + ClO(A) and $Cl + ClOO^* \rightarrow 2\ Cl + O_2$ channels. The average and maximum c.m. total translational energies and anisotropy

parameters for these channels are summarized in Table III.

Table III. Summary of results for each dissociation channel at 248 nm. Energies are all in kcal/mol. The ClO + ClO* and Cl + ClOO*→ 2Cl + O_2* channels were modeled, but this signal is likely to arise from clusters.

channel	$\langle E_T \rangle$	$E_{T,max}$	E_{avail}	$\langle E_T \rangle / E_{avail}$	$E_{T,max}/E_{avail}$	β
Cl + ClOO	34	58	95.4	0.36	0.61	0.6
Cl + O_2 + Cl	65	87	90.7	0.72	0.96	−1.0, 0.1[†]
ClO + ClO	26	45	99.5	0.26	0.45	0.5
Cl + ClOO*	2.3	12	25.1	0.09	0.48	0
ClO + ClO*	2.7	9	9.0	0.30	1.0	0
ClOO→Cl + O_2	6.4	19	90.7 − $E_{T,1°}$.[‡]			isotropic
ClOO→Cl + O_2*	4	15	51.7 − $E_{T,1°}$.[‡]			isotropic

[†] The angular distribution for O_2 corresponded to $-1.0 \le \beta \le -0.5$ and that for Cl to $0.0 \le \beta \le 0.4$, if each was modeled as if it were a two-body dissociation. The best values of −1.0 and 0.1 shown in this table are explained in the "Transition Dipole of the Concerted Channel" section later in this chapter.

[‡]The available energy for the secondary dissociation depends on the primary translational energy, and is thus a distribution.

At 308 nm, two main channels for ClOOCl photolysis were observed: ClO + ClO and 2Cl + O_2 via Cl + ClOO. The signal-to-noise ratio was worse than that at 248 nm, the Cl_2 photolysis signal obscured much of the ClOOCl photolysis signal at m/z = 35, and no O_2^+ signal was observed; therefore, we can not determine whether a concerted process to form 2Cl + O_2 also occurred. Rather, all of the Cl^+ signal was assigned to sequential Cl + ClOO and the spontaneous secondary dissociation of ClOO. Since slow Cl^+ signal was observed, which most likely arose from clusters but could have also arisen from some Cl + ClOO* → 2Cl + O_2* channel. This slow signal was much larger in proportion to the ClOOCl photolysis signal than it was at 248 nm. The average and maximum c.m. total translational energies and

anisotropy parameters for these channels are summarized in Table IV.

Table IV. Summary of results for each dissociation channel at 308 nm. Energies are all given in kcal/mol. The Cl + ClOO*¬ 2Cl + O_2* channels was modeled, but this signal is likely to arise from clusters.

channel	$\langle E_T \rangle$	$E_{T,max}$	E_{avail}	$\langle E_T \rangle / E_{avail}$	$E_{T,max}/E_{avail}$	β
ClO + ClO	27	31	77.3	0.35	0.40	2.0
Cl + ClOO	27	45	73.2	0.37	0.61	1.5
Cl + ClOO*	1.6	5.7	34.2	0.05	0.17	0
ClOO → Cl + O_2	~ 8	20	68.5 - $E_{T,1°}$‡			isotropic
ClOO*→ Cl + O_2*	~14	29.5	29.5 - $E_{T,1°}$‡			isotropic

ClO Photolysis Signal at 248 nm

The angular distribution for the Cl products from the photolysis of ClO was fit by β = 2.0, which differs from the anisotropy parameter β = 1.2 reported by Davis and Lee.[25] The ClO ($A\ ^2\Pi_{3/2} \leftarrow X\ ^2\Pi_{3/2}$) excitation is a parallel transition ($\Delta\Omega = 0$), for which β = 2.0. Davis and Lee explained their observation of β = 1.2 by assuming that ~70% of the dissociation was from the *A* state, with the remaining ~30% occurring via a perpendicular transition (β = −1) from a state of $^2\Sigma$ or $^2\Delta$ symmetry ($\Delta\Omega = \pm 1$).

Their ClO source was from photolysis of the (6,0,0) band of OClO in a jet, which produces a higher-than-thermal yield of spin-orbit excited ClO.[34] Our ClO arose from Cl_2O photolysis and the ensuing chemical reactions, and resided in the quartz cell for over 100 μs after the Cl_2O photolysis occurred. Thus, our ClO was more likely to have a thermal spin-orbit population distribution, which, for a cell temperature of ~200K is ~95% ClO $X\ ^2\Pi_{3/2}$. It is possible that the spin-orbit excited ClO $X\ ^2\Pi_{1/2}$ has enough extra energy to be able to

access the higher $^2\Sigma$ or $^2\Delta$ state while the ClO $X\,^2\Pi_{3/2}$ state can not. In this case, we would only see signal from the ClO ($A\,^2\Pi_{3/2} \leftarrow X\,^2\Pi_{3/2}$) transition, and the two experiments would be consistent.

Transition Dipole of the Concerted Channel and Effects of Excited State Symmetry (248 nm)

The angular distribution of the O_2 peak corresponded to an anisotropy parameter of $-1.0 \leq \beta \leq -0.5$, if we modeled the dissociation as a two-body process. The angular distribution of the Cl counterfragments can be described by $0.0 \leq \beta \leq 0.4$. The low signal-to-noise ratio at $m/z = 32$ and the multiple components at $m/z = 35$ made it difficult to assign more precise values for the anisotropy parameters. β has the form

$$\beta = 2P_2(\cos\chi)$$

where P_2 is the second Legendre polynomial and χ is the angle between the electronic transition moment and the c.m. recoil axis of the fragments. For a given β value, the transition moment resides on a cone with a half-angle χ centered about the recoil axis. For the concerted channel, both β values must correspond to a single electronic transition, so that the transition moment must lie at the intersection of the two cones determined from the O_2 and Cl angular distributions. Furthermore, the transition moment must be unique, so that the two cones must intersect only along one line (that is, the edges of the two cones must just touch.)

For the O_2 products, $\chi = 90°$ for $\beta = -1.0$, and $\chi = 66°$ for $\beta = -0.5$, so that χ must lie between 66° and 90°. For the Cl products, $\chi = 55°$ for $\beta = 0.0$ and $\chi = 47°$ for $\beta = 0.4$. The angles between the c. m. recoil vectors for the ClOOCl dissociation geometry determined from the peak positions in the three-body dissociation analysis are $\angle_{Cl_a,b\text{-}O2} = 142.4°$ and

$\angle_{Cla-Clb} = 75.2°$. Because the angle between the Cl and O_2 c.m. velocity vectors is 142.4°, for the two cones to intersect at the edges the two χ's for the Cl and O_2 angular distributions must add up to 142.4°. This is only possible within the bounds of the observed angular distributions if $\beta_{O2} = -1.0$ ($\chi = 90°$), in which case β_{Cl} must be 0.1 ($\chi = 52°$). Thus, the angular distributions for the products from the concerted dissociation channel are consistent with an electronic transition moment along the O-O bond.

The other two primary dissociation channels, ClO + ClO and Cl + ClOO, were parallel transitions, as indicated by the anisotropy parameters $\beta = 0.5$ and $\beta = 0.6$, respectively. Theory[3] predicts a series of pairs of nearly degenerate states at 248 nm, formed as symmetric (*A*) and antisymmetric (*B*) linear combinations of the ClO antibonding orbitals. The transition moments (as determined from the anisotropy parameter) for these channels suggest that excitation to an antisymmetric *B* state (transition moment along the O-O bond axis) leads to both the ClO + ClO and the concerted 2Cl + O_2 channels, whereas excitation to a symmetric *A* state (transition moment along the Cl-O bond) leads preferentially to dissociation via Cl + ClOO. Thus, the symmetry of the excited state appears to influence the dissociation dynamics.

Comparison with Previous Experiments

Our results indicate that the previous reports of the yield for Cl-atom formation by Cox and Hayman[9] and Molina *et. al.*[10] are qualitatively correct, but somewhat high. One uncertainty in the absolute quantum yield determined by Molina *et al.* at 308 nm is the dependence on the ClOOCl absorption cross section. Using the most recent absorption cross section measurements[12] results in a re-calculated yield for the 2Cl + O_2 channel (7) of $\Phi_7 =$

0.88, in excellent agreement with our results (Φ_7 = 0.83). Furthermore, the high ClO vibrational excitation that we observe could explain their inability to detect ClO products. Recent experiments[35] show that the reaction rate of vibrationally excited ClO with NO is much slower than that for ground state ClO reacting with NO. Since Molina *et. al.* used titration with NO to detect ClO, and our results suggest that the ClO is vibrationally excited, it is not surprising that they did not detect ClO.

Schmidt *et. al.*[13] reported a much lower yield for the Cl + ClOO channel at 250 nm of $\Phi_7 = 0.65 \pm 0.15$, with an average translational energy of $\langle E_T \rangle = 0.42$ eV (~ 10 kcal/mol). At 248 nm, we observe a relative yield for Cl-producing channels of $\Phi_7 = 0.88$, and were able to obtain an upper limit for ClO products that implies that the lower limit for Cl-producing channels must be $\Phi_7 \geq 0.81$. This lower limit is right on the edge of the error bars they give for the Cl yield. Also, we observed that the average translational energy for primary and secondary Cl from the Cl + ClOO → Cl + Cl + O_2 channel was 22 kcal/mol and 3 kcal/mol, respectively. The Cl from the concerted 2Cl + O_2 channel had an average translational energy of 21 kcal/mol. If we only consider our yield for the Cl + ClOO → 2Cl + O_2 channel, Φ = 0.67, we get reasonable agreement with their results. If the very slow products we observed arose from ClOOCl and not clusters, the average translational energy of all the Cl products was ~ 11 kcal/mol with a yield of Φ = 0.89, and the average translational energy if we exclude the Cl products from the concerted channel was ~ 7 kcal/mol with a yield of Φ = 0.70. The best explanation for the discrepancy between our results and the results of Schmidt *et. al.* is that their technique may discriminate against the Cl products with high translational energies.

Stratospheric Implications

From our results at 308 nm, we conclude that in the stratosphere,

$$ClOOCl + h\nu \rightarrow 2Cl + O_2 \qquad \Phi_7 = 0.83 \qquad (7)$$

$$\rightarrow ClO + ClO \qquad \Phi_5 = 0.17 \qquad (5),$$

with an absolute upper limit of $\Phi = 0.31$ for the ClO product channel. The intermediate ClOO (reaction 6) is formed with $E_{int} >> D_e$ and is unlikely to be collisionally stabilized under stratospheric conditions.

Also, we observed highly vibrationally excited ClO and O_2 photoproducts. The role of vibrationally excited states in the stratosphere has recently received some attention. Specifically, the reactions[36,37]

$$O_2 (v \geq 26) + O_2 \rightarrow O_3 + O \qquad (11)$$

and

$$ClO (v \geq 10) + N_2 \rightarrow Cl + N_2O \qquad (12)$$

could potentially be of importance in the stratosphere. The O_2 we observed from the sequential $2Cl + O_2$ channel at 248 nm had an average internal energy of 50 kcal/mol, corresponding to $v = 12$, which is not high enough to exceed the threshold for reaction with O_2. However, the ClO produced from the ClO + ClO channels is highly vibrationally excited, with an average energy per ClO of 37 kcal/mol at 248 nm and 24 kcal/mol at 308 nm. The threshold for reaction with N_2 is 24.3 kcal/mol. Thus, the production of highly excited ClO from ClOOCl photolysis could lead to a small production term for N_2O in the stratosphere. N_2O is currently used as a tracer species, with no stratospheric sources, so discovering a stratospheric source for N_2O could potentially be important. The production of N_2O from ClOOCl photolysis is not likely to be a major perturbation on current models, because 1) the

ClOOCl photolysis mainly occurs for longer wavelengths, where less energy is available and 2) the ClO + ClO channel is minor.

At 248 nm, slow signal was observed at $m/z = 51$ which could arise from the ClO(X) + ClO(A) → ClO + Cl + O channel. This channel is unlikely to be of great importance in the stratosphere, as it requires wavelengths $\lambda \leq 290$ nm and most of the contribution to the ClOOCl photolysis rate occurs for the wavelength range 310 to 470 nm.[12] The ClO(A) fragment predissociates, producing a Cl-atom and an O-atom. Thus, the ClO(X) + ClO(A) channel results in a null cycle for ozone depletion.

Our results confirm that the catalytic cycle involving photolysis of ClOOCl is the dominant mechanism for ozone loss under perturbed polar conditions. However, the production of ClO from ClOOCl photolysis reduces the efficiency of the ClOOCl catalytic cycle for ozone depletion and could shift the predicted partitioning of chlorine-containing species in the stratosphere. Because of the extreme importance of the ClOOCl catalytic cycle in the current models of Antarctic stratospheric ozone depletion, even the small ClO yield ($\Phi_{ClO + ClO} = 0.17$) from ClOOCl photolysis at 308 nm reported in this paper could have a significant effect on the predicted ozone depletion. Further modeling studies are necessary to determine whether the small reduction in the Cl yield may require additional ozone loss mechanisms to balance the ozone budget. This result may be most important in the Arctic vortex, where warmer temperatures decrease ClOOCl concentrations and reduce ozone loss rates.

References

1. L. T. Molina and M. J. Molina, *J. Phys. Chem.* **91**, 433 (1987).

2. T. J. Lee, C. M. Rohlfing, and J. E. Rice, *J. Chem. Phys.* **97**, 6593 (1992).

3. J. F. Stanton, C. M. L. Rittby, R. J. Bartlett, and D. W. Toohey, *J. Phys. Chem.***95**, 2107 (1991).

4. M. P. McGrath, K. C. Clemitshaw, F. S. Rowland, and W. H. Hehre, *Geophys. Res. Lett.* **15**, 883 (1988).

5. F. Jensen and J. Oddershede, *J. Phys. Chem.* **94**, 2235 (1990).

6. M. Schwell, H.-W. Jochims, B. Wassermann, U. Rockland, R. Flesch, and E. Rühl, *J. Phys. Chem.* **100**, 10700 (1996).

7. M Birk, R. R. Friedl, E. A. Cohen, H. M. Pickett, and S. P. Sander, *J. Chem. Phys.* **91**, 6588 (1989).

8. Heat of formation for ClOOCl from S. L. Nickolaisen, R. R. Friedl, and S. P. Sander, *J. Phys. Chem.* **98**, 155 (1994).

9. R. A. Cox and G. D. Hayman, *Nature* **332**, 796 (1988).

10. M. J. Molina, A. J. Colussi, L. T. Molina, R. N. Schindler, and T.-L. Tso, *Chem. Phys. Lett.* **173**, 310 (1990).

11. W. B. DeMore, S. P. Sander, D. M. Golden, R. F. Hampson, M. J. Kurylo, C. J. Howard, A. R. Ravishankara, C. E. Kolb, and M. J. Molina, *Chemical Kinetics and Photochemical Data for Use in Stratospheric Modeling, Evaluation Number 12*, JPL Publication 97-4, JPL (1997).

12. K. J. Huder and W. B. DeMore, *J. Phys. Chem.* **99**, 3905 (1995).

13. S. Schmidt, Th. Benter, and R. N. Schindler, poster at *XXIII Informal Conf. on Photochemistry*, May 10-15 1998, Pasadena, CA, USA.

14. Y. T. Lee, J. D. McDonald, P. R. LeBreton, and D. R. Herschbach, *Rev. Sci. Inst.* **40**, 1402 (1969).

15. T. K. Minton, C. M. Nelson, T. A. Moore, and M. Okumura, *Science* **258**, 1342 (1992).

16. T. K. Minton, P. Felder, R. J. Brudzynski, and Y. T. Lee, *J. Chem. Phys.* **81**, 1759 (1984).

17. M. J. O'Laughlin, B. P. Reid, and R. K. Sparks, *J. Chem. Phys.* **83**. 5647 (1985).

18. D. J. Krajnovich, Ph.D. Thesis, University of California, Berkeley (1983).

19. C. M. Nelson, T. A. Moore, M. Okumura, and T. K. Minton, *J. Chem. Phys.* **100**, 8055 (1994).

20. T. A. Moore, M. Okumura, and T. K. Minton, *J. Chem. Phys.* **107**, 3337 (1997),

21. P. Felder, Habilitationsschrift, University of Zürich, Switzerland (1993).

22. C. Maul and K.-H. Gericke, *Int. Rev. in Phys. Chem.* **16**, 1 (1997).

23. M. J. S. Dewar, *J. Am. Chem. Soc.* **106**, 209 1984.

24. S. W. North, Ph.D. Thesis, University of California, Berkeley (1995).

25. CMLAB1, presented in X. Zhao, Ph.D. Thesis, University of California, Berkeley (1988).

26. H. F. Davis and Y. T. Lee, *J. Phys. Chem.* **100**, 30 (1996).

27.L. V. Gurvich, I. V. Veyts, and C. B. Alcock, *Thermodynamic Properties of Individual Substances, Fourth Edition, Volume 1*, Hemisphere Publishing Corp., p. 182 (1989).

28. R. E. Center and A. Mandl, *J. Chem. Phys.* **57**, 4104 (1972).

29. T. R. Hayes, R. C. Wetzel, and R. S. Freund, *Phys. Rev. A.* **35**, 578 (1987).

30. J. A. Jafri, B. H. Lengsfield, III, C. W. Bauschlicher, Jr., and D. H. Phillips, *J. Chem. Phys.* **83**, 1693 (1985).

31. Y. Matsumi, M. Kawasaki, T. Sato, T. Kinugawa, and T. Arikawa, *Chem. Phys. Lett.* **155**, 486 (1989).

32. Y. Matsumi, K. Tonokura, and M. Kawasaki, *J. Chem. Phys.* **97**, 1065 (1992).

33. P. C. Samartzis, I. Sakellariou, T. Gougousi, and T. Kitsopoulos, *J. Chem. Phys.* **107**, 43 (1997).

34. H. F. Davis and Y. T. Lee, *J. Chem. Phys.* **105**, 8142 (1996).

35. G. S, Tyndall, C. S. Kegley-Owen, J. J. Orlando, and J. G. Calvert, *J. Chem. Soc., Faraday Trans.* **93**, 2675 (1997).

36. J. M. Price, J. A. Mack, C. A. Rogaski, and A. M. Wodtke, *Chem. Phys.* **175**, 83 (1993); R. L. Miller, A. G. Suits, P. L. Houston, R. Toumi, J. A. Mack, and A. M. Wodtke, *Science*

265, 1831 (1994).

37. R. F. Delmdahl and K.-H. Gericke, *Chem. Phys. Lett.* **281**, 407 (1997).

Figure Captions

Figure 1. Structure of ground state ClOOCl, from ref. 7.

Figure 2. TOF spectra of ClO^+ signal from ClOOCl photolysis at 248 nm. The dotted lines correspond to the Cl_2O contribution, which in this case was determined by examining the rising edge of the data at a detector angle of 15°. The dashed line is the remaining signal modeled as ClO + ClO from ClOOCl photolysis. The slow signal was modeled as ClO(X) + ClO(A).

Figure 3. TOF spectra of ClO^+ signal from ClOOCl photolysis at 248 nm. The solid line is the predicted spectra assuming that all of the signal at 30° arises from Cl_2O only and scaling the other angles according to the Cl_2O angular distribution.

Figure 4. TOF spectra of ClO^+ signal at 30° from ClOOCl photolysis at 248 nm, signal averaged for 1,000,000 laser pulses. The solid line is again assuming that all of the signal arises from Cl_2O photolysis.

Figure 5. TOF spectra of ClO^+ signal at 15° from ClOOCl photolysis at 248 nm. The dotted lines correspond to the Cl_2O contribution, which was determined by examining the rising edge of the data.

Figure 6. Optimized c.m. translational energy distributions for the ClO + ClO and the ClO(X) + ClO(A) channels.

Figure 7. TOF spectra of the O_2^+ signal at 30° from ClOOCl photolysis at 248 nm. The fast peak was modeled as arising from the concerted channel. The dotted line indicates where the O_2 products from the secondary dissociation from the fast Cl + ClOO channel would appear; the dot-dashed line indicates the position of the O_2 products from secondary dissociation from the Cl + ClOO* channel.

Figure 8. Optimized c.m. translational energy distribution for the total translational energy release from the concerted Cl + O_1 + Cl channel.

Figure 9. TOF spectra of the Cl^+ signal from ClOOCl photolysis at 248 nm. The short-dashed line indicates the Cl_2O contribution, determined from the m/z = 51 data. The medium-dashed line is from photolyis of ClO in the beam. The long-dashed lines indicate the Cl^+ signal from the ClO + ClO channels fragmenting in the ionizer. The dotted line corresponds to the primary and secondary dissociation from the fast Cl + ClOO channel. The dot-dashed line is from the Cl + O_2 + Cl concerted channel. The dot-dot-dashed line indicates the signal from the primary and secondary dissociation for the slow Cl + ClOO* channel.

Figure 10. Optimized c.m. translational energy distributions for the Cl + ClOO primary channel and the ensuing ClOO secondary dissociation.

Figure 11. TOF spectra of the Cl^+ signal at 15°. The dashed line shows the predicted fit for Cl + ClOO* if a statistical dissociation to the highest calculated ClOO* state that correlates to excited state products. The dotted line indicates the predicted fit for the secondary dissociation of ClOO* to Cl + O_2* assuming a statistical dissociation.

Figure 12. TOF spectra collected at a detector angle of 40° for (**A**) ClO^+ and (**B**) Cl^+ fragments and the predicted TOF distributions for ClOOCl photolysis at 308 nm. The overall ClO^+ fit (solid line) in (**A**) has two components, Cl_2O (dashed line) and the ClOOCl → ClO(X) + ClO(X) channel (dotted line). The overall Cl^+ fit (solid line) in (**B**) is the sum of contributions from photolysis of Cl_2 (long-dashed line), Cl_2O (short-dashed line), ClO → Cl($^2P_{1/2,3/2}$) + O(^3P) (dot-dot-dashed lines), and ClOOCl. The ClOOCl photolysis contributions to the Cl^+ signal include primary and secondary dissociation from the ClOOCl → Cl + ClOO → Cl + Cl + O_2 channel (dotted lines), primary and secondary dissociation from the ClOOCl → Cl + ClOO* → Cl + Cl + O_2* channel which could also arise from clusters (medium-dashed lines), and Cl^+ from the ClO(X) fragmenting in the ionizer (dot-dashed line).

Figure 13. TOF spectra of the Cl^+ signal from Cl_2 photolysis at 308 nm.

Figure 14. Optimized c.m. translational energy distribution for the ClO + ClO channel at 308 nm.

Figure 15. Optimized c.m. translational energy distributions for the Cl + ClOO primary channel and the ensuing ClOO secondary dissociation.

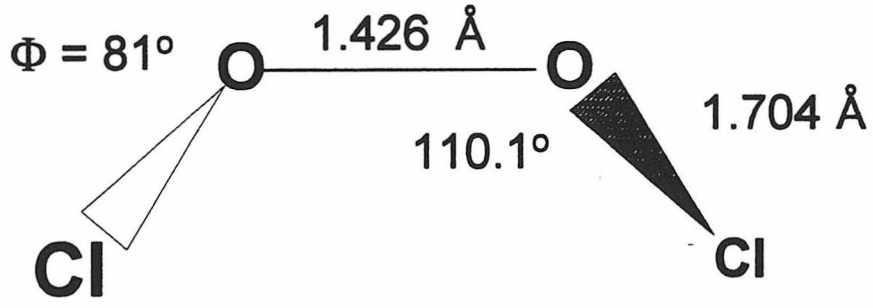

Figure 1.

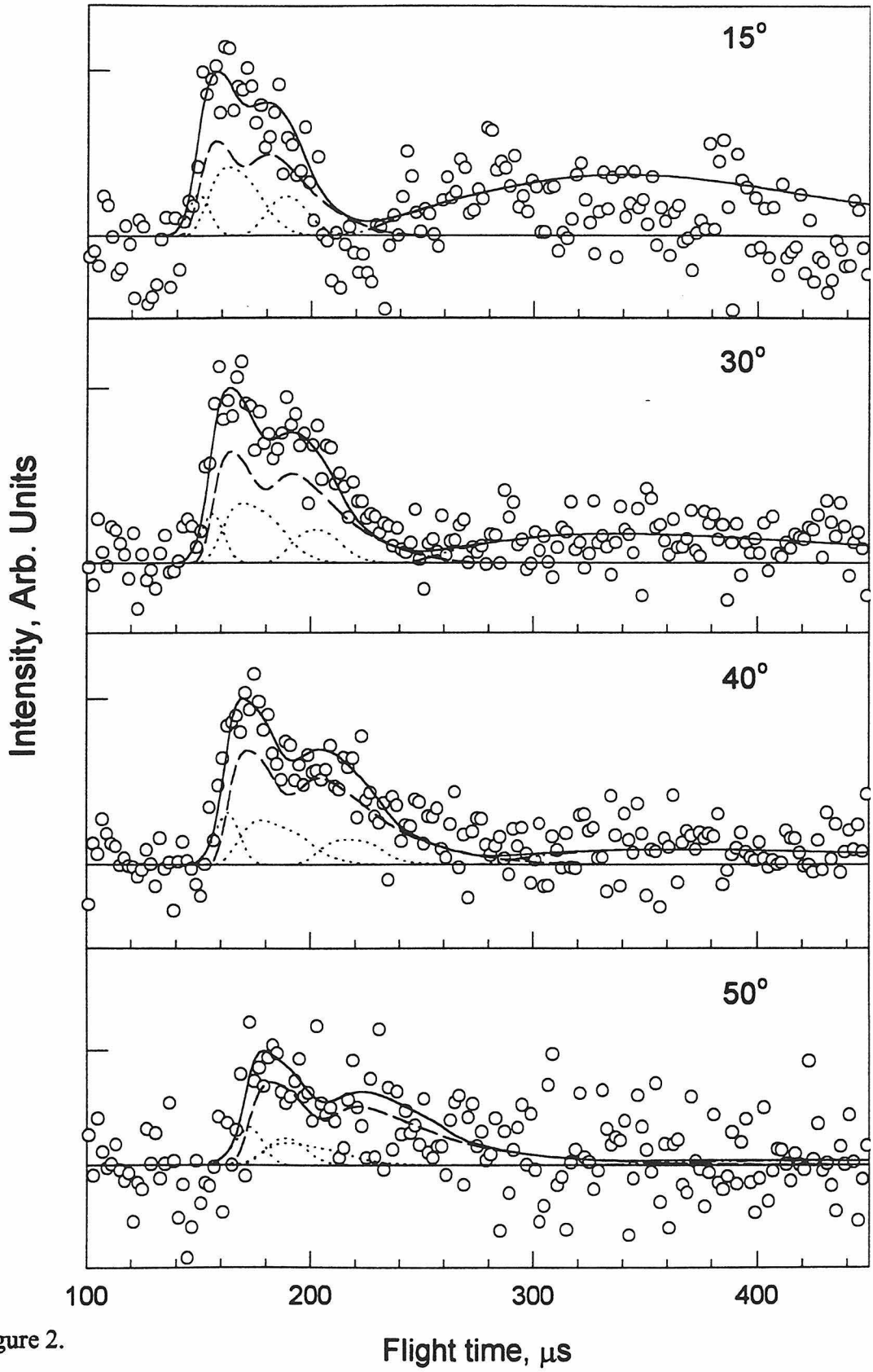

Figure 2.

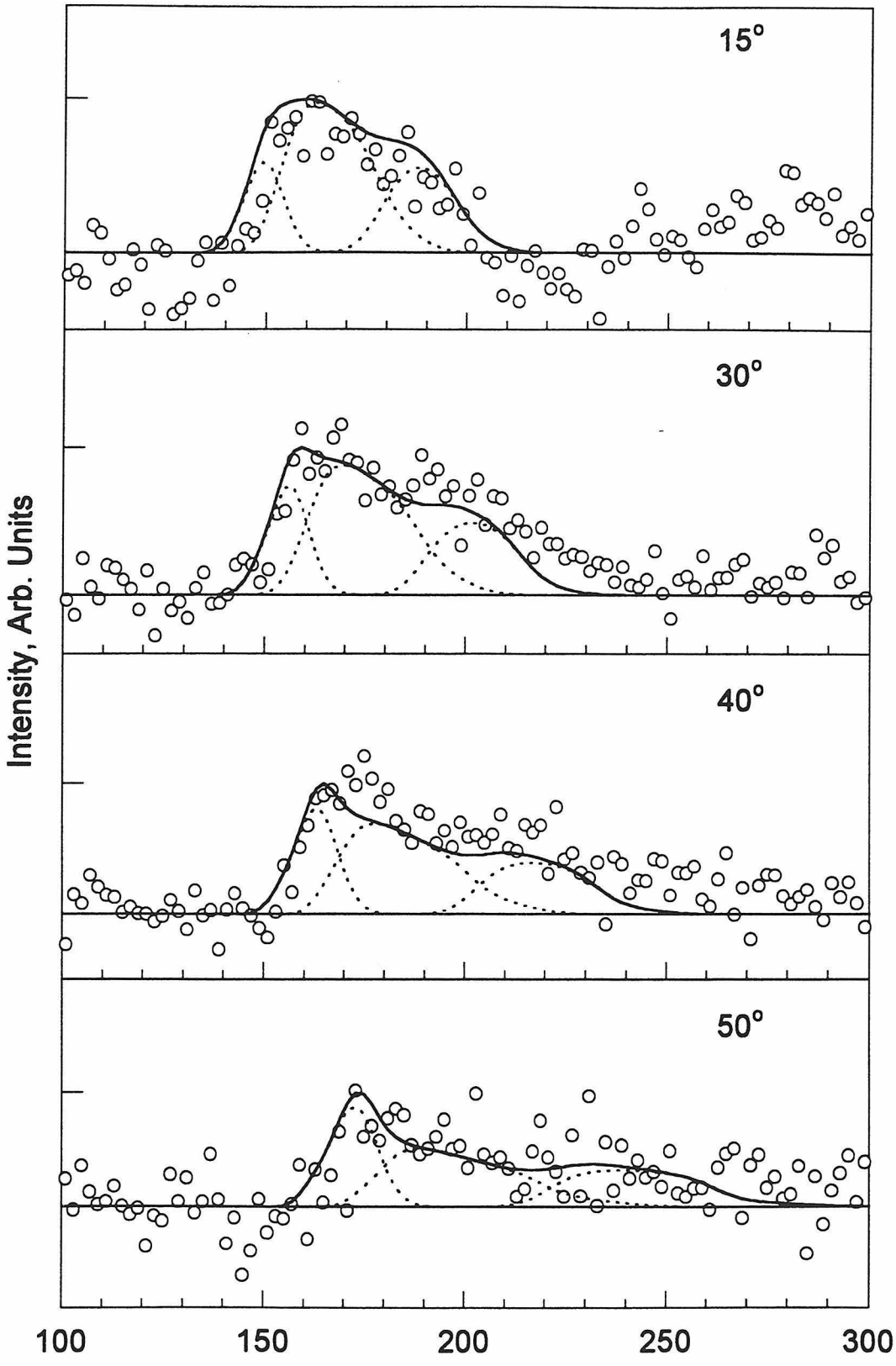
15°
30°
40°
50°
Intensity, Arb. Units
100
150
200
250
300
Flight time, μs

Figure 3.

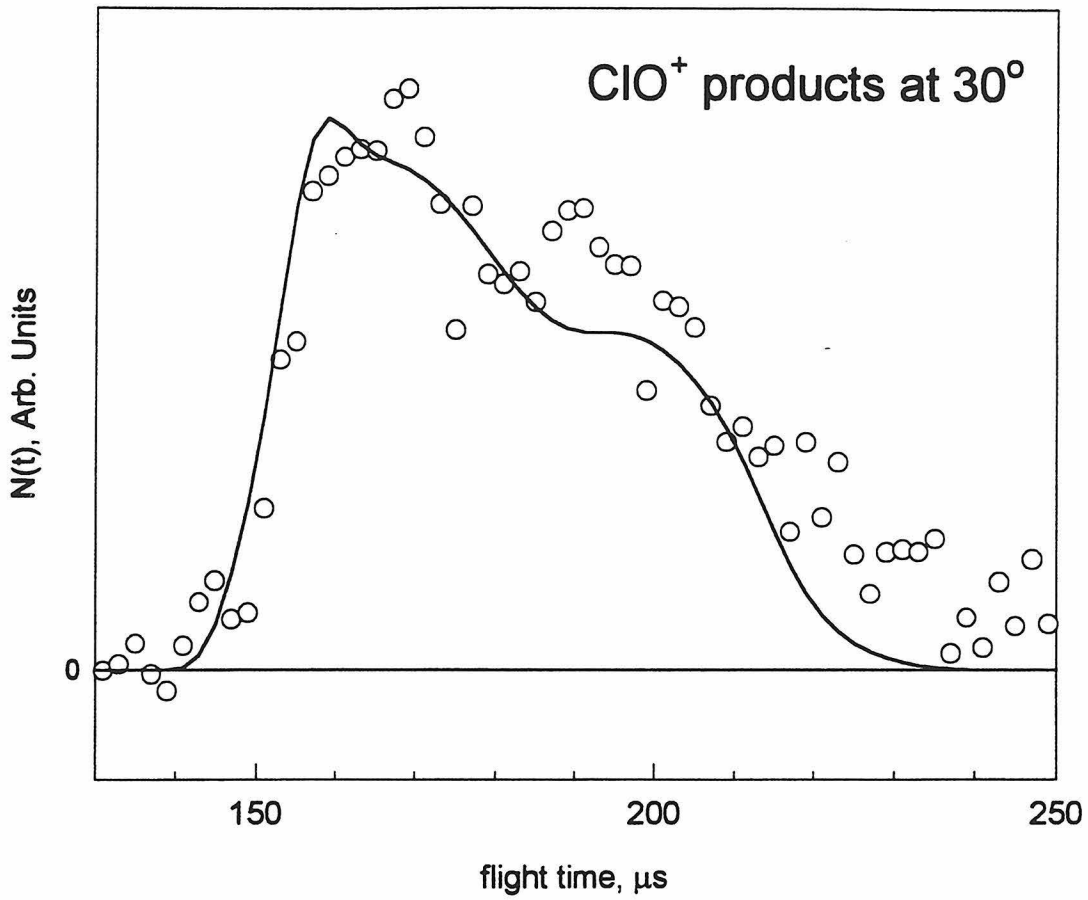

Figure 4.

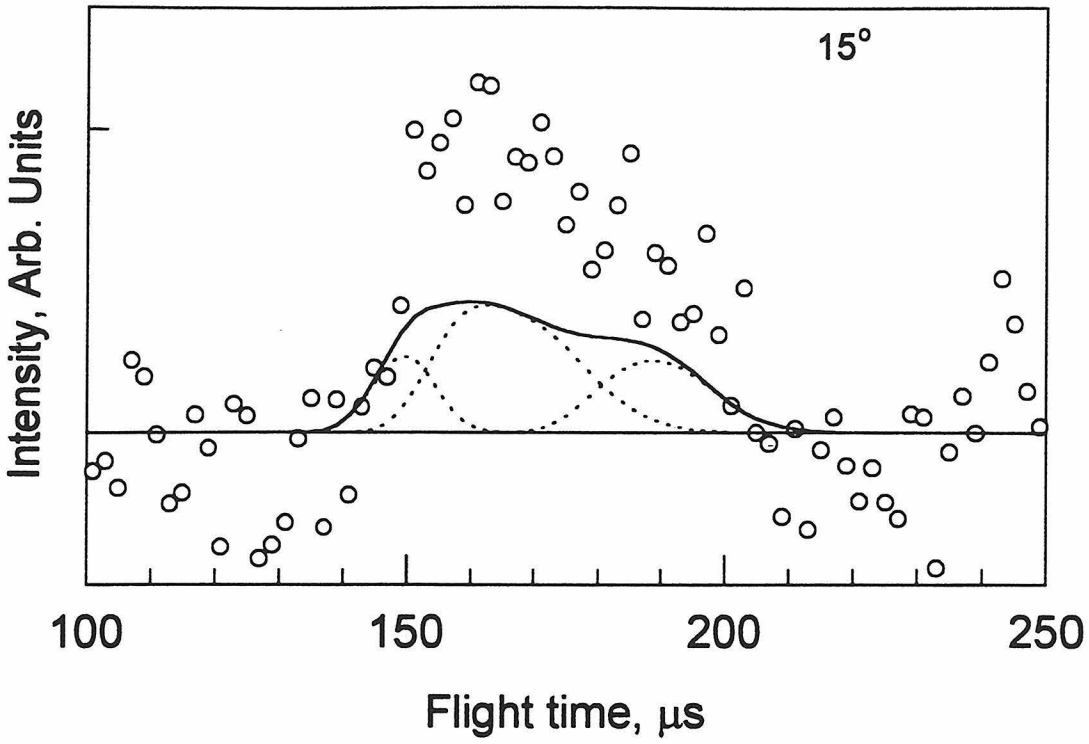

Figure 5.

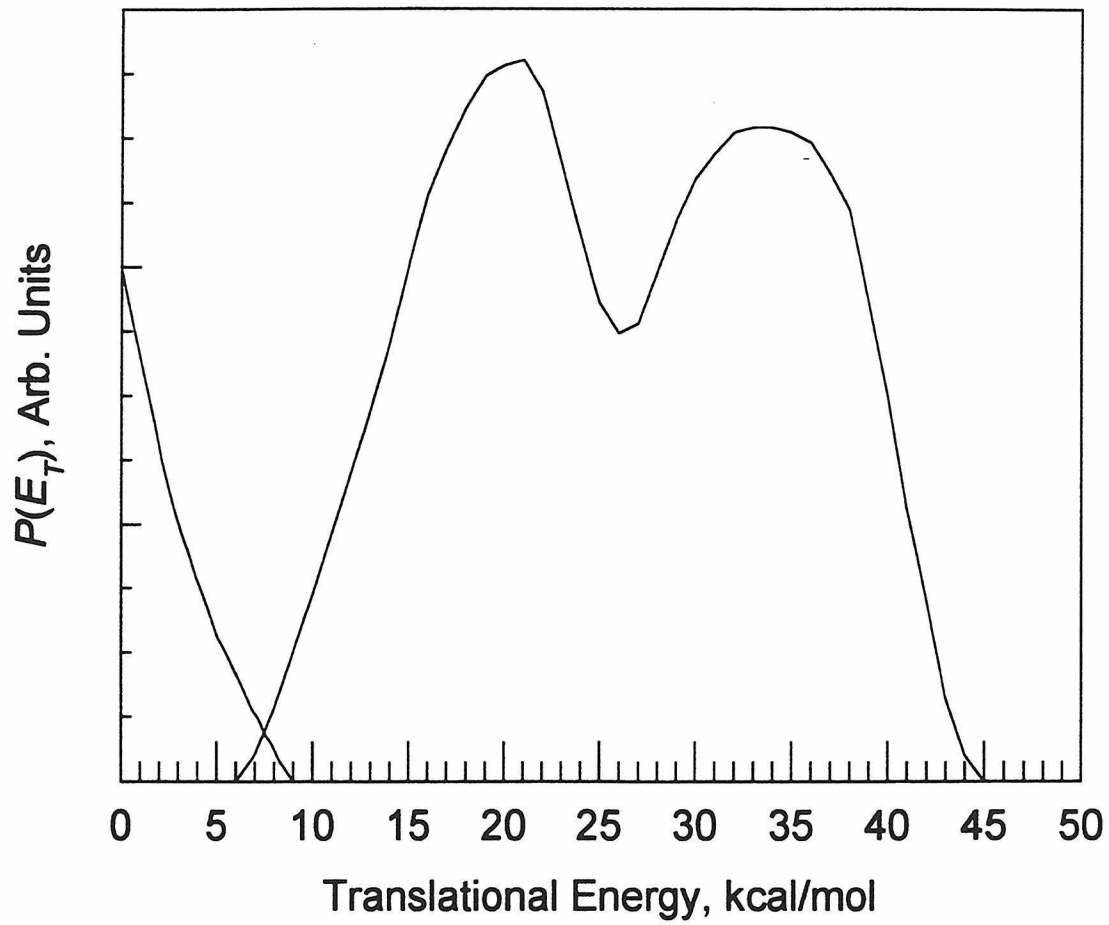
P(E_T), Arb. Units
0
5
10
15
20
25
30
35
40
45
50
Translational Energy, kcal/mol

Figure 6.

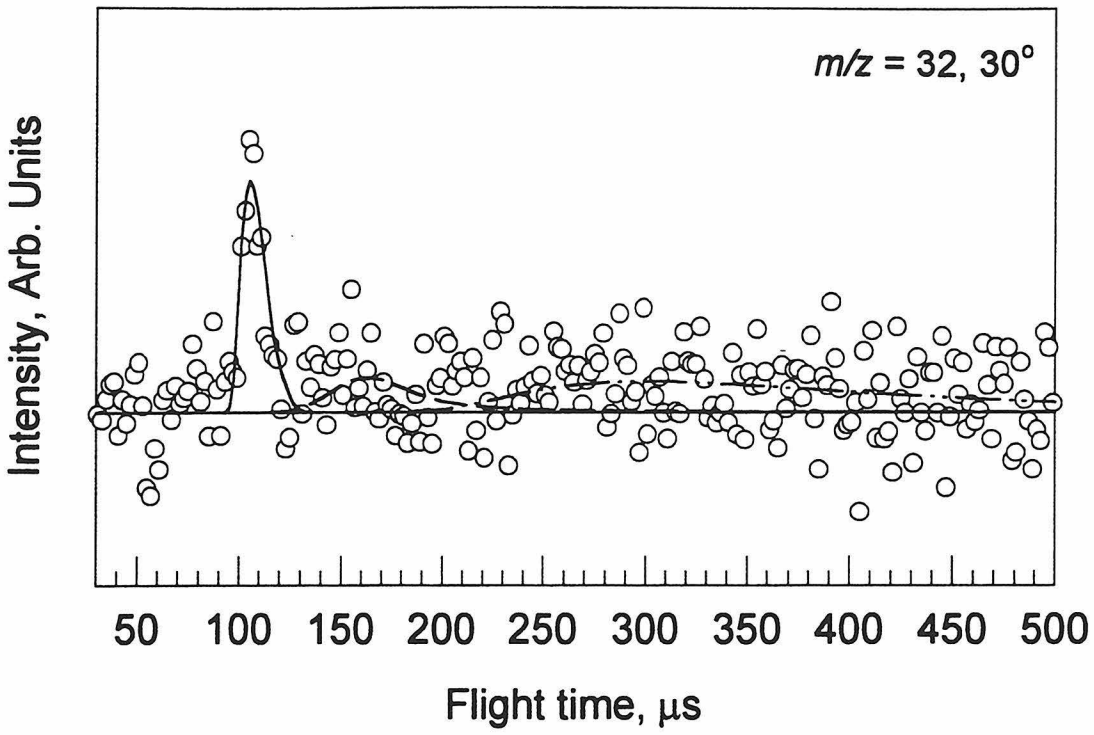
m/z = 32, 30°
Intensity, Arb. Units
50
100
150
200
250
300
350
400
450
500
Flight time, μs

Figure 7.

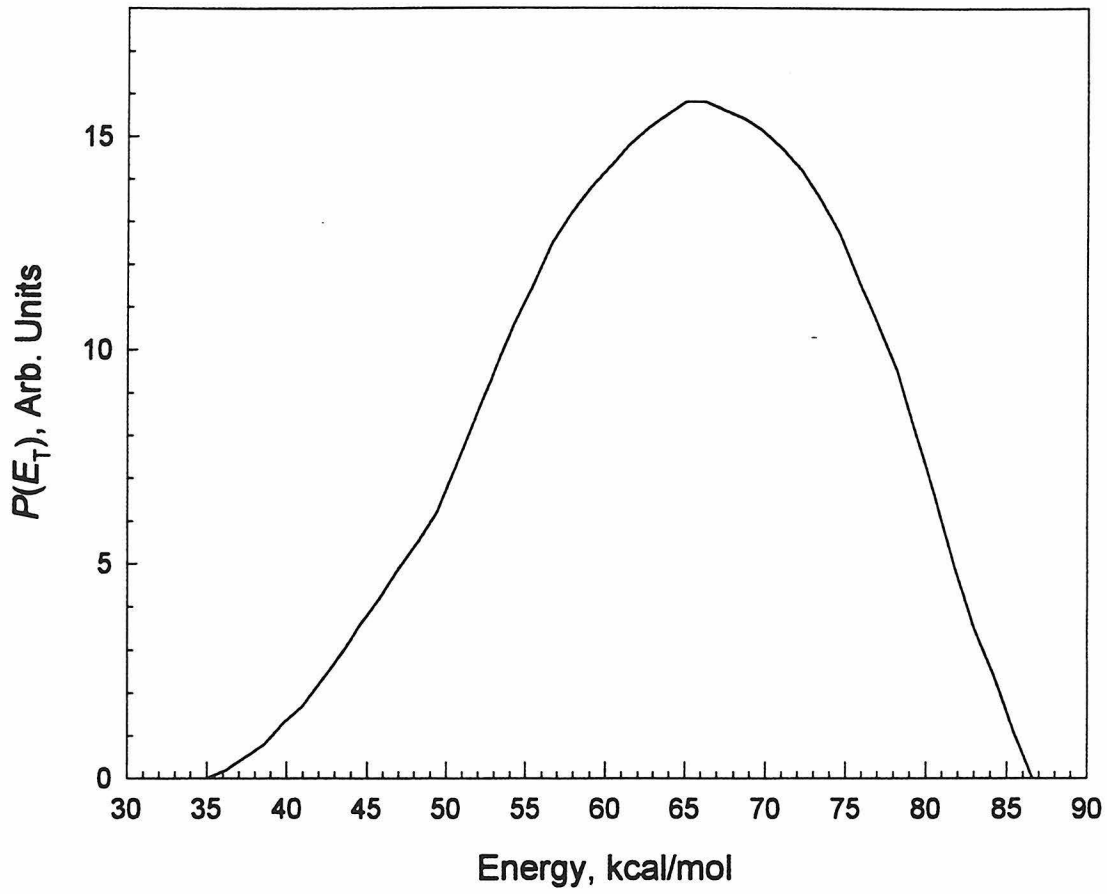
15
10
5
0
$P(E_T)$, Arb. Units
30
35
40
45
50
55
60
65
70
75
80
85
90
Energy, kcal/mol

Figure 8.

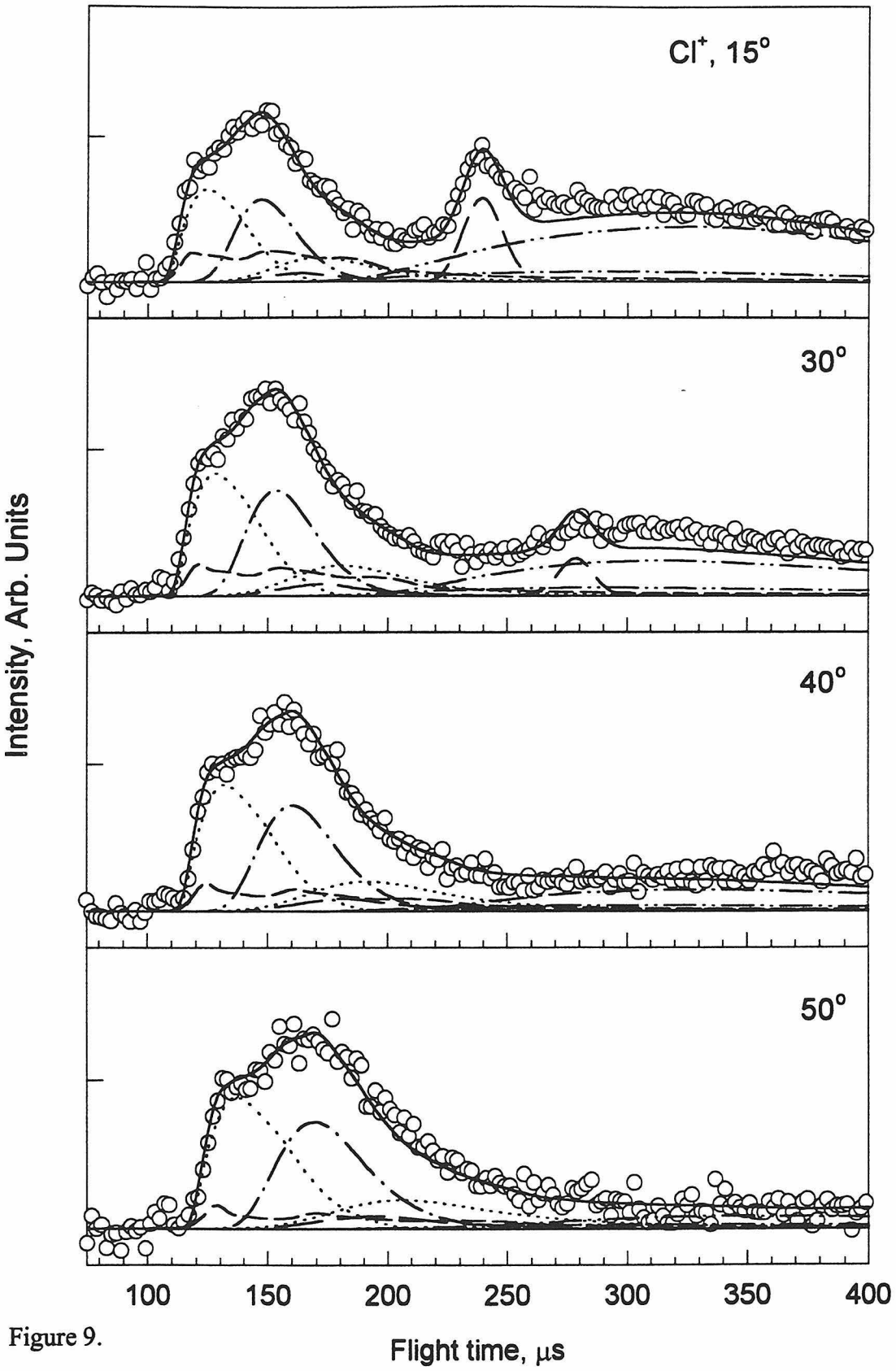
Cl+, 15°
30°
40°
50°
Intensity, Arb. Units
100
150
200
250
300
350
400
Flight time, μs

Figure 9.

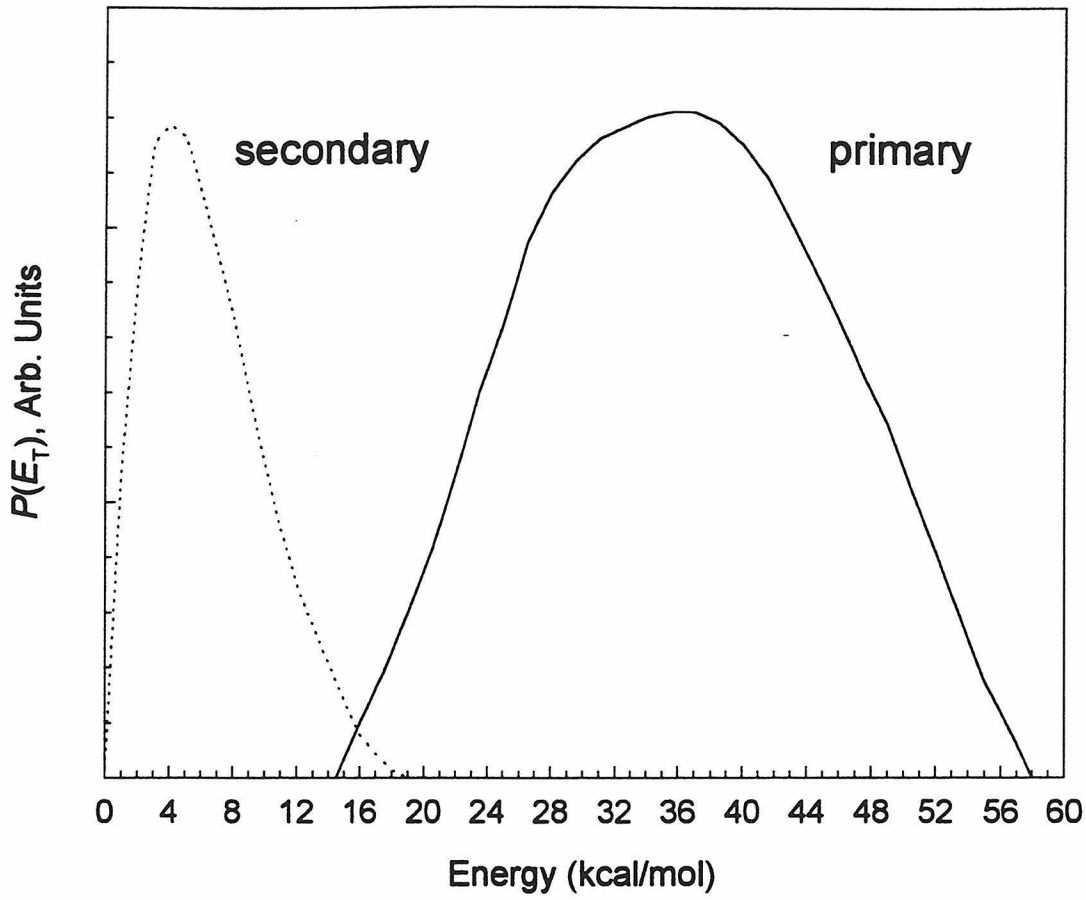
secondary
primary
$P(E_T)$, Arb. Units
0 4 8 12 16 20 24 28 32 36 40 44 48 52 56 60
Energy (kcal/mol)

Figure 10.

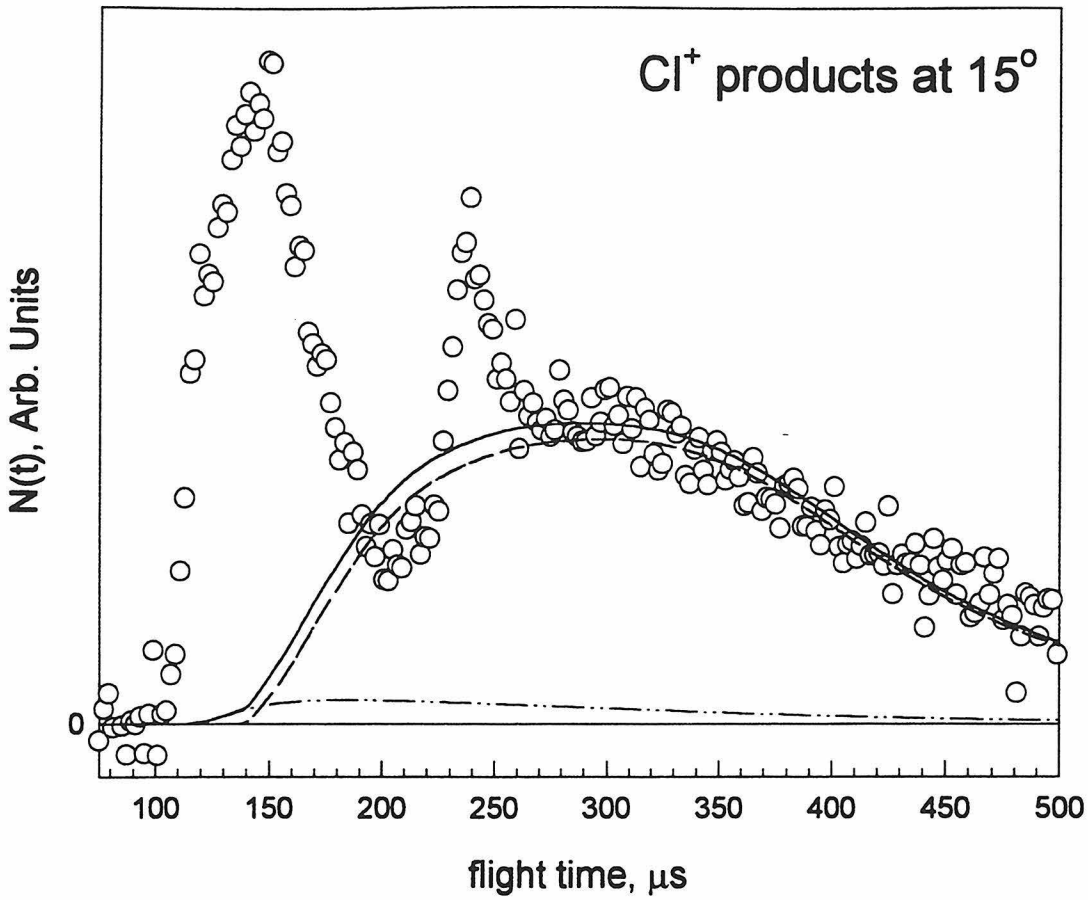
Cl+ products at 15°
N(t), Arb. Units
0
100
150
200
250
300
350
400
450
500
flight time, μs

Figure 11.

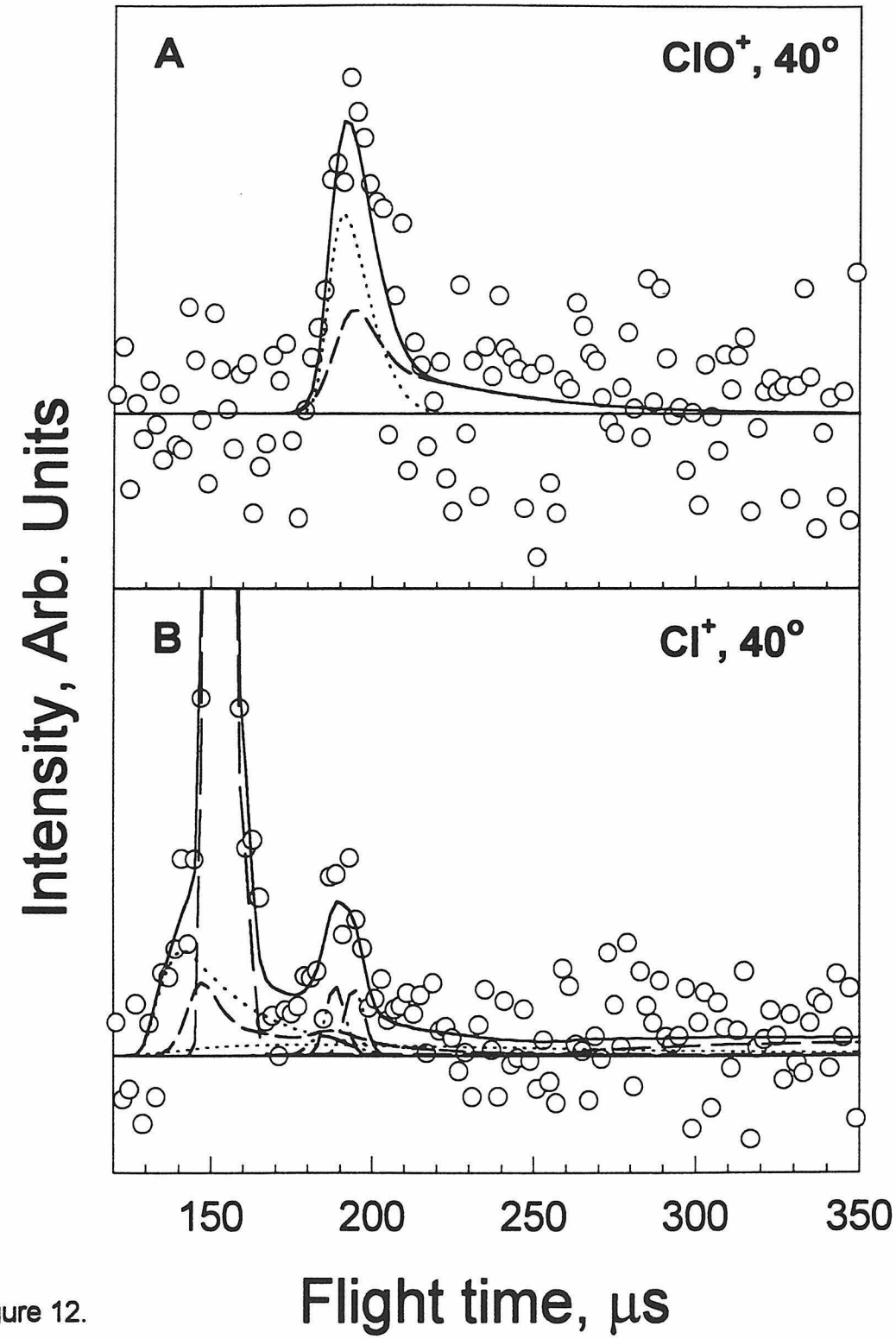
A
ClO+, 40°
B
Cl+, 40°
Intensity, Arb. Units
150
200
250
300
350
Flight time, μs

Figure 12.

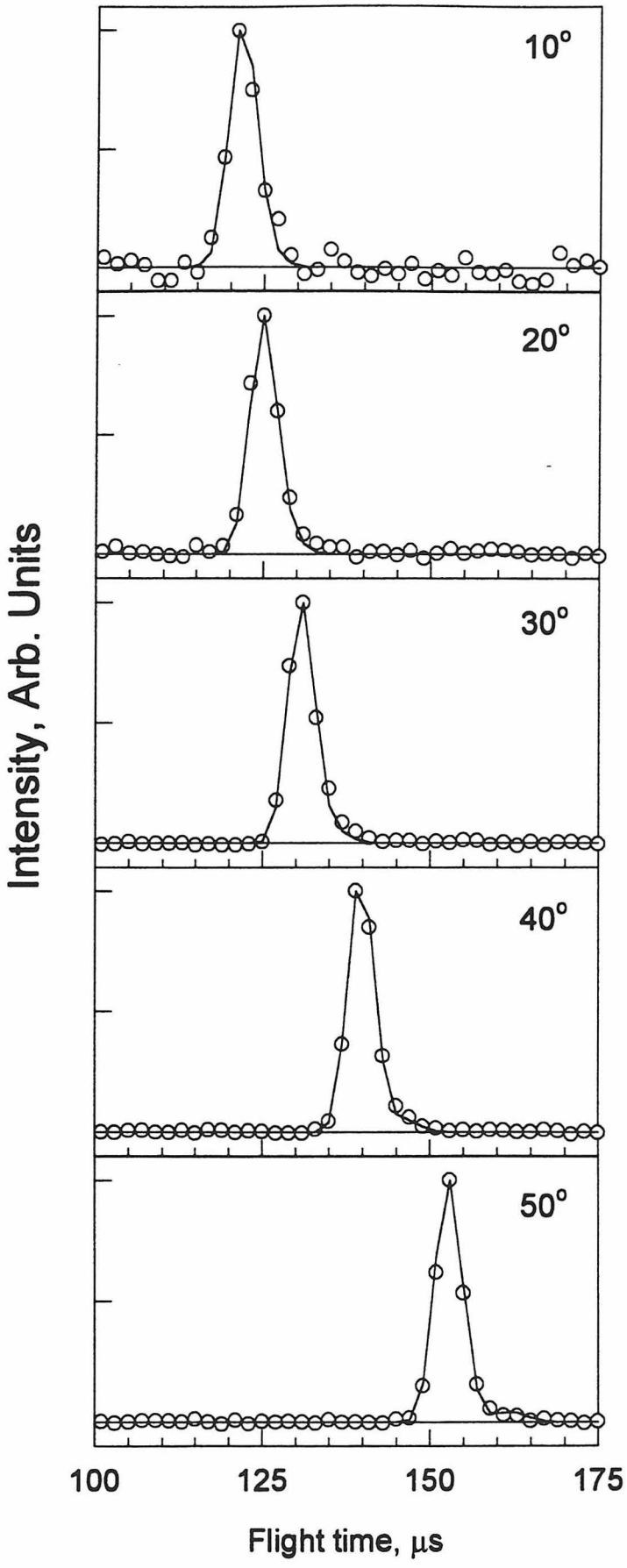
10°
20°
30°
40°
50°
Intensity, Arb. Units
100
125
150
175
Flight time, μs

Figure 13.

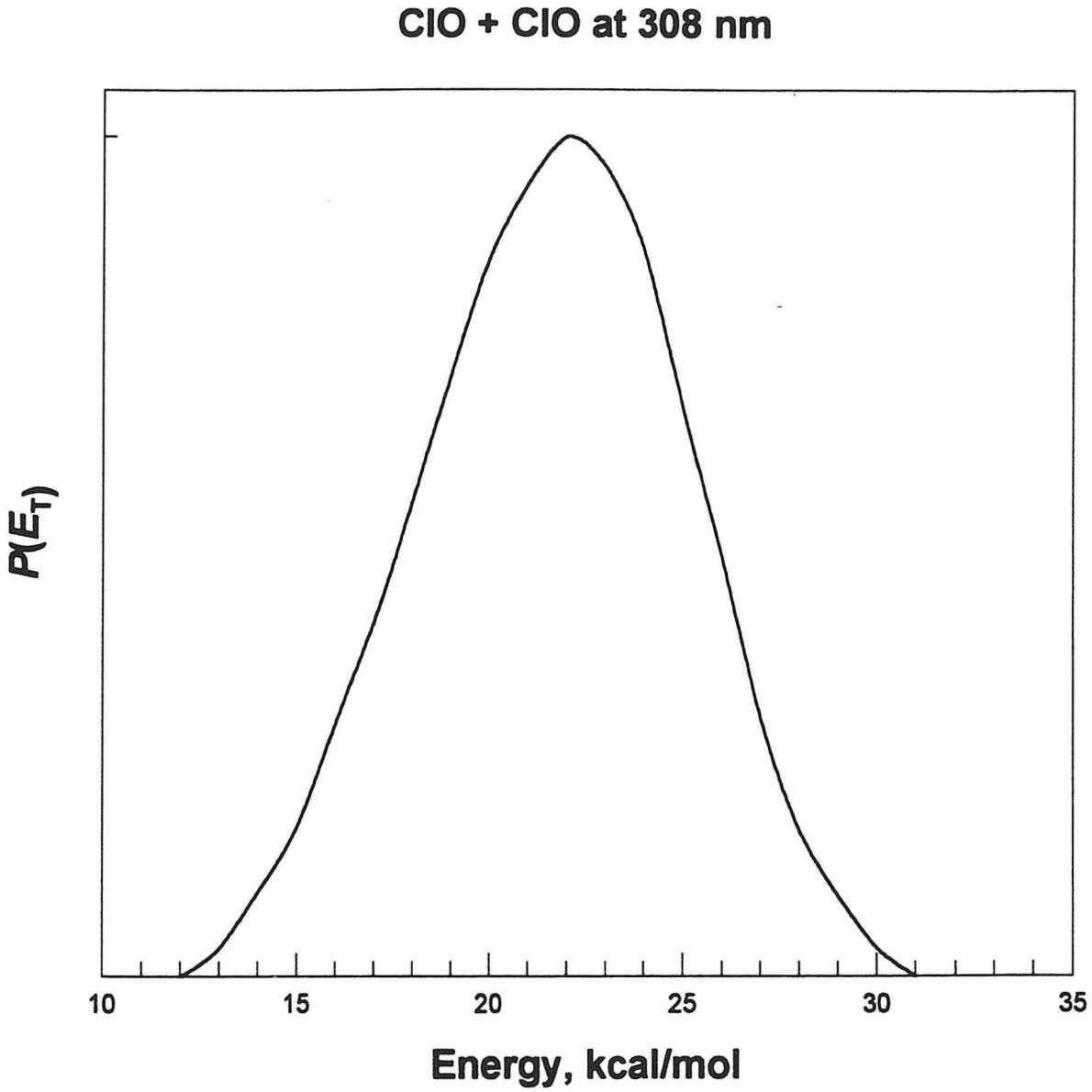

Figure 14.

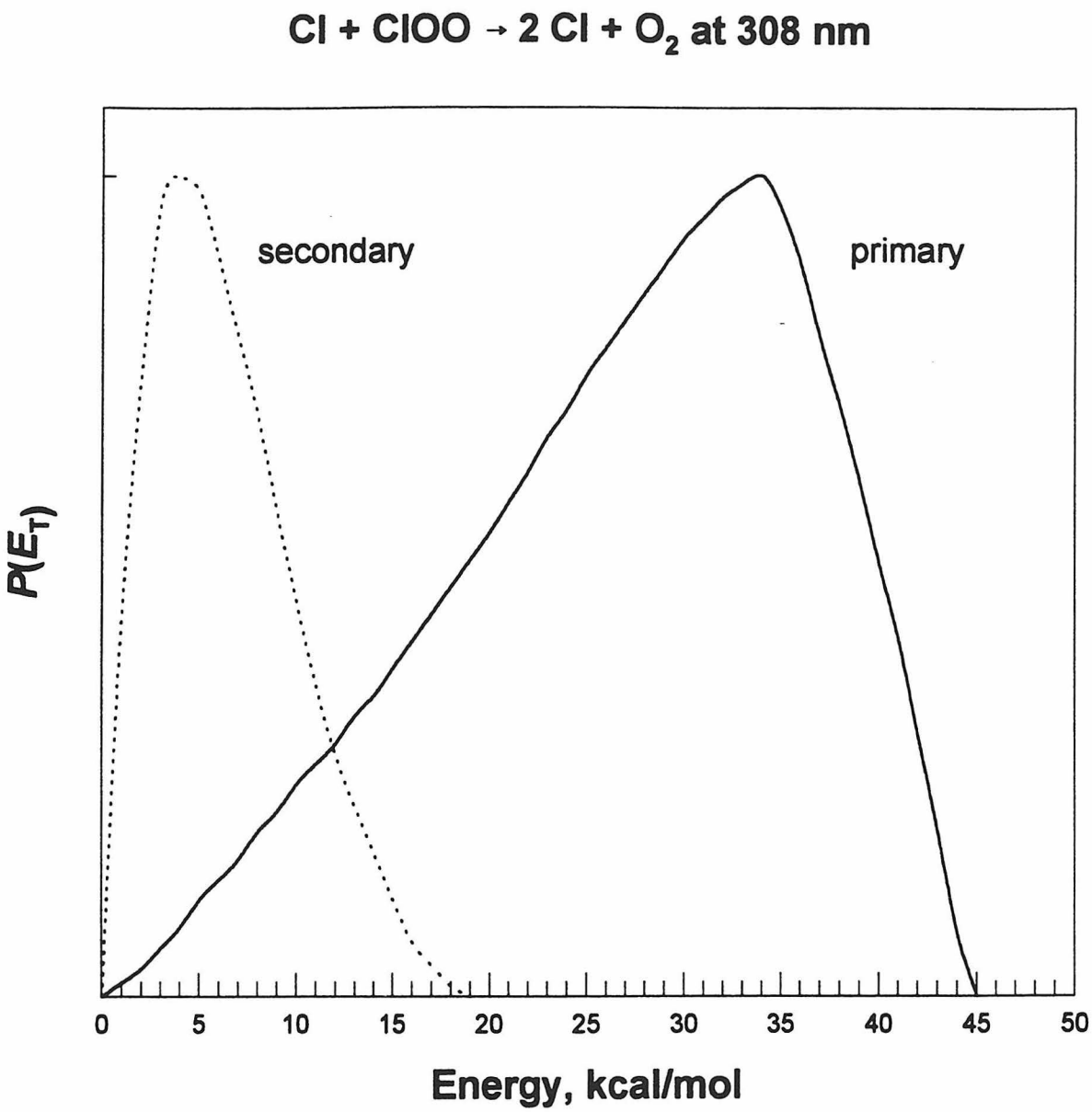
Cl + ClOO → 2 Cl + O2 at 308 nm
secondary
primary
P(ET)
0
5
10
15
20
25
30
35
40
45
50
Energy, kcal/mol

Figure 15.